Title

The Effect of Developmental Heterogeneity and Genetic Variation of Fibroblasts on Cardiac Injury and Repair

Author

Ranjbarvaziri, Sara

Publication Date

2017

Peer reviewed|Thesis/dissertation

UNIVERSITY OF CALIFORNIA

Los Angeles

The Effect of Developmental Heterogeneity and Genetic Variation of Fibroblasts on Cardiac Injury and Repair

A dissertation submitted in partial

satisfaction of the requirements for the

degree Doctor of Philosophy in

Molecular, Cellular and Integrative Physiology

by

Sara Ranjbarvaziri

2017

ABSTRACT OF THE DISSERTATION

The Effect of Developmental Heterogeneity and Genetic Variation of Fibroblasts on Cardiac Injury and Repair

by

Sara Ranjbarvaziri

Doctor of Philosophy in Molecular, Cellular and Integrative Physiology

University of California, Los Angeles, 2017

Professor Reza Ardehali, Committee Chair

Cardiac fibrosis is a pathological process that contributes to adverse cardiac remodeling. It is a consequence of tissue repair processes driven mainly by cardiac fibroblasts (CFbs). In response to stress, CFbs proliferate and secrete extracellular matrix components which, if excessive, leads to scar formation. Scar tissue can interrupt the connections between cardiomyocytes, ultimately compromising the structural integrity and function of the heart. Functional recovery of the myocardium is not only hindered by the formation of fibrotic tissue but also by the irreversible loss of cardiomyocytes. In addition to the key role of CFbs in scar formation, it has been suggested that a subset of CFbs may be the optimal cell source to generate cardiomyocytes through direct reprogramming. Direct

cardiac reprogramming of CFbs represents a promising approach that could lead to regeneration of cardiomyocytes from the endogenous fibroblasts while reducing scar tissue formation. Several studies have demonstrated in vivo direct reprogramming of CFbs leads to an improvement in cardiac function and has been shown to be exceedingly more efficient in the context of recent cardiac injury. Despite the prominent role of CFbs in both scar formation, and in the potential generation of new cardiomyocytes through reprogramming, characterization of these cells is still limited. This is mainly due to lack of reliable markers to identify cardiac fibroblasts, their heterogeneity, and the effects of genetic variation when studying these cells in a diverse population. These constraints prompted us to first identify a panel of surface markers to prospectively identify CFbs. We further performed a comprehensive investigation to identify the developmental heterogeneity of CFbs. We then sought to determine whether developmental origin of CFbs may influence their contribution to formation of scar as well as its effect on their direct reprogramming into iCMs. Finally, by studying CFbs from multiple inbred mouse strains and their response to cardiac insult we aimed to investigate the effect of genetic variation in pathogenesis of cardiac fibrosis.

To undertake a comprehensive study of CFbs, we established a panel of surface markers that can efficiently isolate the majority of CFbs from the adult mouse heart. We employed lineage tracing, transplantation studies, and parabiosis to show that most adult CFbs are derived from the epicardium, a minority arises from endothelial cells, with no contribution from bone marrow or circulating cells. Intriguingly, developmentally distinct CFbs showed similar proliferation rates, and similar gene expression profiles in response to pressure

overload injury. We next sought to determine whether this heterogeneity of CFbs may affect their efficiency to generate cardiomyocytes via direct reprogramming, mainly in the context of injury. Using genetic fate-mapping techniques, transplantation studies and gene expression profiling, we showed that the majority of CFbs originate from a shared mesodermal ancestor as cardiomyocytes while a minority of the CFb population originates from neural crest-derived precursors. We provide compelling evidence that, regardless of their developmental origin, CFbs are able to be successfully converted to functional iCMs through *in vitro* direct reprogramming. However, CFbs generated iCMs with higher efficiency compared to fibroblasts of extra-cardiac organs of identical developmental origin, emphasizing the importance of the physiological microenvironment on cell fate. Remarkably, cardiac injury induced unique re-expression of early developmental genes in CFbs that corresponded to their developmental origin. Finally, we studied the contribution of CFbs from multiple inbred mouse strains following insult to the heart. Our data showed that despite similar increases in proliferation within the different strains, fibroblast activation is a response that correlates with the extent of scar formation. Additionally, by comparing CFbs from multiple strains, we were able to identify potential pathways as therapeutic targets with latent TGF-β binding protein-2 (LTBP2) as a promising diagnostic marker for fibrosis, with relevance to patients with underlying myocardial fibrosis.

Together, our findings suggest that common signaling mechanisms stimulate the pathological response of different CFb populations. However, in the context of direct cardiac reprogramming after injury, the developmental heterogeneity of CFbs may be an

essential contributing factor. Our findings also highlight the importance of genetic variation in cardiac fibrosis. Therefore, therapeutic strategies for reducing pathogenic CFbs should target these common pathways instead of targeting fibroblasts of other sources. It may be crucial to study the effects of injury on different CFb subsets for the development of targeted therapies to promote cardiac repair.

The dissertation of Sara Ranjbarvaziri is approved.

James N Weiss

Aldons J Lusis

William Edward Lowry

Kristina Bostrom

Reza Ardehali, Committee Chair

University of California, Los Angels

2017

DEDICATION

I dedicate my dissertation to patients who suffer from cardiovascular disease.

TABLE OF CONTENTS

LIST OF FIGURES

ACKNOWLEDGEMENTS

I would like to express my special gratitude to my supervisor, Dr. Reza Ardehali, for giving me the opportunity to be a member of his lab. I thank him for his scientific supervision, unwavering support, motivation and enthusiasm, and for believing in me.

I would like to thank the members of my doctoral committee. I especially wish to thank the previous and present members of our laboratory for their experimental help, scientific discussions, and critical comments. I am grateful to everyone who contributed to my research.

Finally, I wish to thank my husband, Ryan, for being a part of our journey in life and science.

VITA/ BIOGRAPHICAL SKETCH

EDUCATION/EXPERIENCES

B.S. Azad University, Iran, Experimental Sciences **2001-2005**

M.S. University of Science and Culture, Iran, Cell & Developmental Biology **2007-2010**

Research Scientist Dalhousie University, Canada, Pharmacology Department **2011-2012**

Staff Research Associate I University of California, Los Angeles, Medicine Department **2012-2014**

Ph.D. University of California, Los Angeles, Molecular, Cellular & Integrative Physiology **Expected 2017**

LIST OF PUBLICATIONS

1. **Ranjbarvaziri S,** James Engel J, Park S, Handel B. V, Zhao P, Ding Y, Sung K, Hsiai T. K, Moore M. D, Novitch B. G, Sahoo D, Nam Y, Ardehali R. Cardiac Microenvironment Supersedes Developmental Origin for Fibroblast-to-Cardiomyocyte Reprogramming. (Manuscript is under preparation).

2. Ranjbarvaziri S*, Park S*, Lay F, Zhao P, Miller M, Lusis J, Ardehali R. Genetic regulation of fibroblasts activation and proliferation in fibrosis. (Manuscript is under revision) * These authors contributed equally

3. Yichen Ding, Jianguo Ma, Adam D. Langenbacher, Kyung In Baek, Juhyun Lee, Chih-Chiang Chang, **Sara Ranjbarvazirj**, Jeffrey J. Hsu, Rajan P. Kulkarni, John Belperio, Wei Shi, Reza Ardehali, Yin Tintut, Linda L. Demer, Jau-Nian Chen, Peng Fei, Tzung K. Hsiai.

Frontier Applications of Light-Sheet Imaging for Elucidating Cardiovascular Development and Disease (Manuscript is under revision)

4. Sereti K*, Kamran P*, Nguyen N*, Zhao P, Ranjbarvaziri S, Engel J, Mikkola H, Ardehali R. (2017) Clonal analysis of cardiomyocyte generation during development and injury. Nature Communication. * These authors contributed equally

5. **Ranjbarvaziri S**, Park S, Nguyen N, Gilmore W, Zhao P, Ardehali R. **(2017)** Generation of Nkx2-5/CreER transgenic mice for inducible Cre expression in developing hearts. Genesis. 55 (8).

6. Ali SR*, **Ranjbarvaziri S***, Talkhabi M, Zhao P, Subat A, Hojjat A, Kamran P, Müller AM, Volz KS, Tang Z, Red-Horse K, Ardehali R. **(2014)** Developmental Heterogeneity of Cardiac Fibroblasts Does Not Predict Pathological Proliferation and Activation. Circulation Research, 115(7), 625-35. (PMID: 25037571) * These authors contributed equally

7. **Ranjbarvaziri S,** Kiani S, Akhlaghi A, Vosough A, Baharvand H, Aghdami N. **(2011)** Quantum Dot Labeling Using Positive Charged Peptides in Human Hematopoietic and Mesenchymal Stem Cells. Biomaterials, 32 (22), 5195-5205. (PMID:21549422)

8. Aghdami N, **RanjbarVaziri S**. Bionanotechnology Strategies for Cell Detection. **(2011)** Bionanotechnology II Global Prospects. 11-39. (Chapter book)

9. **RanjbarVaziri S**, Aghdami N. Applications of quantum dots in cell tracking. **(2010)** Anatomical Science Journal. 2010, 8, 85-95. (Article in Farsi)

10. Aghdami N, **RanjbarVaziri S**. Imaging of molecular targets, Quantum dots as cell highlighters in stem cell transplantation. (**2008**) Bioforum Europe journal.12 (11) 34-36.

CHAPTER 1

Introduction

1.1 Heart failure and Cardiac fibrosis

For most of the last century, cardiovascular disease (CVD) has been one of the leading causes of morbidity and mortality in the entire world and in the United States in particular [1]. Progression of CVD that develops into heart failure is mainly associated with pathological remodeling of the heart [2, 3]. Cardiac fibrosis and cardiomyocyte hypertrophy are both hallmarks of cardiac remodeling of the failing myocardium. Unlike other organs, the heart has very limited regenerative capacity following injury. The process of cardiac repair mainly involves the removal of necrotic cardiomyocytes followed by fibrosis that act to preserve myocardial structural and functional integrity. Cardiac fibrosis refers to a progressive condition in which excess fibrous matrix, mainly secreted by cardiac fibroblasts, results in stiffened heart tissue, ultimately leading to abnormalities in cardiac contractility and conductance [4].

Many clinical interventions for treating CVD aim to inhibit or reverse cardiac fibrosis. Despite substantial improvements in therapeutic strategies, these interventions may lead to a partial recovery of cardiac contractility and thereby only delay the progression towards heart failure [5]. Therefore, there is an urgent need for innovative and effective approaches for targeting cardiac disease processes linked to fibroblast function.

1.2 The role of fibroblasts in cardiac physiology and pathophysiology

Cardiac mesenchymal cells — often referred to 'fibroblasts', derived from the Latin *fibra* (fibre or filament) and the Greek *blastos* (germ or sprout) — are among the most abundant interstitial cells in the myocardium [6]. In the healthy heart, cardiac fibroblasts play a central role in formation and maintenance of cardiac connective tissue. These cells are involved in synthesizing and secreting the extracellular matrix (ECM) proteins, including collagens, fibronectin, laminins, and tenascins. Cardiac fibroblasts also produce matrix metalloproteinases (MMP) and tissue inhibitors of metalloproteinase (TIMP) thereby enabling homeostatic maintenance of the ECM. In addition to the maintenance of connective tissue, cardiac fibroblasts express a wide array cytokines and paracrine factors that influence development, growth, and functional adaptation of other cardiac cells, cardiomyocytes in particular, during development as well as in both physiological and pathophysiological settings [7].

In response to cardiac stress, fibroblasts — the primary effectors of scar formation — proliferate and/or become activated. Activated fibroblasts, also known as myofibroblasts, are nearly absent in the healthy heart and are remarkably distinguishable from resident fibroblasts. Compared to quiescent fibroblasts, activated fibroblasts are more mobile, secrete excessive ECM proteins, and express higher levels of contractile proteins. This excess deposition of ECM leads to the development of fibrous tissue. After cardiac injury, cardiac fibroblasts and their activated counterparts play an integral role in providing tensile strength, lack of which may lead to ventricular wall rupture [1]. Eventually, in the

normal non-cardiac wound healing process, activated fibroblasts are removed, allowing the scar tissue to regress and the injured area to recellularize. By contrast, in cardiac injury, due to lack of sufficient regeneration, cardiomyocytes fail to repopulate the injured area and activated fibroblasts persistently remain in the area. This in turn leads to maturation of scar tissue and ultimately chamber dilation and heart failure [8].

One of the impediments to developing new mechanistically based strategies to target fibroblast function in cardiac diseases has been an incomplete understanding of their true identity [7]. This is mainly due to the multi-lineage derivation of fibroblasts and subsequent difficulty in determining specific markers. To date, a common expression marker has not been identified which can specifically label all subpopulations of cardiac fibroblasts [7]. Instead, research has mainly relied on the use of semi-specific markers to differentiate fibroblasts from other cell types. As an example, fibroblast specific protein 1 (FSP1) has been widely used to identify fibroblasts. However, FSP1 has been shown to mark monocytes, smooth muscle cells, and cancer cells in addition to fibroblasts [7, 9]. Lack of commonly expressed fibroblast-specific marker(s) has prevented research to better understand the origin and function of cardiac fibroblasts in disease states. Therefore, it is imperative to delineate and validate a robust set of markers to isolate cardiac fibroblasts. To this end, in this Thesis we first seek to develop a panel of surface markers that would most specifically allow us to account for the majority of cardiac fibroblasts without contamination from other cell types.

1.3 Origin of cardiac fibroblasts

During heart development, fibroblasts have shown to be originated from multiple neighboring mesenchymal tissues [7]. Several studies from both avian and mouse models showed that the pro-epicardium — a sprout-like cluster of extra-cardiac cells — provides the source for a thin layer of epithelium that progressively envelops the embryonic heart. This thin layer, also known as the epicardium, then undergoes epithelial-to-mesenchymal-transition (EMT) and contributes to the majority of cardiac fibroblasts and vascular smooth muscle cells [6]. Despite knowledge of the origin of cardiac fibroblasts during development, the source of scar forming fibroblasts in the injured myocardium still remains controversial. This is mainly due to lack of clear-cut lineage studies. Several sources have been suggested as potential contributors after injury to the heart. Using *Tie1*$^{Cre/+}$;*Rosa26*$^{lacZ/+}$ mice, in which endothelial cells and their descendants are marked by LacZ, Zeisberg et al. demonstrated that a subset of activated fibroblasts in the fibrotic area are of endothelial origin through endothelial-to-mesenchymal transition (EndMT) [10]. However, there are several concerns regarding the significance of these findings. The Tie1 promoter is not specific to endothelial cells since it also expresses in a small fraction of hematopoietic cells. The researchers also used FSP1-GFP transgenic mice which do not exclusively label fibroblasts, but also mark myeloid lineage cells [9]. This may confound interpretations of fibroblast lineage studies given the abundance of immune cells after cardiac injury [10, 11]. Additionally, using chimeric mice, it has been suggested that bone-marrow-derived cells also contribute to a significant percentage of

both quiescent and activated fibroblasts after cardiac injury. However, other studies suggest that bone marrow contributions to cardiac fibroblasts after injury are minor.

These uncertainties prompted us to design a series of experiments using different lineage tracing transgenic mouse models ($Tbx18^{Cre/+}$ [12] and $Wt1^{CreERT2/+}$ [13-16] for epicardium; $Tie2^{Cre}/+$ for endothelium [17]; $Pax3^{Cre/+}$ for neural crest [18]) to investigate the precise source of fibroblasts after pressure overload injury. We also perform transplantation and parabiosis studies to test whether there is any contribution from bone marrow or circulation to fibroblast population in the heart. We further explore the implications of fibroblasts' developmental heterogeneity in normal physiology and after cardiac injury.

1.4 Cardiac fibroblasts in repair

The functional recovery of the damaged heart is not only hindered by the formation of fibrotic tissue but also by the irreversible loss of millions to billions of cardiomyocytes which cannot be restored [19]. Therefore, to fully restore heart function it is necessary to keep the balance between generations of new and functional cardiomyocytes along with reducing the scar tissue. While heart transplantation is an effective therapy for end-stage heart failure, it is limited by the number of donor organs available and requires significant lifelong care and immunosuppression treatment [16]. The current cell-based strategies using stem/progenitor cells to repair the damaged tissue are facing several obstacles, including inefficient delivery systems, lack of an optimal cell type, and low survival rate in

transplanted cells [19]. Moreover, these approaches can only limit the severity of initial cardiac damage — none of them can reverse fibrosis once the process has begun.

Direct conversion of a somatic cell to cardiomyocytes, on the other hand, holds great promise in the field of cardiac regenerative medicine [19, 20]. In fact, cardiac fibroblasts are thought to be the optimal cell type for autologous generation of cardiomyocytes. This is mainly due to the abundance of these cells in the scar area, their proliferative properties, and their tendency to persist for long periods of time. Furthermore, a recent study by Furtado et al. suggests that a subpopulation of cardiac fibroblasts may be more amenable in cardiac reprogramming due to expression of cardiogenic genes at higher levels when compared to fibroblasts of other organs [21]. Several studies have directly converted both mouse and human fibroblasts into induced cardiomyocytes *in vitro* by overexpressing different combinations of cardiac-specific factors (e.g., Gata4, Mef2c, and Tbx5). Additionally, reprogramming of endogenous cardiac fibroblasts into functional cardiomyocytes has been performed *in vivo* after cardiac injury [22-24]. These studies have shown that reprogrammed cardiomyocytes are not identical but similar to endogenous cardiomyocytes in both morphology and functionality. The generated cardiomyocytes have been shown to restore contractile cardiac function by improving ejection fraction while reducing scar volume. Furthermore, cardiac reprogramming could be modulated to generate different subtypes of cardiomyocytes (i.e., ventricular, atrial, and nodal cells) [25-27] which can potentially be used for different cardiac disease settings. For example, induced ventricular cardiomyocytes are needed to repair ischemic

damage to the ventricular myocardium, while nodal cells can be used to restore proper cardiac rhythm and electrical conduction [28].

Despite the advancements made in the field of direct reprogramming, low efficiency and presence of residual epigenetic memory to the original cell population remain as obstacles for bringing this technology closer to the clinic [28]. Epigenetic memory (or transcriptional remnants) refers to characteristics of the initial cell type that persist after direct reprogramming and which thereby may impact the function of the desired reprogrammed cell type [29]. Thus, choosing a starting cell type that has similar ontogeny to the terminal cell type may overcome some of the limitations associated with this issue. Given the heterogeneity of cardiac fibroblasts, we investigate whether there is a distinct population of cardiac fibroblasts that is more amenable to cardiomyocyte reprogramming. In particular, we examine whether there exists a subpopulation of cardiac fibroblasts that share embryonic origin with cardiomyocytes; due to its retained developmental memory, this could in principle lead to a higher efficiency in generating cardiomyocytes.

Several studies have revealed the higher efficiency of *in vivo* reprogramming with prior injury compared to *in vitro* reprogramming. Additionally, functional improvement after *in vivo* reprogramming is greater than expected, suggesting that factors beyond cell intrinsic differences may also be involved. It is possible that presence of stimulatory factors after injury may enhance conversion of cardiac fibroblasts to cardiomyocytes. These uncertainties prompted us to perform a comprehensive investigation to identify the developmental heterogeneity of cardiac fibroblasts and determine whether developmental origin or the microenvironment of the cardiac fibroblasts is the dominant

factor for efficient reprogramming. Our findings provide insight for the molecular mechanism underlying the beneficial effect of *in vivo* reprogramming for potential therapeutic interventions toward cardiogenesis.

1.5 The role of genetic variation of fibroblasts in cardiac fibrosis

Heart failure resulting from prolonged interstitial and perivascular fibrosis is a highly heterogeneous disorder influenced by many genetic and environmental factors. The unbiased genome-wide association study (GWAS) was designed to identify genetic variations on complex traits such as heart failure [30]. However, multiple large-scale GWAS studies have provided limited success in identifying genetic signals driving heart failure [31]. This is partly due to paucity of quantitative phenotypic data as well as diverse environmental factors. Therefore, it has proven challenging to develop treatments for heart failure and cardiac fibrosis that are applicable for a diverse population. Indeed, the efficacy of currently available therapies and detection strategies varies widely between different patient populations. The Hybrid Mouse Diversity Panel (HMDP) is a collection of over 100 genotyped inbred strains of mice and serves as a unique tool for mimicking in mice the genetic variance and substantial diversity of heart failure development seen in humans. In a comprehensive study by Rau et al., mice within the HMDP were phenotypically characterized following chronic treatment with the β-adrenergic agonist isoproterenol (ISO) [31]. Excessive stimulation of β-adrenergic receptors in the heart was linked to increased CFb proliferation and collagen synthesis. Chronic treatment of the HMDP with ISO resulted in a wide range of severity in cardiac hypertrophy and associated

fibrosis across the different strains. These findings support the hypothesis that genetic variation influences the development and progression of cardiac dysfunction and pathological fibrosis. However, these studies evaluated changes at the cardiac tissue level and did not delineate the roles of specific cell types to each strain's respective phenotype. While previous studies have sought to identify genetic markers uniquely associated with heart failure in a specific genetic background, here we characterize fibroblasts of multiple strains with different cardiac fibrosis severities in response to ISO treatment. Using this valuable tool, we investigate the molecular mechanisms that regulate the specific contributions of these cells to scar development. Findings from our study may lead to improved diagnosis and tailored treatments based on the genetic makeup of individuals in the population.

1.6 The overall goal of our study

Cardiac fibroblasts are diverse in ontogeny and play a crucial role in development and functional operation of the healthy and diseased heart. In this Thesis, we provide a framework for studying the developmental origin of cardiac fibroblasts in pathogenic fibrosis induced by pressure overload injury (Chapter 2). We further study whether developmental heterogeneity and/or physiological environment of these cells can affect their potential therapeutic target in direct fibroblasts-to-cardiomyocytes reprogramming (Chapter 3). Finally, we investigate the effect of genetic variation on cardiac fibroblasts response to injury (Chapter 4). We believe that data from our studies will be essential in the development of therapies to reduce the scar and promote cardiac repair.

1. Fan, D., et al., Cardiac fibroblasts, fibrosis and extracellular matrix remodeling in heart disease. Fibrogenesis Tissue Repair, 2012. 5(1): p. 15.

2. Nowbar, A.N., et al., 2014 global geographic analysis of mortality from ischaemic heart disease by country, age and income: statistics from World Health Organisation and United Nations. Int J Cardiol, 2014. 174(2): p. 293-8.

3. Xu, J. and T. Kisseleva, Bone marrow-derived fibrocytes contribute to liver fibrosis. Exp Biol Med (Maywood), 2015. 240(6): p. 691-700.

4. Rohr, S., Arrhythmogenic implications of fibroblast-myocyte interactions. Circ Arrhythm Electrophysiol, 2012. 5(2): p. 442-52.

5. Travers, J.G., et al., Cardiac Fibrosis: The Fibroblast Awakens. Circulation research, 2016. 118(6): p. 1021-1040.

6. Gourdie, R.G., S. Dimmeler, and P. Kohl, Novel therapeutic strategies targeting fibroblasts and fibrosis in heart disease. Nat Rev Drug Discov, 2016. 15(9): p. 620-638.

7. Ali, S.R., et al., Developmental Heterogeneity of Cardiac Fibroblasts Does Not Predict Pathological Proliferation and Activation. Circulation Research, 2014. 115(7): p. 625-635.

8. Davis, J. and J.D. Molkentin, Myofibroblasts: trust your heart and let fate decide. J Mol Cell Cardiol, 2014. 70: p. 9-18.

9. Kong, P., et al., Lack of specificity of fibroblast-specific protein 1 in cardiac remodeling and fibrosis. Am J Physiol Heart Circ Physiol, 2013. 305(9): p. H1363-72.

10. Zeisberg, E.M., et al., Endothelial-to-mesenchymal transition contributes to cardiac fibrosis. Nat Med, 2007. 13(8): p. 952-61.

11. Ruiz-Villalba, A., et al., Interacting resident epicardium-derived fibroblasts and recruited bone marrow cells form myocardial infarction scar. J Am Coll Cardiol, 2015. 65(19): p. 2057-66.

12. Cai, C.-L., et al., A myocardial lineage derives from Tbx18 epicardial cells. Nature, 2008. 454(7200): p. 104-108.

13. Quinn, T.A., et al., Electrotonic coupling of excitable and nonexcitable cells in the heart revealed by optogenetics. Proceedings of the National Academy of Sciences of the United States of America, 2016. 113(51): p. 14852-14857.

14. von Gise, A., et al., WT1 regulates epicardial epithelial to mesenchymal transition through β-catenin and retinoic acid signaling pathways. Developmental biology, 2011. 356(2): p. 421-431.

15. Zhou, B. and W.T. Pu, Genetic Cre-loxP assessment of epicardial cell fate using Wt1-driven Cre Alleles. Circulation research, 2012. 111(11): p. e276-e280.

16. Rudat, C. and A. Kispert, Wt1 and epicardial fate mapping. Circ Res, 2012. 111(2): p. 165-9.

17. Zeisberg, E.M., et al., Endothelial-to-mesenchymal transition contributes to cardiac fibrosis. Nat. Med., 2007. 13: p. 952-61.

18. Lang, D., et al., Pax3 functions at a nodal point in melanocyte stem cell differentiation. Nature, 2005. 433: p. 884-7.

19. Sanganalmath, S.K. and R. Bolli, Cell therapy for heart failure: a comprehensive overview of experimental and clinical studies, current challenges, and future directions. Circ Res, 2013. 113(6): p. 810-34.

20. Qian, L. and D. Srivastava, Direct cardiac reprogramming: from developmental biology to cardiac regeneration. Circ Res, 2013. 113(7): p. 915-21.

21. Furtado, M.B., et al., Cardiogenic genes expressed in cardiac fibroblasts contribute to heart development and repair. Circ Res, 2014. 114(9): p. 1422-34.

22. Qian, L., et al., In vivo reprogramming of murine cardiac fibroblasts into induced cardiomyocytes. Nature, 2012. 485(7400): p. 593-598.

23. Kuishi, Y., et al., In Vivo Cardiac Reprogramming by a Single Polycistronic Vector Improves Cardiac Function after Myocardial Infarction. Journal of Cardiac Failure. 21(10): p. S189.

24. Mohamed, T.M.A., et al., Chemical Enhancement of In Vitro and In Vivo Direct Cardiac Reprogramming Clinical Perspective. Circulation, 2017. 135(10): p. 978-995.

25. Fu, Y., et al., Direct reprogramming of mouse fibroblasts into cardiomyocytes with chemical cocktails. Cell Res, 2015. 25(9): p. 1013-24.

26. Ieda, M., et al., Direct reprogramming of fibroblasts into functional cardiomyocytes by defined factors. Cell, 2010. 142(3): p. 375-86.

27. Nam, Y.J., et al., Induction of diverse cardiac cell types by reprogramming fibroblasts with cardiac transcription factors. Development, 2014. 141(22): p. 4267-78.

28. Burridge, P.W., A. Sharma, and J.C. Wu, Genetic and Epigenetic Regulation of Human Cardiac Reprogramming and Differentiation in Regenerative Medicine. Annu Rev Genet, 2015. 49: p. 461-84.

29. Morris, S.A. and G.Q. Daley, A blueprint for engineering cell fate: current technologies to reprogram cell identity. Cell Res, 2013. 23(1): p. 33-48.

30. Stranger, B.E., E.A. Stahl, and T. Raj, Progress and promise of genome-wide association studies for human complex trait genetics. Genetics, 2011. 187(2): p. 367-83.

31. Rau, C.D., A.J. Lusis, and Y. Wang, Genetics of common forms of heart failure: challenges and potential solutions. Curr Opin Cardiol, 2015. 30(3): p. 222-7.

CHAPTER 2

Developmental Heterogeneity of Cardiac Fibroblasts Does Not Predict Pathological Proliferation and Activation

*This chapter is reprinted from Ali et al., Developmental Heterogeneity of Cardiac Fibroblasts Does Not Predict Pathological Proliferation and Activation, Circulation Research, 115(7):625-35. http://circres.ahajournals.org/content/115/7/625.long

Developmental Heterogeneity of Cardiac Fibroblasts Does Not Predict Pathological Proliferation and Activation

Shah R. Ali,* Sara Ranjbarvaziri,* Mahmood Talkhabi, Peng Zhao, Ali Subat, Armin Hojjat, Paniz Kamran, Antonia M.S. Müller, Katharina S. Volz, Zhaoyi Tang, Kristy Red-Horse, Reza Ardehali

Rationale: **Fibrosis is mediated partly by extracellular matrix–depositing fibroblasts in the heart. Although these mesenchymal cells are reported to have multiple embryonic origins, the functional consequence of this heterogeneity is unknown.**

Objective: **We sought to validate a panel of surface markers to prospectively identify cardiac fibroblasts. We elucidated the developmental origins of cardiac fibroblasts and characterized their corresponding phenotypes. We also determined proliferation rates of each developmental subset of fibroblasts after pressure overload injury.**

Methods and Results: **We showed that $Thy1^+CD45^-CD31^-CD11b^-Ter119^-$ cells constitute the majority of cardiac fibroblasts. We characterized these cells using flow cytometry, epifluorescence and confocal microscopy, and transcriptional profiling (using reverse transcription polymerase chain reaction and RNA-seq). We used lineage tracing, transplantation studies, and parabiosis to show that most adult cardiac fibroblasts derive from the epicardium, a minority arises from endothelial cells, and a small fraction from Pax3-expressing cells. We did not detect generation of cardiac fibroblasts by bone marrow or circulating cells. Interestingly, proliferation rates of fibroblast subsets on injury were identical, and the relative abundance of each lineage remained the same after injury. The anatomic distribution of fibroblast lineages also remained unchanged after pressure overload. Furthermore, RNA-seq analysis demonstrated that Tie2-derived and Tbx18-derived fibroblasts within each operation group exhibit similar gene expression profiles.**

Conclusions: **The cellular expansion of cardiac fibroblasts after transaortic constriction surgery was not restricted to any single developmental subset. The parallel proliferation and activation of a heterogeneous population of fibroblasts on pressure overload could suggest that common signaling mechanisms stimulate their pathological response. (*Circ Res*. 2014;115:625-635.)**

Key Words: aging ■ cardiac fibroblasts ■ fibrosis ■ growth and development

Cardiac fibrosis underlies the pathological response of the mammalian heart to certain insults, such as a pressure overload injury, and this process is largely mediated through cardiac fibroblasts. The functions and characteristics of cardiac fibroblasts in scar formation and tissue remodeling are being actively explored.[1] However, the study and analysis of cardiac fibroblasts are limited by imprecise definitions for this cell type and, concomitantly, by lack of specific markers to aid in their identification. Several other interstitial cell types, such as mesenchymal and inflammatory cells, express certain markers commonly used for identifying cardiac fibroblasts. One such example is fibroblast-specific protein 1 that is expressed in both fibroblasts and macrophages in the liver.[2] Therefore, it is imperative to delineate and validate a robust set of markers to isolate cardiac fibroblasts.

Editorial, see p 602
In This Issue, see p 601

It is thought that injury induces the expression of α-smooth muscle actin (α-SMA) in a fraction of cells expressing fibroblast markers leading to their activation. These activated cells, termed myofibroblasts, secrete extracellular matrix to increase collagen content and hence cause histological fibrosis. Accumulating evidence supports the existence of heterogeneity among cardiac fibroblasts.[1] For example, several developmental origins have been suggested for cardiac fibroblasts, such as the bone marrow (BM),[3] embryonic endothelium,[4] circulation,[5] neural crest,[6,7] and epicardium.[8] Nevertheless, it is not known whether certain fibroblast subtypes, on the basis of their developmental origin, have a propensity toward proliferation and activation after

Original received February 21, 2014; revision received July 15, 2014; accepted July 17, 2014. In June 2014, the average time from submission to first decision for all original research papers submitted to *Circulation Research* was 15 days.

From the Departments of Pathology and Developmental Biology, Institute for Stem Cell Biology and Regenerative Medicine, Stanford University School of Medicine, CA (S.R.A.); Department of Internal Medicine, Division of Cardiology, and Broad Stem Cell Research Center, University of California Los Angeles School of Medicine (S.R., M.T., P.Z., A.S., A.H., P.K., Z.T., R.A.); and Division of Blood and Marrow Transplantation, Department of Medicine (A.M. S.M.) and Department of Biology (K.S.V., K.R.-H.), Stanford University, CA.

*These authors contributed equally to this article.

The online-only Data Supplement is available with this article at http://circres.ahajournals.org/lookup/suppl/doi:10.1161/CIRCRESAHA.115.303794/-/DC1.

Correspondence to Reza Ardehali, MD, PhD, Department of Internal Medicine, Division of Cardiology, and Broad Stem Cell Research Center, University of California Los Angeles School of Medicine, Los Angeles, CA 90095. E-mail RArdehali@mednet.ucla.edu

Nonstandard Abbreviations and Acronyms	
α-SMA	α-smooth muscle actin
BM	bone marrow
EMT	epithelial-to-mesenchymal transition
EndMT	endothelial-to-mesenchymal transition
HSC	hematopoietic stem cell
PI	propidium iodide
TAC	transaortic constriction

profibrotic cardiac injuries. Indeed, it remains unclear whether fibroblasts from different lineages exhibit phenotypic or transcriptional disparities. Understanding the developmental origin of cardiac fibroblasts may enable identification of fibroblast subsets that are directly involved in fibrosis and may thus help to develop novel treatment strategies to target fibrosis.

Herein, we define a set of surface markers that distinguish cardiac fibroblasts from other cell types in the heart. We use fate-mapping models, BM transplantation, and parabiosis studies in the setting of physiological aging as well as pressure overload injury to determine the developmental sources of cardiac fibroblasts and to elucidate whether pathological activation of fibroblasts is developmentally determined. We demonstrate that cardiac fibroblasts derive primarily from the epicardium, whereas a smaller fraction originates from the endothelial lineage, and a minority from the neural crest. Our work further shows that circulating, hematopoietic, and stromal cells do not contribute to the cardiac fibroblast pool. Interestingly, we did not observe any differences in proliferation rate among cardiac fibroblasts of different developmental origins after pressure overload injury. Rather, our findings show that fibroblasts from distinct lineages have a similar phenotype and gene expression profile in a given context, such as aging and injury.

Methods

An expanded Materials and Methods is available in the Online Data Supplement.

Mice

$Pax3^{Cre/+}$, $Tie2^{Cre/+}$, $Wt1^{CreERT2/+}$, $Myh11^{Cre/+}$-GFP, $Vav1^{Cre/+}$, CAG-dsRed, and C57Bl/6 mice strains were obtained from the Jackson Laboratory and have been described previously. Tbx18Cre transgenic mice, Myh6-GFP, and $R26R^{mT/mG}$ reporter mice were gifts from Sylvia Evans (San Diego, CA), Deepak Srivastava (San Francisco, CA), and Liqun Luo (Stanford, CA), respectively. All procedures were performed with the approval of the University of California, Los Angeles Animal Research Committee or the Institutional Animal Care and Use Committee at Stanford University. Two operators blinded to the genotype and experimental design performed all animal surgeries.

Isolation of Cardiac Fibroblasts

Mice were injected with heparin and euthanized, then the heart was dissected out and perfused with Hanks' balanced salt solution. The hearts were cut into small pieces and digested with Liberase Blendzyme TH and TM (Roche) in Medium 199 plus DNase I and polaxamer at 37°C for 1 hour. Cells were passed through a 70-μm cell strainer (BD Falcon) and centrifuged. The cell pellet was resuspended in staining buffer (3% fetal bovine serum in Hanks' balanced salt solution) containing the relevant $Thy1^+HE^-$ (HE refers to hematopoietic and endothelial lineages) surface marker antibodies (Online Table I) and incubated in the dark for 30 minutes at room temperature.

Parabiosis

Mice of the same weight, size, and sex were paired ≥2 to 3 weeks before the surgery, after being observed for at least a week to make sure that they were compatible.[9] Mice were anesthetized by isoflurane in O_2. Toe pinch was used as an indicator of the pain response. After shaving the corresponding lateral aspects of each mouse, the site was disinfected using an alcohol swab and povidone/iodine. Matching skin incisions are made from the olecranon to the knee joint of each mouse, and the subcutaneous fascia was bluntly dissected to create ≈0.5 cm of free skin. One partner had the procedure done on the right side and the other on the left. The right olecranon of 1 animal is attached to the left olecranon of the other by a single 4-0 silk suture and tie. The partners' knee joints were similarly connected. The dorsal and ventral skins were then approximated by staples or by continuous suture, and the animals were warmed with heating pads and monitored until recovery. Parabiotic pairs were housed 1 pair per cage and given acidified water (pH 2.5). After 4 weeks of anastomosis, blood samples from each animal in a parabiont pair were analyzed using flow cytometry. Animal pairs with <90% blood chimerism were excluded from our studies. Biological replicates were used, and the experiment was repeated 3 times in the laboratory (n=4–6 per sample; minimum n=3 to observe statistical significance, with more to account for possible animal death).

BM Transplant

C57BL/6 mice (*H2b*, $Thy1.1^+CD45.2^+dsRed^+$) served as donors for hematopoietic stem cells (HSCs), green fluorescent protein (GFP)-expressing or dsRed-expressing C57BL/6 mice (*H2b*; $Thy1.2^+CD45.2^+GFP^+$) were used as donors for nonhematopoietic BM cells for transplantation into C57BL/6 (*H2b*, $Thy1.1^+CD45.2^+$) recipients. Donors were 6 to 12 weeks old, recipients were 8 weeks old at transplant. BM was flushed from tibiae and femora into Hanks' balanced salt solution/2% fetal bovine serum, enriched for c-Kit (3C11) cells by magnetic column separation (CD117 MicroBeads, MACS Separation Columns LS; Miltenyi Biotec, Auburn, CA), and KTLS ($c\text{-}Kit^+$, Thy1.1lo, lineage marker$^-$, $Sca\text{-}1^+$)-HSC were purified by FACS (fluorescence-activated cell sorting)-sorting, selecting for $c\text{-}Kit^+$, $Thy1.2^{lo\text{-}neg}$, $Sca\text{-}1^+$, Lin^- (CD3, CD4, CD5, CD8α, B220, Gr1, Mac1, and Ter119). A total of 1000 FACS-purified HSCs were infused per recipient mouse. For cotransfer of nonhematopoietic cells, BM was flushed from tibiae, femora, and pelvis. Nonhematopoietic cells were extracted by magnetic column depletion of $CD45^+$ cells (CD45 MicroBeads; Miltenyi Biotec). C57BL/6.CD45.2 recipients received a lethal 1050 cGy dose total body γ-irradiation, ≈5 hours before tail-vein injection of a radioprotective dose of 1000 KTLS-HSC. In cotransfer experiments, 5×10^6 $CD45^-$ stromal/nonhematopoietic cells were injected simultaneously with the HSCs. Biological replicates were used, and the experiment was performed 3 times.

Statistical Analysis

Statistical testing was performed with Microsoft Excel version 12.2.8 and GraphPad Prism. Results are presented as mean±SEM and were compared using a 2-tailed Student *t* test or 2-way ANOVA (significance was assigned for $P<0.05$).

Results

$Thy1^+HE^-$ Cells Exhibit a Fibroblast Phenotype In Vitro and In Vivo and Encompass the Majority of Cardiac Fibroblasts

We applied a panel of surface markers to identify cardiac fibroblasts: Thy1 as an inclusive surface protein ($Thy1^+$) given its association with cardiac fibroblasts,[10,11] and exclusion of hematopoietic cells ($CD45^-Ter119^-$), macrophages ($CD11b^-$),[2] and endothelial cells ($CD31^-$). In accordance with the reported proportion of cardiac fibroblasts in mice,[12] this combination (hereafter called $Thy1^+HE^-$) marked ≈30% of the cells in adult mouse hearts (Figure 1A). Using cardiomyocyte-specific and smooth muscle reporter transgenic mice, we show that cardiomyocytes and vascular smooth muscle cells are excluded from the $Thy1^+HE^-$ population (Online Figure IA and IB). In comparison with age-matched whole heart controls, $Thy1^+HE^-$ cells exhibit markedly elevated expression of fibroblast- and

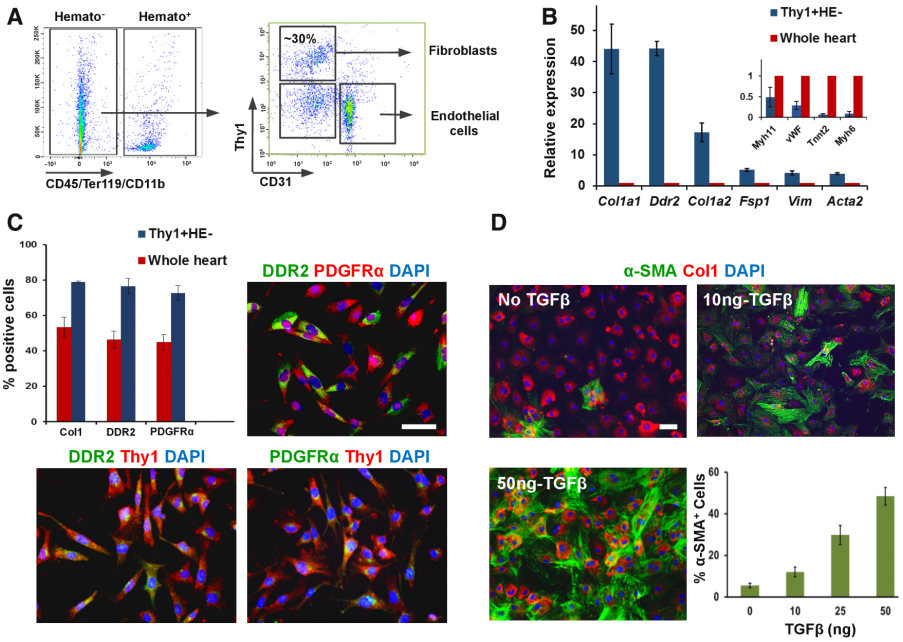

Figure 1. Characterization of Thy1⁺HE⁻cells. A, After gating for cells on forward and side scatter axes, and excluding doublets, cells that were negative for CD45, Ter119, CD11b, and CD31 could be divided into Thy1⁺ and Thy1⁻ populations. Of these 2 fractions, the Thy1⁺ cells were designated as fibroblasts and selected for analysis in all experiments. **B**, Relative gene expression in Thy1⁺HE⁻ cells from 8-week-old mice with reference to age-matched whole heart controls for fibroblast- and nonfibroblast-associated genes (inset; using *GAPDH* as reference gene; n=3 mice). **C**, Thy1⁺HE⁻ cells highly express the fibroblast markers collagen I (Col1), platelet-derived growth factor receptor α (PDGFRα), and discoidin domain-containing receptor 2 (DDR2) in comparison with the whole heart by flow cytometry. Sorted cells retain a mesenchymal morphology and maintain expression of these proteins after 3 passages. **D**, Exposure to transforming growth factor (TGF)-β1 induces expression of α-smooth muscle actin (α-SMA) in cultured Thy1⁺HE⁻ cells in a dose-dependent manner (scale bar, 50 μm). All error bars represent SEM. DAPI indicates 4′,6-diamidino-2-phenylindole.

extracellular matrix (ECM)-associated genes (Figure 1B), whereas cardiomyocyte and vascular cell–related genes are expressed at low levels (Figure 1B, inset). Because individual fibroblast markers may be found on multiple cell types, we hypothesized that individual fibroblasts may not express every fibroblast-associated marker. We quantified the fraction of Thy1⁺HE⁻ cells from whole hearts coexpressing known fibroblast markers using flow cytometry, and we demonstrate an enriched expression of collagen I (Col1), discoidin domain-containing receptor 2 (DDR2), and platelet-derived growth factor receptor α (PDGFRα) in the Thy1⁺HE⁻ population compared with the whole heart control (Figure 1C). In addition, immunostaining of Thy1⁺HE⁻ cells isolated from freshly digested hearts showed robust expression of DDR2 and PDGFRα (Online Figure IC). Notably, expression of α-SMA or CD146 (markers associated with smooth muscle cells and

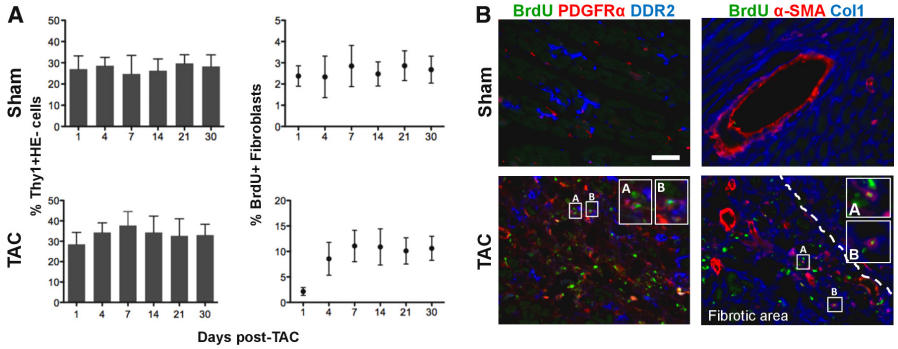

Figure 2. Proliferation of cardiac fibroblasts after pressure overload injury. A, The percent of Thy1⁺HE⁻ cells undergoes a small, nonsignificant increase upon transaortic constriction (TAC) injury, but plateaus after 7 days post injury. Similarly, the percentage of bromodeoxyuridine (BrdU⁺) fibroblasts increases from a baseline of 2% to 10% at 7 days after TAC, then remains constant through 30 days post TAC (n=4 mice per group). **B**, Immunohistochemistry of heart sections in **A** shows colocalization of BrdU with cells expressing fibroblast and myofibroblast markers in TAC (**bottom**) compared with sham sections (**top**; scale bar, 50 μm). All error bars represent SEM.

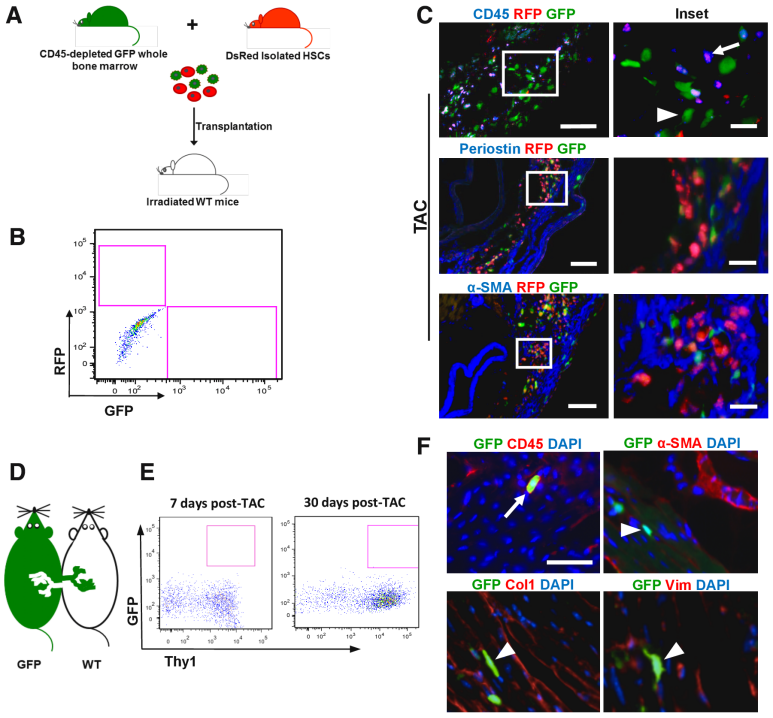

Figure 3. Hematopoietic, bone marrow stromal, and circulating cells do not generate cardiac fibroblasts. A, Schematic depicts the model of bone marrow transplantation in which red fluorescent protein (RFP⁺) hematopoietic stem cells (HSCs) and CD45-GFP⁺ (green fluorescent protein) bone marrow (BM) stromal cells were intravenously delivered in a host mouse after myeloablation. **B**, GFP⁺ and RFP⁺ cells are not present in the Thy1⁺HE⁻ fraction 30 days after transaortic constriction (TAC) or sham in BM-recipient mice (n=4). **C**, Immunohistochemistry (IHC) shows that RFP⁺ cells stain primarily with CD45. Representative TAC sections were stained with Periostin and α-smooth muscle actin (α-SMA) from the fibrotic areas in the subepicardium of the free ventricle wall. **D**, Schematic demonstrates surgical anastomosis of unlabeled and GFP-labeled adult female mice to achieve parabiosis. **E**, Thy1⁺HE⁻ sorted cells from wild-type (WT) mouse hearts 7 and 30 days after parabiosis do not express GFP (n=4). **F**, IHC staining for CD45, collagen I (Col1), α-SMA and Vimentin (Vim; arrows indicate cells that costain for the marker of interest, and arrowheads indicate cells that do not costain with the marker). Scale bar, 50 μm for merged panel and 12.5 μm for the inset. DAPI indicates 4′,6-diamidino-2-phenylindole.

pericytes, respectively) was rarely detected in the Thy1⁺HE⁻ cells (Online Figure IC). Sorted Thy1⁺HE⁻ cells were cultured in vitro for several passages (Online Figure ID), and they retained expression of fibroblast-associated ECM and structural proteins. Cultured cells also expressed the fibroblast markers Thy1, DDR2, and PDGFRα (Figure 1C), further demonstrating the fibroblast phenotype of Thy1⁺HE⁻ cells (fibroblast-specific protein 1 marked a heterogeneous population of cells, including some hematopoietic cells. We therefore restricted our analysis to the aforementioned fibroblast-associated markers).

In culture, treatment of Thy1⁺HE⁻ cells with transforming growth factor-β1 resulted in upregulation of α-SMA in a dose-dependent manner (Figure 1D).[13] Furthermore, RNA-seq of Thy1⁺HE⁻ cells isolated 7 days after transaortic constriction (TAC) or sham operation revealed an increased expression of ECM and ECM regulatory genes, activated fibroblast genes, and cell cycle genes in the TAC relative to sham specimens (Online Figure IE, IF, and IG), as would be predicted following fibrosis.[14] This provides additional validation for the use of the Thy1⁺HE⁻ panel of markers to isolate cardiac fibroblasts.

To determine whether the Thy1⁺HE⁻ population encompasses all cardiac fibroblasts, we isolated Thy1⁻HE⁻ cells from adult wild-type (WT) mouse hearts and examined the expression of the fibroblast-associated markers DDR2 and PDGFRα. We observed rare cells that costained for both markers, suggestive of a fibroblast phenotype (Online Figure IH). Further fractionation revealed the Thy1⁻HE⁻ cells to include CD146⁺ cells (pericyte-associated marker) and CD105⁺ cells (mesenchymal stem cell marker), which stained for DDR2 and PDGFRα (Online Figure II). However, the absolute number of such cells was orders of magnitude lower than the Thy1⁺HE⁻ population. These data demonstrate that few cardiac fibroblasts are excluded from the Thy1⁺HE⁻ population.

Cell Proliferation and Programmed Cell Death After TAC Injury

Next, we sought to determine whether increased fibrosis on pressure overload TAC injury occurs through fibroblast proliferation as opposed to an increase in ECM production from a fixed number of fibroblasts (Online Figure IIA and IIB). Adult mice (8 weeks old) underwent TAC or sham operation and were analyzed. Masson's trichrome staining of the respective tissue revealed sparse global fibrosis at 4 days after injury that increased by day 7 and persisted at 2 weeks (Online Figure IIC) in the TAC hearts. Using flow cytometry, we observed an increase in the number of Thy1⁺HE⁻ cells as well as an increase in the fraction of Thy1⁺HE⁻ cells on TAC injury relative to sham (Figure 2A; Online Figure IID). In accordance, ≈10% of the Thy1⁺HE⁻ cells derived from the operated mice were bromodeoxyuridine (BrdU⁺) at 7 days after TAC and remained at this level at 4 weeks, compared with 2% in the sham mice (P=0.008; n=3 mice/group/time point; Figure 2A). Immunohistochemistry of TAC specimens showed BrdU⁺ cells that costained with the fibroblast markers DDR2 and PDGFRα. BrdU⁺ cells also costained with α-SMA and Col1 (Figure 2B). Together, these data suggest that fibroblast proliferation in response to TAC occurs primarily during the first week after injury.

To determine whether apoptosis of fibroblasts occurs after TAC injury, we analyzed for Annexin V and propidium iodide (PI) expression on Thy1⁺HE⁻ cells from WT mice at 1, 4, 7, and 14 days after injury. We observed a significant increase in fibroblasts undergoing late apoptosis (defined by Annexin V⁺PI⁺

staining) 4 days post TAC (Online Figure IIE) compared with sham. At all other time points, the extent of apoptosis was equivocal between the 2 surgical groups (Online Figure IIE). It is possible, however, that nonapoptotic pathways (necrosis, elimination by the reticulo-endothelial system, etc) also lead to clearance of fibroblasts. We therefore examined for the presence of necrotic cells among the Thy1^{+}HE^{-} fibroblasts by analyzing the uptake of PI. We observed rare necrosis of fibroblasts at the time points studied (7 and 14 days after sham and TAC), with no significant increase in necrosis in the TAC relative to the sham fibroblasts (Online Figure IIF). These data further support that the first week after pressure overload injury is the most dynamic period with respect to cell turnover. Fibroblast apoptosis peaks during this time but is counteracted by a more robust generation of new fibroblasts. The time course of these cellular changes suggests a discrete temporal period for potential therapeutic interventions.

BM and Circulating Cells Do Not Generate Cardiac Fibroblasts During Development, Aging, or After Pressure Overload Injury

Hematopoietic cells have been reported to contribute to the formation of scar tissue after cardiac injury.[5] To rigorously test this hypothesis, we transplanted GFP-labeled whole BM cells or red fluorescent protein (RFP)-labeled HSCs along with CD45-depleted GFP-labeled BM stromal cells into adult mice after myeloablation.[15] Eight weeks after engraftment, TAC and sham operations were performed (Figure 3A). We observed labeled cells grossly in both surgical groups[16] (Online Figure IIIA). However, there were no GFP^{+} nor RFP^{+} cells in the Thy1^{+}HE^{-} population 30 days after TAC and sham surgery in either transplant model (Figure 3B). Moreover, HSC-derived RFP^{+} cells expressed the hematopoietic marker CD45 rather than fibroblast markers (Figure 3C).

To further confirm whether circulating cells can be a cell of origin for cardiac fibroblasts, we surgically paired WT and GFP-labeled female mice to achieve parabiosis (Figure 3D). Blood chimerism was obtained by 4 weeks after anastomosis (Online Figure IIIB and IIIC) and GFP^{+} cells were observed in the hearts of both mice. To determine whether pressure overload injury facilitates fibroblast or fibroblast-like cell generation by circulating cells, we performed TAC injury on the WT mouse of WT-GFP parabiont pairs 4 weeks after surgical anastomosis. Heart/body weight ratio demonstrated cardiac hypertrophy after TAC injury (Online Figure IIID). Flow cytometric analysis (Figure 3E) and immunohistochemistry (Figure 3F; Online Figure IIIE) at 7 and 30 days after injury did not reveal any GFP^{+} circulating cells expressing the Thy1^{+}HE^{-} set of markers; instead, the hematopoietic marker CD45 could be detected in GFP^{+} cells (Figure 3F).

Analysis of the BM transplantation and parabiosis models excludes a hematopoietic or BM stromal contribution to cardiac fibrosis during pressure overload injury. However, a potential developmental contribution of hematopoietic progenitors or lineages to cardiac fibroblasts cannot be excluded; such a phenomenon could reconcile the transplantation data with previous studies.[17] To examine whether cardiac fibroblasts have an embryonic hematopoietic origin, we generated Vav$^{Cre/+}$;R26R$^{mT/mG}$ mice, in which GFP labels hematopoietic progenitors and their progeny (Online Figure IIIF).[18] We did not observe any GFP expression in the Thy1^{+}HE^{-} cell compartment (Online Figure IIIG). Collectively, these distinct models exclude a hematopoietic, BM stromal, or circulating cell origin for cardiac fibroblasts during development, physiological aging, or on pressure overload.[19]

Endothelial-Derived Cells Generate Cardiac Fibroblasts

It has been reported that endothelial-to-mesenchymal transition (EndMT) contributes to cardiac fibrosis on TAC injury.[4] Whether EndMT, which is known to occur during development to generate heart valves,[20] also contributes to cardiac fibroblasts during aging and injury remains unclear. We generated Tie2$^{Cre/+}$;R26R$^{mT/mG}$ mice, in which Tie2-derived progeny is indelibly labeled with GFP (Figure 4A). At 7 and 30 days after sham and TAC operations, ≈20% of Thy1^{+}HE^{-} cells were GFP^{+} in both groups (P=0.35; n=5 mice/TAC/time point and n=3 mice/sham/time point; Figure 4B). Therefore, the relative proportion of endothelial-derived fibroblasts remains the same despite proliferation after pressure overload, suggesting that fibroblast division on injury is not restricted to the EndMT-derived fibroblast subset.

Immunohistochemistry demonstrated that GFP^{+} cells expressed DDR2 and PDGFRα, as well as Col1 and Vim, in both sham and TAC hearts (Figure 4C; Online Figure IVA and IVB). Tie2-derived fibroblasts were found in association with most blood vessels, whereas no single vascular territory exhibited a disproportionate number of GFP^{+} fibroblasts. Some GFP^{+} cells, predominantly in the fibrotic areas of TAC hearts, co-localized with α-SMA expression, demonstrating the capacity of this lineage to express myofibroblast markers (Figure 4C).

Pax3-Derived Cells Contribute to Cardiac Fibroblasts

The neural crest is a migratory population of cells that originates from the dorsal aspect of the neural tube. Neural crest–derived lineages have been fate-mapped using the Pax3Cre transgenic model[21] and the cardiac neural crest has been postulated to contribute to the cardiac mesenchyme.[22] Thy1^{+}HE^{-} fibroblasts from WT hearts after sham and TAC operations did not express Pax3, as evidenced by RNA-seq analysis (data not shown). We therefore generated Pax3$^{Cre/+}$;R26R$^{mT/mG}$ mice to ascertain the cardiac contribution of neural crest cells (Figure 5A). We observed many GFP^{+} cells in the outflow tract, consistent with the previously described contribution of neural crest cells (Figure 5B).[22]

The fraction of Thy1^{+}HE^{-} cells that were GFP^{+} remained ≈5% in both TAC and sham groups at 7 and 30 days post injury (Figure 5C; P=0.4; n=5/TAC/time point and n=3/sham/time point). Most GFP^{+} cells expressed the neural markers, Smi32 and NF160, on immunohistochemistry (Online Figure VA). However, we also observed rare, scattered GFP^{+} cells in the atria and ventricles that stained with Col1 and Vim (Figure 5D). We did not detect expression of Pax3 in the GFP^{+} cells at both the mRNA (data not shown) and protein levels in adult hearts (Online Figure VB), which argues against ectopic expression of Pax3 in cardiac fibroblasts. However, we cannot exclude transient Pax3 expression in cardiac fibroblasts during development. These data support a limited contribution of Pax3-expressing neural crest cells to cardiac fibroblasts, which warrants further inquiry.

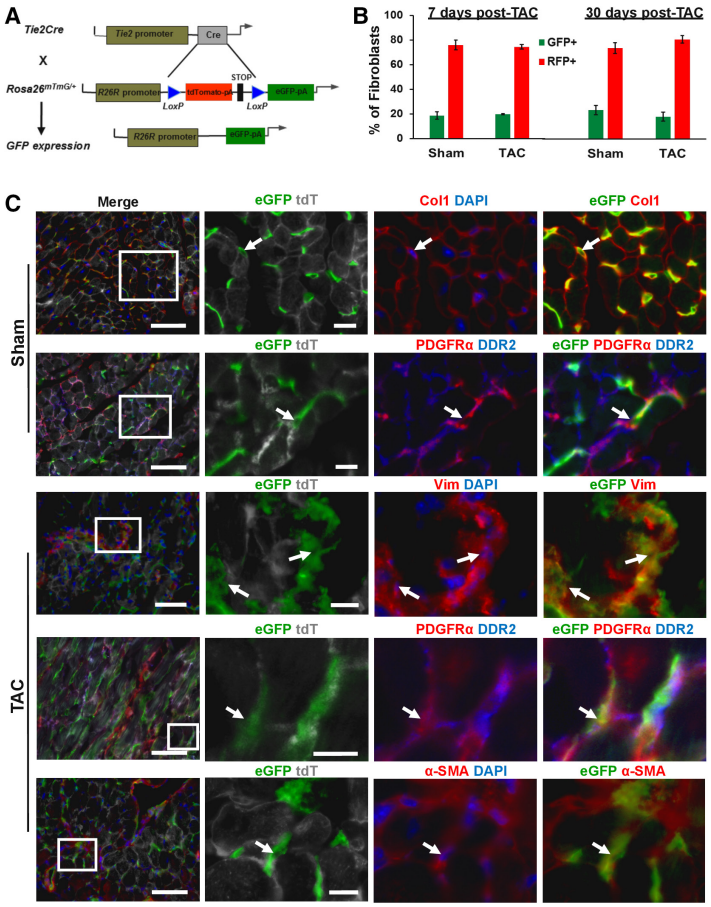

Figure 4. Lineage tracing of Tie2Cre$^{mT/mG}$ model during aging and injury demonstrates endothelial-derived fibroblasts. A, Gene construct of Tie2Cre$^{mT/mG}$ mice. **B**, Proportion of GFP$^+$ (green fluorescent protein) and red fluorescent protein (RFP$^+$) cells in sham and transaortic constriction (TAC) hearts at 7 and 30 days after operation (P>0.05; n=6 mice/TAC/time point and n=4 mice/sham/time point, 2-tailed t test with P>0.05). **C**, Immunohistochemistry of TAC and sham sections with collagen I (Col1; red), platelet-derived growth factor receptor α (PDGFRα; red), Vimentin (Vim; red), α-smooth muscle actin (α-SMA; red), and discoidin domain-containing receptor 2 (DDR2; blue; arrows indicate GFP$^+$ cell that costain for the respective markers). Scale bar, 50 μm for merged panel and 12.5 μm for the inset. All error bars represent SEM. DAPI indicates 4′,6-diamidino-2-phenylindole.

Epicardial Cells Form Cardiac Fibroblasts During Development But Not After Pressure Overload Injury

It has been reported widely that cardiac fibroblasts may be derived from the epicardium,[23] which forms from the migrating cells of the transient proepicardium after E9.5 in mice.[24] We generated Tbx18$^{Cre/+}$;R26R$^{mT/mG}$ mice (Figure 6A) to determine whether epicardium-derived fibroblasts preferentially proliferate in response to pressure overload injury.[25] The GFP$^+$ cells in the Thy1$^+$HE$^-$ population remained at ≈75% in both sham and TAC groups at 7 and 30 days post injury (P=0.35; n=5 mice/TAC/time point and n=3 mice/sham/time point; Figure 6B). We observed dispersed

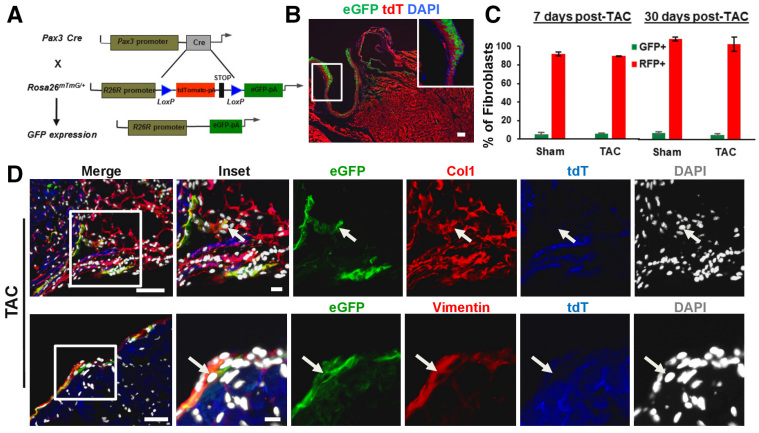

Figure 5. Pax3-derived cells can become cardiac fibroblasts. A, Schematic of the Pax3Cre$^{mT/mG}$ model. **B**, GFP$^+$ (green fluorescent protein) cells in the outflow tract demonstrate neural crest contribution to the large vessels. **C**, The percentage of GFP$^+$ fibroblasts in sham and transaortic constriction (TAC) hearts 7 and 30 days after operation (n=3 each). **D**, Immunohistochemistry of TAC sections with collagen I (Col1) and Vimentin (red; arrows indicate positive cell for the stained marker). Scale bar, 50 μm for merged panel and 12.5 μm for the inset. All error bars represent SEM. DAPI indicates 4′,6-diamidino-2-phenylindole; and tdT, tdTomato.

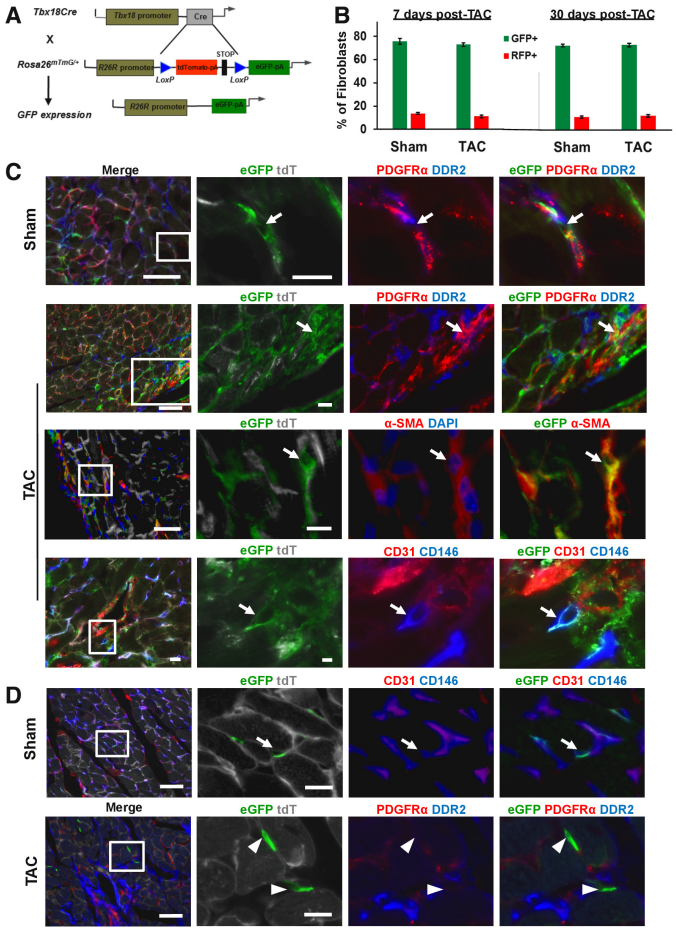

Figure 6. The majority of cardiac fibroblasts are derived from epicardium during aging and after pressure overload injury. A, Schematic showing recombination in the Tbx18Cre$^{mT/mG}$ model. **B**, Flow cytometry analysis indicates the percentage of Thy1$^+$HE$^-$ cells derived from Tbx18-expressing cells in sham and transaortic constriction (TAC) hearts both 7 and 30 days after surgery (n=6 mice/TAC/time point and n=4 mice/sham/time point; 2-tailed *t* test *P*>0.05). **C**, Costaining of sham and TAC sections with platelet-derived growth factor receptor α (PDGFRα; red) and discoidin domain-containing receptor 2 (DDR2; blue). Representative TAC sections were also stained with α-smooth muscle actin (α-SMA), endothelial (CD31), and pericyte-associated (CD146) markers. **D**, After tamoxifen induction in Wt1CreER$^{mT/mG}$ mice, immunohistochemistry on sham and TAC hearts was performed with PDGFRα (red) and DDR2 (blue; n=4 mice/surgical group). Sections were also stained with CD31 and CD146 (arrows indicate cells that costain and arrowheads indicate cells that do not costain for the respective markers). Scale bar, 50 μm for merged panel and 12.5 μm for the inset. All error bars represent SEM. tdT indicates tdTomato.

GFP$^+$ cells that costained with Vim, DDR2, PDGFRα, and Col1 in sham and TAC heart sections (Figure 6C; Online Figures VIA, VIIA, and VIIB). We also observed GFP-labeled cells whose phenotype (CD146$^+$CD31$^-$) and anatomic location (intimate proximity to CD31$^+$ endothelial cells of small capillaries) is characteristic of pericytes (Figure 6C). In the TAC hearts we also observed a significant amount of GFP$^+$ cells remote from the vasculature (ie, not associated with blood vessels) that costained with α-SMA. Moreover, the majority of epithelial-to-mesenchymal transition (EMT)–derived fibroblasts were observed throughout the interstitium of left and right ventricular free walls.

To determine whether there is reactivation of the epicardium and subsequent EMT on pressure overload injury, we administered tamoxifen to adult Wt1$^{CreERT2/+}$;R26R$^{mT/mG}$ mice[26] before a sham or TAC operation, followed by tamoxifen delivery during the week after surgery (Online Figure VIB and VIC). On analysis 1 week after the sham operation, we observed rare epicardial and myocardial GFP expression, which did not colocalize with expression of fibroblast markers (Figure 6D; Online Figure VIE). Notably, 1 week after the operation, we observed a 5-fold increase in the abundance of GFP$^+$ cells in both the epicardium and the myocardium of TAC when compared with that in sham hearts (Online Figure VID). As in the sham model, these cells did not express fibroblast markers or α-SMA: many were CD146$^+$CD31$^+$ (endothelial markers) and a smaller fraction were CD146$^+$CD31$^-$ (pericyte markers; Figure 6D), suggesting that in contrast to the effects of ischemic injury,[27] Wt1-expressing cells may not generate fibroblasts in adulthood or on pressure overload injury. These data therefore argue against EMT as the signaling mechanism that underlies proliferation in the epicardial-derived fraction of fibroblasts after injury. On the contrary, the observed pattern of costaining suggests the following explanations: (1) endogenous endothelial expression of WT1 is induced after injury, (2) expression of WT1 in pericytes, and (3) potential generation of pericytes from the epicardium in adulthood and after injury (the expression of Wt1 in endothelial cells has been reported previously).[27]

Characterization of Pax3-, Tie2-, and Tbx18-Derived Fibroblasts In Vitro and In Vivo

To compare the phenotypic characteristics and gene expression profiles of fibroblasts from different developmental sources, we isolated GFP$^+$ Thy1$^+$HE$^-$ cells from each of the 3 Cre models and expanded them in culture. All fibroblast subsets exhibited a spindle-like morphology characteristic of mesenchymal cells and expressed Col1 (Figure 7A). On addition of transforming

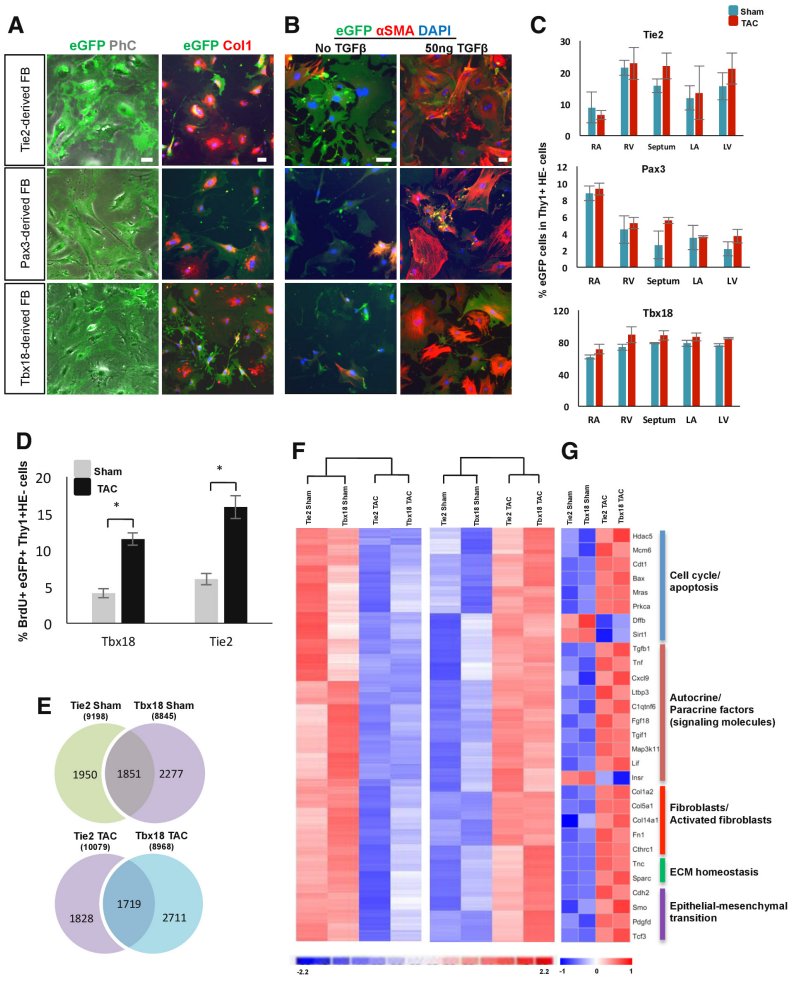

Figure 7. Characterization of Pax3-, Tie2-, and Tbx18-derived cardiac fibroblasts during aging and after pressure overload injury. **A**, Sorted eGFP$^+$Thy1$^+$HE$^-$ cells from each lineage exhibit a similar morphology in culture; all traced fibroblasts highly express the fibroblast-associated marker collagen I (Col1). **B**, All 3 lineage-traced fibroblast subsets express α-smooth muscle actin (α-SMA) after exposure to transforming growth factor (TGF)-β1. **C**, The majority of Tie2-derived fibroblasts are located in the ventricles and septum, compared with Pax3-derived fibroblasts that are primarily found in the right atrium. Tbx18-derived fibroblasts are evenly distributed among the different chambers. **D**, The percentage of bromodeoxyuridine (BrdU$^+$) cells in Tbx18-derived and Tie2-derived fibroblasts increases to a similar extent 7 days after sham and transaortic constriction (TAC). **E**, Venn diagram showing the overlap and discrepancies between genes expressed (reads per kilobase of exon model per million mapped reads [RPKM], ≥11) in the sham and TAC. There is extensive overlap of genes expressed in the Tbx18$^-$ and Tie2-derived fibroblasts in each operation (sham or TAC), respectively (numbers in parentheses indicate the total number of genes expressed in each sample [RPKM >0]). **F,** Selected heat map of RNA-seq data shows differentially expressed genes (using hierarchical clustering) between the 2 lineage-tracing models in sham and TAC mice. Individual genes are up- and downregulated similarly in the sham groups in both Cre models. The gene profile was significantly altered after TAC in a similar way for both Cre models. **G**, Heat map showing fibroblast and fibrosis-related gene expression with expression fold change >1.5 after TAC operation. Scale bar, 50 μm. All error bars represent SEM. DAPI indicates 4′,6-diamidino-2-phenylindole; FB, fibroblast; LA, left atrium; LV, left ventricle; RA, right atrium; and RV, right ventricle.

growth factor-β1 to the culture medium, fibroblasts from all subsets expressed the activated fibroblast marker, α-SMA (Figure 7B). In vitro BrdU uptake assays showed that the relative proliferation rate (based on BrdU optical density) is similar among all 3 developmental subsets at individual time points after BrdU exposure, and this rate increases in parallel in all subsets over time (Online Figure VIIIA).

We next studied the anatomic distribution of each fibroblast subset in sham and TAC hearts 7 days after injury (Figure 7C; Online Figure VIIIB): Tbx18-derived fibroblasts seemed evenly distributed throughout all cardiac chambers, whereas Tie2-derived fibroblasts exhibited a trend toward preferential localization in the ventricles and septum. The majority of Pax3-derived fibroblasts were localized in the right atrium. Interestingly, the relative abundance of each subset with respect to individual chambers did not change on TAC injury.

To directly measure the in vivo proliferative capacity of the fibroblast subsets on TAC injury, we administered BrdU to Tbx18$^{Cre/+}$;R26R$^{mT/mG}$ and Tie2$^{Cre/+}$;R26R$^{mT/mG}$ mice starting at the time of surgery until analysis 7 days later (Figure 7D). The

fraction of BrdU$^+$ fibroblasts in the sham group was similar between the 2 models (≈5% for Tbx18 versus ≈6% for Tie2; P=0.13; n=3 mice/group) and significantly increased after TAC injury (≈13% for Tbx18, ≈15% for Tie2; P=0.07; n=3 mice/group). Similar percentages of BrdU$^+$ fibroblasts were observed in WT hearts (Figure 2A). These data directly confirm that on pressure overload injury, there is a balanced proliferation in each developmental subset of fibroblasts. Collectively, these findings suggest that the developmental origin affects the anatomic distribution of cardiac fibroblasts but does not result in phenotypic differences with respect to the expression of fibroblast-associated genes, the propensity toward activation in response to appropriate stimuli, or their proliferation rate.

Tbx18- and Tie2-Derived Fibroblasts Have Similar Transcriptional Profiles Upon Pressure Overload Injury

In an effort to determine phenotypic similarities among the different fibroblast developmental subsets, we performed RNA-seq of Tie2-derived and Tbx18-derived fibroblasts isolated 7 days post TAC or sham operation. To quantify and compare the gene expression level within and between the sham and TAC groups (ie, Tie2-derived and Tbx18-derived fibroblasts), we calculated and normalized the expression level of the genes through reads per kilobase of exon model per million mapped reads as described previously.[28] The total number of expressed genes (reads per kilobase of exon model per million mapped reads, ≥1) in Tie2 sham and Tbx18 sham was 9198 and 8845, respectively (Figure 7E). Among them, 1950 genes in Tie2 sham and 2277 genes in Tbx18 sham showed a high level of expression (reads per kilobase of exon model per million mapped reads, ≥11), with 1851 common genes between these 2 groups (Figure 7F). Of 10079 genes expressed in Tie2 TAC, 1828 genes showed a high level of expression, whereas 2711 genes of 8968 genes expressed in Tbx18 TAC were highly expressed (Figure 7F). Among the common genes expressed in sham and TAC fibroblasts were fibroblast- and fibrosis-related markers, whose expression increased after TAC operation (Figure 7G; Online Table III). For example, fibroblast-related genes, such as Col1a1, Col1a2, Postn, Thy1, and DDR2, were expressed at approximately the same level between Tie2 sham and Tbx18 sham fibroblasts; expression of these genes increased in the respective TAC fibroblasts. ECM homeostasis-related genes showed a dynamic variation between sham and TAC fibroblasts: Sparc, Timp1, Mmp14, and Mmp2 showed upregulation in TAC compared with sham fibroblasts, whereas Timp2 and Mmp2 expression levels did not show a significant change (Online Table III). Upregulation of transforming growth factor, tumor necrosis factor, LIF (leukemia inhibitory factor) signaling components on TAC injury suggests a role for these factors during and after pressure overload injury and cardiac hypertrophy. These data further attest that developmentally distinct fibroblasts have parallel gene expression patterns that change similarly in response to pressure overload injury, providing evidence for comparable phenotypes.

Discussion

The lack of cardiac fibroblast–specific markers has made it challenging to investigate the lineage origin of these cells and their response to injury. The previously reported markers are either not specific for fibroblasts because they are expressed by other interstitial cells or they only mark a subpopulation of fibroblasts. Here, we identified a panel of surface markers (Thy1$^+$HE$^-$) and validated its use for prospective identification of cardiac fibroblasts using several approaches: (1) immunohistochemical and flow cytometric analysis using a combination of fibroblast markers in the context of their anatomic location, (2) global- and fibroblast-specific gene expression analysis, (3) in vivo proliferation in response to injury, and (4) in vitro characterization. This set of core surface markers may form the basis for further refinement and fractionation of cardiac fibroblasts to delineate phenotypically or pathologically distinct fibroblast subsets in future studies.

We used several experimental tools to demonstrate that the progeny of BM and circulating cells can migrate to the heart, especially in the context of injury,[16] but they do not adopt a fibroblast phenotype. Use of the Thy1$^+$HE$^-$ markers may exclude fibrocytes, which are putative circulating hematopoietic-derived cells that participate in the process of fibrosis and scar formation in the heart after injury.[29] However, given previous reports of inflammatory cells that express fibroblast markers but do not deposit ECM (and thus phenotypically are not fibroblasts), better characterization of this cell population is needed, especially given the results from our BM transplantation, parabiosis, and the lineage-tracing hematopoietic models described above.[2] Moreover, a recent study demonstrated the near-complete absence of hematopoietic-associated genes (eg, CD45, CD34) in cardiac fibroblasts.[30] However, it is possible that pressure overload injury may not be the ideal injury model to study the possible recruitment of circulating progenitors to the heart (to generate fibroblasts), perhaps, because of a less severe inflammatory response as compared with other injury models.

Although it has been shown previously that epicardial cells generate cardiac fibroblasts, our work demonstrates that although EMT is an important developmental process, its induction after injury does not generate fibroblasts (unlike during development). We found rare cells staining for epicardial markers after TAC injury dispersed throughout the myocardium rather than localized to the fibrotic regions, but this likely represents ectopic expression by interstitial and endothelial cells as these cells did not coexpress fibroblast markers. It is possible, however, that epicardial cells undergo EMT on injury and generate mesenchymal cells that are confined to the subepicardial location without migration to the area of fibrosis. It is technically possible that inefficient recombination in the used inducible system or the short time course before analysis may have led to underrepresentation of fibroblasts being generated from EMT in the Wt1-CreERT2 model (although we show that proliferation peaks by 1 week post injury).

Our data corroborate some of the findings of Zeisberg et al[4] in identifying endothelial-derived fibroblasts as a subset of cardiac fibroblasts but differs in the absence of evidence for active EndMT on TAC injury. We show that the relative proportion of endothelial-derived fibroblasts remains the same after injury in the setting of a global increase in fibroblasts. By itself, this finding could certainly be explained by EndMT occurring after pressure overload, as this could lead to increased labeling using the Tie2Cre model. However, based on the data obtained with the Tbx18Cre and Pax3Cre models, as well as the fact that the percentage of endothelial-derived fibroblasts remains the same post injury, it can be inferred that proliferation of existing fibroblasts, rather than

EndMT, is the primary response to pressure overload. The differences between the 2 studies could be explained by the use of different transgenic fate-mapping mouse models. In our study, we used the Tie2Cre rather than the Tie1Cre model. Developmental studies have demonstrated that the Tie1 promoter drives gene expression in endothelial cells from embryonic day E10 until birth as well as in a small fraction of hematopoietic cells (≈12%–20% of the adult erythroid, myeloid, and lymphoid cells).[31] Although the expression pattern is similar to Tie1Cre mice, Tie2 expression starts as early as embryonic day E8.5, hence making it potentially a more suitable mouse model to lineage trace a greater proportion of endothelial cells.[32] Moreover, experimental differences such as the length of time from injury to analysis as well as the use of fibroblast-specific protein 1 and α-SMA as markers for the identification of cardiac fibroblasts[4] could explain the discrepancies observed between the 2 studies. Fibroblast-specific protein 1 marks the myeloid lineage in addition to fibroblasts,[33] which may confound interpretation of fibroblast lineage studies given the abundance of BM-derived cells after TAC injury.

Recently, a comprehensive study by Moore-Morris et al[34] was published that corroborates our findings herein using a collagen1a1-GFP reporter mouse, which could identify cardiac fibroblasts based on the expression of GFP. Although they used an alternate method for labeling cardiac fibroblasts, they used similar genetic models (Tbx18Cre, Wt1Cre, Wt1CreER, Tie2Cre, and others) and sought to clarify the embryonic lineages that generate fibroblasts in the heart. In line with our data, they showed that the epicardial and endothelial lineages are the primary contributors (ie, no apparent contribution from hematopoietic cells). On aortic banding injury of adult mice, moreover, they did not observe reactivation of EMT or EndMT; furthermore, fibroblasts of epicardial and endothelial origins had similar gene expression patterns in the setting of aortic banding. Therefore, the independent report by Moore-Morris et al that takes advantage of a unique transgenic reporter model for cardiac fibroblasts validates the findings in this study.

In spite of their developmental heterogeneity, fibroblasts from disparate subsets proliferate at a parallel rate on TAC. The developmental programs that generate fibroblasts in utero do not seem to mediate proliferation after injury, as confirmed by Moore et al. These data suggest that ontogeny does not determine the pathological proliferation of cardiac fibroblasts elicited by pressure overload. It is more likely that a shared mechanism stimulates division of embryonically distinct fibroblast subsets. Moreover, the data derived from the RNA-seq studies could lead to a precise understanding of the signaling pathways that regulate each developmental subset and the entire fibroblast population in response to injury.

Prospective isolation of cardiac fibroblasts using our panel of surface markers may facilitate future studies to characterize signaling pathways that regulate the response of this pathologically important cell type to injury and especially to determine the molecular mechanisms that drive proliferation on injury. Identification of such mechanisms would be therapeutically relevant, as inhibiting fibroblast proliferation may prevent deposition of scar tissue and, thereby, minimize fibrosis.[35,36]

Acknowledgments

We acknowledge Konstantina-Ioanna Sereti for critical reading of the article and Dr Matt Schibler for assistance with confocal images. We would also like to acknowledge Dr Xinmin Li and Jian Zhou of the University of California, Los Angeles (UCLA) Clinical Microarray Core with their assistance in RNA sequencing. Flow Cytometry experiments were performed in UCLA Broad Stem Cell Research Center Flow Cytometry Core Resource. S.R. Ali, S. Ranjbarvaziri, and R. Ardehali conceived the project and designed the experiments. S.R. Ali, S. Ranjbarvaziri performed the majority of the experiments and analyzed data from all experiments with R. Ardehali. Figures were prepared by S.R. Ali, S. Ranjbarvaziri, and M. Talkhabi. M. Talkhabi, P. Kamran, and Z. Tang assisted with immunohistochemistry, A. Subat assisted with experimental breeding, and A. Hojjat assisted with RNA-seq experiments. K.S. Volz performed the BrdU experiments. P. Zhao performed the surgeries. A.M.S. Müller performed bone marrow transplantation. K. Red-Horse provided Tbx18Cre/+;R26RmT/mG mice. S.R. Ali, S. Ranjbarvaziri, and R. Ardehali wrote the article.

Sources of Funding

This work was supported in part by a grant from the California Institute of Regenerative Medicine (RC1-00354-1; to R. Ardehali) and from the American Heart Association (AHA-BGA 12BGIA8960008; to R. Ardehali). S.R. Ali was supported by the Howard Hughes Medical Institute Medical Research Fellowship, Stanford Medical Scholars Program, Paul and Daisy Soros Fellowship, and AHA Student Scholarship in Cardiovascular Disease. Confocal laser scanning microscopy was performed at the California NanoSystems Institute Advanced light microscopy/Spectroscopy Shared Resource Facility at UCLA, supported with funding from National Institutes of Health-National Center for Research Resources shared resources grant (CJX1-443835-WS-29646) and National Science Foundation Major Research Instrumentation grant (CHE-0722519).

Disclosures

None.

References

1. Krenning G, Zeisberg EM, Kalluri R. The origin of fibroblasts and mechanism of cardiac fibrosis. *J Cell Physiol*. 2010;225:631–637.
2. Österreicher CH, Penz-Österreicher M, Grivennikov SI, Guma M, Koltsova EK, Datz C, Sasik R, Hardiman G, Karin M, Brenner DA. Fibroblast-specific protein 1 identifies an inflammatory subpopulation of macrophages in the liver. *Proc Natl Acad Sci USA*. 2011;108:308–313.
3. Ogawa M, LaRue AC, Drake CJ. Hematopoietic origin of fibroblasts/myofibroblasts: Its pathophysiologic implications. *Blood*. 2006;108:2893–2896.
4. Zeisberg EM, Tarnavski O, Zeisberg M, Dorfman AL, McMullen JR, Gustafsson E, Chandraker A, Yuan X, Pu WT, Roberts AB, Neilson EG, Sayegh MH, Izumo S, Kalluri R. Endothelial-to-mesenchymal transition contributes to cardiac fibrosis. *Nat Med*. 2007;13:952–961.
5. van Amerongen MJ, Bou-Gharios G, Popa E, van Ark J, Petersen AH, van Dam GM, van Luyn MJ, Harmsen MC. Bone marrow-derived myofibroblasts contribute functionally to scar formation after myocardial infarction. *J Pathol*. 2008;214:377–386.
6. Bergwerff M, Verberne ME, DeRuiter MC, Poelmann RE, Gittenberger-de Groot AC. Neural crest cell contribution to the developing circulatory system: implications for vascular morphology? *Circ Res*. 1998;82:221–231.
7. Waldo K, Miyagawa-Tomita S, Kumiski D, Kirby ML. Cardiac neural crest cells provide new insight into septation of the cardiac outflow tract: aortic sac to ventricular septal closure. *Dev Biol*. 1998;196:129–144.
8. Gittenberger-de Groot AC, Vrancken Peeters MP, Mentink MM, Gourdie RG, Poelmann RE. Epicardium-derived cells contribute a novel population to the myocardial wall and the atrioventricular cushions. *Circ Res*. 1998;82:1043–1052.
9. Kamran P, Sereti K-I, Zhao P, Ali SR, Weissman IL, Ardehali R. Parabiosis in mice: a detailed protocol. 2013:e50556.
10. Hudon-David F, Bouzeghrane F, Couture P, Thibault G. Thy-1 expression by cardiac fibroblasts: lack of association with myofibroblast contractile markers. *J Mol Cell Cardiol*. 2007;42:991–1000.
11. Sirish P, Li N, Liu JY, Lee KS, Hwang SH, Qiu H, Zhao C, Ma SM, López JE, Hammock BD, Chiamvimonvat N. Unique mechanistic insights into the beneficial effects of soluble epoxide hydrolase inhibitors in the prevention of cardiac fibrosis. *Proc Natl Acad Sci USA*. 2013;110:5618–5623.
12. Souders CA, Borg TK, Banerjee I, Baudino TA. Pressure overload induces early morphological changes in the heart. *Am J Pathol*. 2012;181:1226–1235.

13. Evans RA, Tian YC, Steadman R, Phillips AO. TGF-beta1-mediated fibroblast-myofibroblast terminal differentiation-the role of Smad proteins. *Exp Cell Res*. 2003;282:90–100.
14. Manabe I, Shindo T, Nagai R. Gene expression in fibroblasts and fibrosis: involvement in cardiac hypertrophy. *Circ Res*. 2002;91:1103–1113.
15. Bianco P, Riminucci M, Gronthos S, Robey PG. Bone marrow stromal stem cells: nature, biology, and potential applications. *Stem Cells*. 2001;19:180–192.
16. Xia Y, Lee K, Li N, Corbett D, Mendoza L, Frangogiannis NG. Characterization of the inflammatory and fibrotic response in a mouse model of cardiac pressure overload. *Histochem Cell Biol*. 2009;131:471–481.
17. Chu PY, Mariani J, Finch S, McMullen JR, Sadoshima J, Marshall T, Kaye DM. Bone marrow-derived cells contribute to fibrosis in the chronically failing heart. *Am J Pathol*. 2010;176:1735–1742.
18. Stadtfeld M, Graf T. Assessing the role of hematopoietic plasticity for endothelial and hepatocyte development by non-invasive lineage tracing. *Development*. 2005;132:203–213.
19. Ross R, Everett NB, Tyler R. Wound healing and collagen formation. VI. The origin of the wound fibroblast studied in parabiosis. *J Cell Biol*. 1970;44:645–654.
20. Hinton RB, Yutzey KE. Heart valve structure and function in development and disease. *Annu Rev Physiol*. 2011;73:29–46.
21. Lang D, Lu MM, Huang L, Engleka KA, Zhang M, Chu EY, Lipner S, Skoultchi A, Millar SE, Epstein JA. Pax3 functions at a nodal point in melanocyte stem cell differentiation. *Nature*. 2005;433:884–887.
22. Stoller JZ, Epstein JA. Cardiac neural crest. *Semin Cell Dev Biol*. 2005;16:704–715.
23. Rinkevich Y, Mori T, Sahoo D, Xu PX, Bermingham JR Jr, Weissman IL. Identification and prospective isolation of a mesothelial precursor lineage giving rise to smooth muscle cells and fibroblasts for mammalian internal organs, and their vasculature. *Nat Cell Biol*. 2012;14:1251–1260.
24. Männer J, Pérez-Pomares JM, Macías D, Muñoz-Chápuli R. The origin, formation and developmental significance of the epicardium: a review. *Cells Tissues Organs*. 2001;169:89–103.
25. Cai CL, Martin JC, Sun Y, Cui L, Wang L, Ouyang K, Yang L, Bu L, Liang X, Zhang X, Stallcup WB, Denton CP, McCulloch A, Chen J, Evans SM. A myocardial lineage derives from Tbx18 epicardial cells. *Nature*. 2008;454:104–108.
26. Zhou B, Ma Q, Rajagopal S, Wu SM, Domian I, Rivera-Feliciano J, Jiang D, von Gise A, Ikeda S, Chien KR, Pu WT. Epicardial progenitors contribute to the cardiomyocyte lineage in the developing heart. *Nature*. 2008;454:109–113.
27. Zhou B, Honor LB, He H, et al. Adult mouse epicardium modulates myocardial injury by secreting paracrine factors. *J Clin Invest*. 2011;121:1894–1904.
28. Mortazavi A, Williams BA, McCue K, Schaeffer L, Wold B. Mapping and quantifying mammalian transcriptomes by RNA-Seq. *Nat Methods*. 2008;5:621–628.
29. Krenning G, Zeisberg EM, Kalluri R. The origin of fibroblasts and mechanism of cardiac fibrosis. *J Cell Physiol*. 2010;225:631–637.
30. Furtado MB, Costa MW, Pranoto EA, Salimova E, Pinto AR, Lam NT, Park A, Snider P, Chandran A, Harvey RP, Boyd R, Conway SJ, Pearson J, Kaye DM, Rosenthal NA. Cardiogenic genes expressed in cardiac fibroblasts contribute to heart development and repair. *Circ Res*. 2014;114:1422–1434.
31. Gustafsson E, Brakebusch C, Hietanen K, Fässler R. Tie-1-directed expression of Cre recombinase in endothelial cells of embryoid bodies and transgenic mice. *J Cell Sci*. 2001;114:671–676.
32. Braren R, Hu H, Kim YH, Beggs HE, Reichardt LF, Wang R. Endothelial FAK is essential for vascular network stability, cell survival, and lamellipodial formation. *J Cell Biol*. 2006;172:151–162.
33. Kong P, Christia P, Saxena A, Su Y, Frangogiannis NG. Lack of specificity of fibroblast-specific protein 1 in cardiac remodeling and fibrosis. *Am J Physiol Heart Circ Physiol*. 2013;305:H1363–H1372.
34. Moore-Morris T, Guimarães-Camboa N, Banerjee I, et al. Resident fibroblast lineages mediate pressure overload-induced cardiac fibrosis. *J Clin Invest*. 2014;124:2921–2934.
35. Wynn TA, Ramalingam TR. Mechanisms of fibrosis: therapeutic translation for fibrotic disease. *Nat Med*. 2012;18:1028–1040.
36. Friedman SL, Sheppard D, Duffield JS, Violette S. Therapy for fibrotic diseases: nearing the starting line. *Sci Transl Med*. 2013;5:167sr1.

Novelty and Significance

What Is Known?

- Cardiac fibroblasts are a developmentally heterogeneous population, reported to have embryonic origins from the hematopoietic system, endothelium, epicardium, and neural crest.
- Cardiac fibroblasts play a key role in regulating normal myocardial integrity, as well as reverse remodeling that occurs after injury.
- Reactivation of certain developmental gene programs might prime a subset of fibroblast to be preferentially activated after myocardial injury.

What New Information Does this Article Contribute?

- We characterize a combination of surface markers that can be used to prospectively identify and isolate the majority of cardiac fibroblasts using FACS (fluorescence-activated cell sorting).
- The cardiac fibroblast pool is primarily derived from the epicardial and endothelial lineages, with no ostensible contribution from hematopoietic or circulating cells.
- On injury, cardiac fibroblasts from different lineages exhibit similar proliferation rates and gene expression patterns, suggesting that cardiac fibroblasts are functionally identical in spite of distinct developmental origins.

Studies of cardiac fibroblasts have been limited by a lack of universally accepted markers that enable accurate identification and characterization of this developmentally heterogeneous population. Moreover, previous reports implied that a subset of developmentally distinct fibroblasts is preferentially activated on injury. We used a panel of surface markers to isolate cardiac fibroblasts and studied their developmental origins using lineage-tracing experiments. We found that most cardiac fibroblasts are derived from the epicardium and the endothelium during development. Using multiple models, we show that hematopoietic cells do not generate cardiac fibroblasts. Importantly, we discovered that epicardial- and endothelial-derived fibroblasts proliferate at a similar rate and have a similar pattern of gene expression in response to pressure overload–induced stress/injury. These findings suggest that developmental origin of cardiac fibroblasts does not affect their pathological propensity; rather, cardiac fibroblasts may be functionally similar. Our findings suggest that therapeutic targets for pathological cardiac fibrosis should aim to identify the common signaling pathways that are activated on injury in all fibroblasts.

Circulation Research
Journal of the American Heart Association

Developmental Heterogeneity of Cardiac Fibroblasts Does Not Predict Pathological Proliferation and Activation

Shah R. Ali, Sara Ranjbarvaziri, Mahmood Talkhabi, Peng Zhao, Ali Subat, Armin Hojjat, Paniz Kamran, Antonia M.S. Müller, Katharina S. Volz, Zhaoyi Tang, Kristy Red-Horse and Reza Ardehali

Circ Res. 2014;115:625-635; originally published online July 18, 2014;
doi: 10.1161/CIRCRESAHA.115.303794
Circulation Research is published by the American Heart Association, 7272 Greenville Avenue, Dallas, TX 75231

Print ISSN: 0009-7330. Online ISSN: 1524-4571

SUPPLEMENTAL MATERIAL.

Mice

Pax3$^{Cre/+1}$, Tie2$^{Cre/+2}$, Wt1$^{CreERT2/+3}$, Myh11cre/+-GFP[4], Vav1$^{Cre/+5}$, CAG-dsRed and C57Bl/6 mice strains were obtained from the Jackson Laboratory and have been described previously. Tbx18Cre transgenic mice[6], Myh6-GFP[7] and R26R$^{mT/mG}$[8] reporter mice were gifts from Sylvia Evans (San Diego, CA) and Liqun Luo (Stanford, CA) respectively. All procedures were carried out with the approval of the University of California, Los Angeles (UCLA) Animal Research Committee or the Institutional Animal Care and Use Committee at Stanford University. Two operators blinded to the genotype and experimental design performed all animal surgeries.

Tamoxifen.

Tamoxifen (Sigma) was dissolved in corn oil (Sigma) by sonication at a concentration of 20mg/ml. Tamoxifen was administered by gavage over two weeks starting one week prior to surgery to the Wt1$^{CreERT2+/}$;R26R$^{mT/mG}$ mice. Mice received a total of six doses of 4mg during this period.

Genotyping.

The following primers were used for genotyping:
Cre: 5'-GCGGTCTGGCAGTAAAAACTATC-3' and
5'-GTGAAACAGCATTGCTGTCACTT-3';
mT/mG: 5'-CTCTGCTGCCTCCTGGCTTCT-3',
5'-CGAGGCGGATCACAAGCAATA-3'
and 5'-TCAATGGGCGGGGGTCGTT-3′

Transaortic Constriction

Adult mice weighing 25± 5 g were randomly divided into sham and TAC groups (n=4-6 per group; minimum n=3 to observe statistical significance, with more to account for possible animal death). Biological replicates were used, and the experiments were repeated 2-3 times in the lab. The number of animals used for each group was estimated based on mortality rate of 4-8% upon transaortic constriction, as well as in accordance with past studies using this injury model. Although there was a small variation in the severity and extent of cardiac fibrosis, there was a near-uniform degree of LV dysfunction. Animals were anesthetized by an i.p. injection of ketamine/xylazine (100 mg/10 mg/kg). Endotracheal intubation was performed using a blunt 20-gauge needle that was then connected to a volume-cycled rodent ventilator (SAR-830/P; CWE, Inc.) with a tidal volume of 0.2 ml and a respiratory rate of 120/min. The chest was entered in the second intercostal space at the top left aortic arch, the transverse aorta was isolated, and aortic constriction was performed by tying a 7-0 nylon suture ligature against a 27-gauge blunt needle. The needle was then removed to yield a constriction 0.4 mm in diameter. In sham-operated control mice, the entire procedure was identical except that aortic constriction was not performed. The chest tube was used to evacuate the pneumothorax, and it was removed once negative pressure was re-established. The chest was closed in layers using 5-0 Vicryl sutures. Ventilation was maintained until sufficient spontaneous breathing occurred, followed by extubation and removal of the chest tube. The whole surgical procedure was

performed under aseptic conditions. For analysis, animals were randomly divided to 1, 2, and 4 weeks post-operation groups.

BrdU detection by flow cytometry for in vivo proliferation studies

BrdU powder (Sigma) was dissolved in saline (10mg/ml). BrdU was injected intraperitoneally after aortic constriction surgery. Mice were supplied BrdU-added water (1 mg/ml) until analysis (as described earlier). BrdU water was changed every two days. BrdU intracellular staining was performed according to instructions of the BD Pharmingen™ BrdU Flow Kits. In short, cells were fixed and permeabilized in Cytofix/Cytoperm Buffer (BD), followed by incubation in Cytoperm Permeabilization Buffer plus (BD) and DNase treatment (BD) and exposure to fluorescent anti-BrdU antibody. Cells were washed and resuspended in staining buffer and analyzed using flow cytometry.

Echocardiography

In vivo cardiac morphology was assessed by transthoracic echocardiography in live mice as described (23), including the following indices: left ventricular size (end-diastolic and end-systolic dimension), wall thickness (posterior wall thickness), and ventricular function (ejection fraction). ECHO was performed on mice sedated with isoflurane vaporized (2.5% for induction, 1.0% for maintenance) in oxygen. The animal's chest was shaved and positioned in the left lateral decubitus position for ultrasonic imaging with Vevo 770 high-resolution ECHO system equipped with a 35 MHz transducer. LV chamber dimensions and PWT were obtained from M-mode images; LV systolic function is also assessed from these measurements by calculating EF. All mice underwent echocardiography one week after TAC or sham. Studies and analysis were performed blinded to heart condition.

Isolation and culture of Cardiac Fibroblasts (CF)

Before sacrifice, mice were injected with heparin, then the heart was dissected out and perfused with HBSS. The hearts were cut into small pieces and digested with Liberase Blendzyme TH and TM (Roche) in Medium 199 plus DNAse I and polaxamer in 37°C for 1h. Cells were passed through a 70μm cell strainer (BD Falcon) and centrifuged. The cell pellet was resuspended in staining buffer (3% FBS in HBSS) containing the relevant Thy1+HE- surface marker antibodies (Supplemental Table 1) and incubated in the dark for 30 min at room temperature. Thy1+HE- cells were cultured on a 0.1% gelatin-coated 6-well plates in DMEM supplemented with 15% FBS and antibiotics. The medium was changed 24 hours after the primary culture, followed by changes every 48h. After first passage cells were washed and cultured in serum-free culture medium supplemented with 0.5 mg/ml insulin and 0.5 mg/mL transferrin. At confluence, cells were randomly treated either with 0, 10, 25 or 50 ng/mL TGF-β1. After 4 days, untreated and TGF-β treated cells were washed, fixed in 4% paraformaldehyde and stained for expression of Col1 and α-SMA. Cell counts were performed on ImageJ using the 'Cell Counter' plug-in and performed by two people blinded to the cell type and condition.

Flow cytometry analysis

Digested cells from adult mice hearts were suspended in staining buffer (3% FBS in HBSS) containing the relevant surface marker antibodies (Supplementary Table 1). These were incubated in the dark for 30 minutes at room temperature. After

three washing steps, a secondary antibody conjugated to Alexa flour 488 was added. For intracellular staining of Col1, cells were fixed with 4% PFA for 15 min at room temperature before staining. In all steps, a permeabilization buffer containing 0.2% saponin (Sigma) was used. To analyze the anatomic localization of fibroblasts, after perfusion with HBSS, we separate left and right atria, and also left and right ventricles and septum from each heart under the dissecting microscope (Leica). Biological replicates (n=3) were used.

Quantitative RT-PCR

Total RNA from hearts and sorted cardiac fibroblasts (Thy1+HE- cells) were extracted using TRI reagent (Sigma) and RNeasy MinElute Cleanup Kit (Qiagen) according to manufacturer's instructions. The concentration and quality of extracted RNA were measured using a NanoDrop ND-1000 Spectrophotometer (Thermo Scientific). Complementary DNAs (cDNAs) were synthesized using an Omniscript RT Kit (Qiagen). For quantitative RT-PCR, we used a QuantiTect SYBR Green PCR Kit (Qiagen), amplified cDNA and gene specific primers (Supplemental Table 2) on a PRISM 7900HT Sequence Detection System (Applied Biosystems). PCR conditions included initial denaturation at 94°C for 3 min, 35 cycles of denaturation at 94°C for 45 s, annealing at 55°C for 45 s, and extension at 72 °C for 45 s, followed by a final extension at 72°C for 10 min. The mean cycle threshold (Ct) values from triplicate measurements were used to calculate gene expression, with normalization to GAPDH as an internal control. We used the ddCt method to analyze relative gene expression in sorted samples compared to whole-heart control samples. Technical replicates (n=3) and biological replicates (n=3) were performed. The experiment was repeated three times in the lab.

RNA Sequencing

Thy1+HE- cells were isolated from sham and TAC operated hearts 7 days after operation (n=3 per group), and then sorted again directly into RNA Later solution (Ambion). (Number of mice was based on risk of surgical survival as well as expense). Total RNA was extracted using RNeasy miniElute Cleanup Kit (Qiagen) according to manufacturer's instructions. The cDNA library was generated using the reagents provided in the Illumina ® TruSeq™ RNA Sample Preparation v2 Kit (Illumina). The clustering was performed on a cBot cluster generation system using an Illumina HiSeq single read cluster generation kit (Illumina) according to the manufacturer's instructions. The amplified cDNA library was sequenced on an Illumina HiSeq 2500 for estimating transcript abundance (1X50 reads and >12 million reads/sample). The raw reads were generated by HiSeq 2500 sequencing control software, and Fastq files were analyzed using NextGene software (Softgenetics, PA) for calculating Reads Per Kilobase of transcript per Million mapped reads (RPKM). The analyses were performed by the UCLA Clinical Microarray Core Facility, which was blinded to the identity of cell type and surgical group. The statistical analyses were performed using Partek genomics Suite 6.6. Thresholds for selecting significant genes were set at >= 1.5-fold and $p<0.05$. Genes that met both criteria simultaneously were considered as significant changes. Global functional analyses, network analyses and canonical pathway analyses were performed using Ingenuity Pathway Analysis (Ingenuity® Systems, www.ingenuity.com). The RNA sequencing data were submitted to GEO and were assigned the following accession numbers: GSE51620.

In vitro proliferation assay

The relative proliferation of Thy1+HE- cells derived from each lineage (Tie2Cre, Pax3Cre and Tbx18Cre) was analyzed with a BrdU cell proliferation kit following the product manual (Millipore). In brief, 10^3 Thy1+HE- cells were seeded into a well of a 96 well culture plate. BrdU was added into culture after cells were attached at day 0 and at day 3. BrdU incorporation was detected 1, 3 and 5 days later using a microplate reader (BIO-RAD Model 3550). The proliferation absorbance were calculated using the following formula:
Proliferation absorbance = actual absorbance − background absorbance.

Apoptosis assay

PI and Annexin V-FITC Apoptosis Detection Kit I (BD Pharmingen) were used according to the manufacturer's instructions to assess cell death in Thy1+HE- cells. Briefly, adult mouse hearts were digested and sorted for Thy1+HE- cells at 1, 4, 7, and 14 days after TAC and sham surgery. Immediately after sorting cells, FACS Calibur (BD Biosciences) was used to analyze late apoptotic cells as Annexin V+/PI+ double-positive cells or PI+ cells for necrotic cells.

Cytospun preparation

Aliquots of 10-50 × 10^4 cells in 200 µl PBS were cytocentrifuged at 800 rpm for 4 minutes on glass slides. Cytospin slides were dried for 10 minutes and were fixed with Paraformaldehyde 4% for 15 minutes.

Histology and immunohistochemistry

Heart tissues were fixed for 6 hours at 4°C in 4% paraformaldehyde (Electron Microscopy Sciences) in PBS (Fisher Scientific), washed in PBS, immersed in a solution of 30% sucrose (Sigma) in PBS at 4°C overnight, embedded in Tissue-Tek OCT Compound (Sakura), and transferred to a bath of 2-Methylbutane (Fisher Scientific) on dry ice. Frozen tissue slides were prepared at 7-µm thickness using a cryostat (Leica) and stored at -80°C. Masson's trichrome staining (Sigma) was performed according to manufacturer's instructions. For immunohistochemistry, slides were dried at room temperature for 20 minutes, washed 3 times for 10 minutes each in PBS, permeabilized in PBS containing 0.25% Triton X-100 (Fisher Scientific) for 10 minutes at room temperature followed by washing in PBS-T (PBS containing 0.05% Tween-20 (Fisher)) twice for 5 minutes. The tissue slides were incubated with blocking buffer (10% normal goat serum (Sigma) in PBS) for 30 minutes at room temperature. The tissue slides were then incubated with primary antibodies (Supplemental Table 1) diluted in blocking buffer overnight at 4 °C followed by 1 hour at room temperature. After washing three times for 10 minutes with PBS-T, the tissue slides were incubated with the secondary antibody (Supplemental Table 1) for 1 hr at room temperature, washed three times for 10 minutes with PBST, and then mounted with DAPI-containing mounting media (Vector). We used mounting media without DAPI for slides stained with the secondary antibody Alexa Fluor 350. Tyramide Signal Amplification Kit (Invitrogen) was used for double staining using Alexa Fluor 350 according to the manufacturer's protocol. The immunostained slides were observed and analyzed using a Leica fluorescent microscope (LEICACTR6500).

Parabiosis

Mice of the same weight, size and sex were paired at least two to three weeks before the surgery, to make sure that they are compatible. Mice are anesthetized by isoflurane in O_2. Toe pinch was used as an indicator of the pain response. After shaving the corresponding lateral aspects of each mouse, the site was disinfected using an alcohol swab and povidone/iodine. Matching skin incisions are made from the olecranon to the knee joint of each mouse, and the subcutaneous fascia was bluntly dissected to create approximately 0.5 cm of free skin. One partner had the procedure done on the right side, and the other on the left. The right olecranon of one animal is attached to the left olecranon of the other by a single 4-0 silk suture and tie. The partners' knee joints were similarly connected. The dorsal and ventral skins were then approximated by staples or by continuous suture, and the animals were warmed with heating pads, and monitored until recovery. Parabiotic pairs were housed one pair per cage, and given acidified water (pH 2.5). After 4 weeks blood samples from each animal in a parabiont pair were analyzed using flow cytometry. Animal pairs with lower 90% blood chimerism were excluded from our studies

Bone Marrow Transplant

C57BL/6 mice (*H2b*, Thy1.1+CD45.2+ dsRed+) served as donors for hematopoietic stem cells (HSC), GFP- or dsRed-expressing C57BL/6 mice (*H2b*; Thy1.2+CD45.2+GFP+) were used as donors for non-hematopoietic bone marrow (BM) cells for transplantation into C57BL/6 (*H2b*, Thy1.1+CD45.2+) recipients. Donors were 6-12 weeks old, recipients were 8 weeks old at transplant. BM was flushed from tibiae and femora into HBSS/2% FBS, enriched for c-Kit (3C11) cells by magnetic column separation (CD117 MicroBeads, MACS Separation Columns LS; Miltenyi Biotec, Auburn, CA), and 'KTLS-HSC' were purified by FACS-sorting, selecting for c-Kit+, Thy1.2$^{lo\text{-}neg}$, Sca-1+, Lin- (CD3, CD4, CD5, CD8α, B220, Gr1, Mac1 and Ter119). 1000 FACS-purified HSC were infused per recipient mouse. For co transfer of non-hematopoietic cells, BM was flushed from tibiae, femora, and pelvis. Non-hematopoietic cells were extracted by magnetic column depletion of CD45+ cells (CD45 MicroBeads; Miltenyi Biotec). C57BL/6.CD45.2 recipients received a lethal 1050 cGy dose total body gamma irradiation, ~5h prior to tail-vein injection of a radioprotective dose of 1,000 KTLS HSC. In co-transfer experiments $5x10^6$ CD45- non-hematopoietic/stromal cells were injected simultaneously with the HSC. Biological replicates were used, and the experiment was performed three times.

Online Table I: Antibodies used for Flow Cytometry and Immunofluorescence

Antibody	Catalog no.	Vendor
Collagen 1	ab34710	Abcam
CD45	14-0451-82	eBioscience
Cd90/Thy1	553016	BD Biosciences
Vimentin	ab8978	Abcam
S100A4	ab27957	Abcam
CD31	ab28364	Abcam
CD31	557355	BD Biosciences
DDR2	MAB25381	R&D Systems
Periostin	ab14041	Abcam
Smi32	Smi-32R	Covance Inc.
BrdU	ab6326	Abcam
160kD Neurofilament Medium	ab7794	Abcam
CD146	ab75769	Abcam
α-Smooth Muscle Actin	A2547	Sigma-Aldrich
PDGFR-α	sc-338	Santa Cruz Biotechnology
PDGFR- β	3164	Cell Signaling
Anti-Mouse CD 90.1 APC-eFluor 780	47-0900-82	eBioscience
Anti-Mouse CD 90.2 APC-eFluor 780	47-0902-82	eBioscience
Anti-Mouse CD11b PE-Cyanine7	25-0112-81	eBioscience
Anti-Mouse CD1 PE-Cyanine7	25-0311-81	eBioscience
Anti-Mouse TER-119 PE-Cyanine7	25-5921-81	eBioscience
Anti-Mouse CD45 PE-Cyanine5	15-0451-81	eBioscience
Anti-Mouse CD45 PE-Cyanine5	48-0451-82	eBioscience
Donkey Anti-Rabbit Alexa Fluor 647	A-31573	Invitrogen
Rabbit Anti-Mouse Alexa Fluor 647	A-21239	Invitrogen
Chicken Anti-Rat Alexa Fluor 647	A-21472	Invitrogen
Goat Anti-Rabbit Alexa Fluor 350	A-11046	Invitrogen
Goat Anti-Mouse Alexa Fluor 350	A-11045	Invitrogen
Goat Anti-Rabbit Alexa Fluor 594	A-11037	Invitrogen
Goat Anti-Rabbit Alexa Fluor 488	A-21206	Invitrogen
Goat Anti-Mouse Alexa Fluor 488	A-11001	Invitrogen
TSA™ Kit #7, with HRP—Goat Anti-Mouse IgG and Alexa Fluor 350 Tyramide	T-20917	Invitrogen
TSA™ Kit #17, with HRP—Goat Anti-Rabbit IgG and Alexa Fluor 350 Tyramide	T-20917	Invitrogen

Online Table II: qPCR Primers

Gene	Forward Primer	Reverse Primer
S100a4	GGAGCTGCCTAGCTTCCTG	TCCTGGAAGTCAACTTCATTGTC
Col1	GCCAAGAAGACATCCCTGAAG	TGTGGCAGATACAGATCAAGC
Col1a2	GCCACCATTGATAGTCTCTCC	CACCCCAGCGAAGAACTCATA
Acta2	TGACGCTGAAGTATCCGATAGA	CGAAGCTCGTTATAGAAAGAGTGG
Vim	CGGCTGCGAGAGAAATTGC	CCACTTTCCGTTCAAGGTCAAG
Ddr2	CTGTGGGAGACCTTCACCTT	TAGATCTGCCTCCCTTGGTC
Gapdh	TTGTCTCCTGCGACTTCAAC	GTCATACCAGGAAATGAGCTTG
Vwf	GCTCCAGCAAGTTGAAGACC	GCAAGTCACTGTGTGGCACT
Actb	TTCTTTGCAGCTCCTTCGTT	ATGGAGGGGAATACAGCCC
Pax3	ACTACCCAGACATTTACACCAGG	AATGAGATGGTTGAAAGCCATCAG
PDGFR-α	GGACTTACCCTGGAGAAGTGAGAA	ACACCAGTTTGATGGATGGGA
Fn1	AAGGCTGGATGATGGTGGAC	TGAAGCAGGTTTCCTCGGTTG
Myh11	GGCTACACTGCGCAATACCAC	GATGCGGATGCCTTCCAAC
Tnnt2	GAAGTTCGACCTGCAGGAAA	TTCCCACGAGTTTTGGAGAC
Myh6	ACATGAAGGAGGAGTTTGGG	GCACTTGGAGCTGTAGGTCA

Online table III.

Differentially expressed genes in fibroblasts derived from Tie2Cre and Tbx18Cre mice after sham and TAC operations based on RPKM values (RPKM > 11).

		Sham		TAC		
	Gene	**Tie2**	**Tbx18**	**Tie2**	**Tbx18**	**Description**
Fibroblast	**Col1a1**	80.0314	95.8383	646.4613	712.7813	collagen, type I, alpha 1
	Col1a2	96.2915	116.5658	459.5582	545.4914	collagen, type I, alpha 2
	Col3a1	115.3566	207.1719	596.5724	1040.372	collagen, type III, alpha 1
	Col5a1	32.7424	31.2378	85.5528	86.1304	collagen, type V, alpha 1
	Postn	72.2368	52.9055	740.5395	448.3678	periostin, osteoblast specific factor
	Fn1	17.9933	25.9464	290.2151	194.9573	Fibronectin 1
	Ddr2	29.0605	40.1488	19.2445	30.7169	discoidin domain receptor tyrosine kinase 2
	Thy1	19.1403	38.6514	27.5472	93.164	Thy-1 cell surface antigen
ECM Homeostasis	**Tns1**	28.4275	26.1888	27.6148	31.6598	tensin 1
	Sparc	408.4202	447.9847	1587.441	2046.029	secreted protein, acidic, cysteine-rich
	Timp1	20.0221	15.9939	46.7784	148.1267	TIMP metallopeptidase inhibitor 1
	Timp2	253.8434	247.2642	209.5109	294.0806	TIMP metallopeptidase inhibitor 2
	Timp3	341.246	216.4087	236.3808	166.6386	TIMP metallopeptidase inhibitor 3
	Mmp14	24.2605	32.6318	46.5415	73.5397	matrix metallopeptidase 14
	Mmp2	146.1947	154.6572	178.2829	273.9883	matrix metallopeptidase 2
	Mmp23	16.7036	12.9698	20.9731	26.2247	matrix metallopeptidase 23
Autocrine / Paracrine factors (Signaling molecules)	**Tgfb1i1**	13.5097	17.3364	15.4534	30.1916	transforming growth factor beta 1 induced transcript 1
	Tgfb3	19.7593	19.3452	59.3214	34.2881	transforming growth factor, beta 3
	Tgfbi	28.1405	16.2618	17.3993	20.1667	transforming growth factor, beta-induced, 68kDa
	Tgfbr1	15.0678	14.6785	11.6977	14.078	transforming growth factor, beta receptor 1
	Tgfbr2	31.5393	43.9599	24.3327	47.9357	transforming growth factor, beta receptor II
	Tgfbr3	42.2138	47.2823	14.3668	27.2264	transforming growth factor, beta receptor III
	Ctgf	81.451	117.1423	195.2079	250.5535	connective tissue growth factor
	Fgfr1	20.539	22.1367	25.126	30.0622	fibroblast growth factor receptor 1
	Bmp1	14.7556	12.9104	23.2762	30.5738	bone morphogenetic protein 1
	Pdgfra	61.8699	84.6227	22.1991	54.0437	platelet-derived growth factor receptor, alpha polypeptide

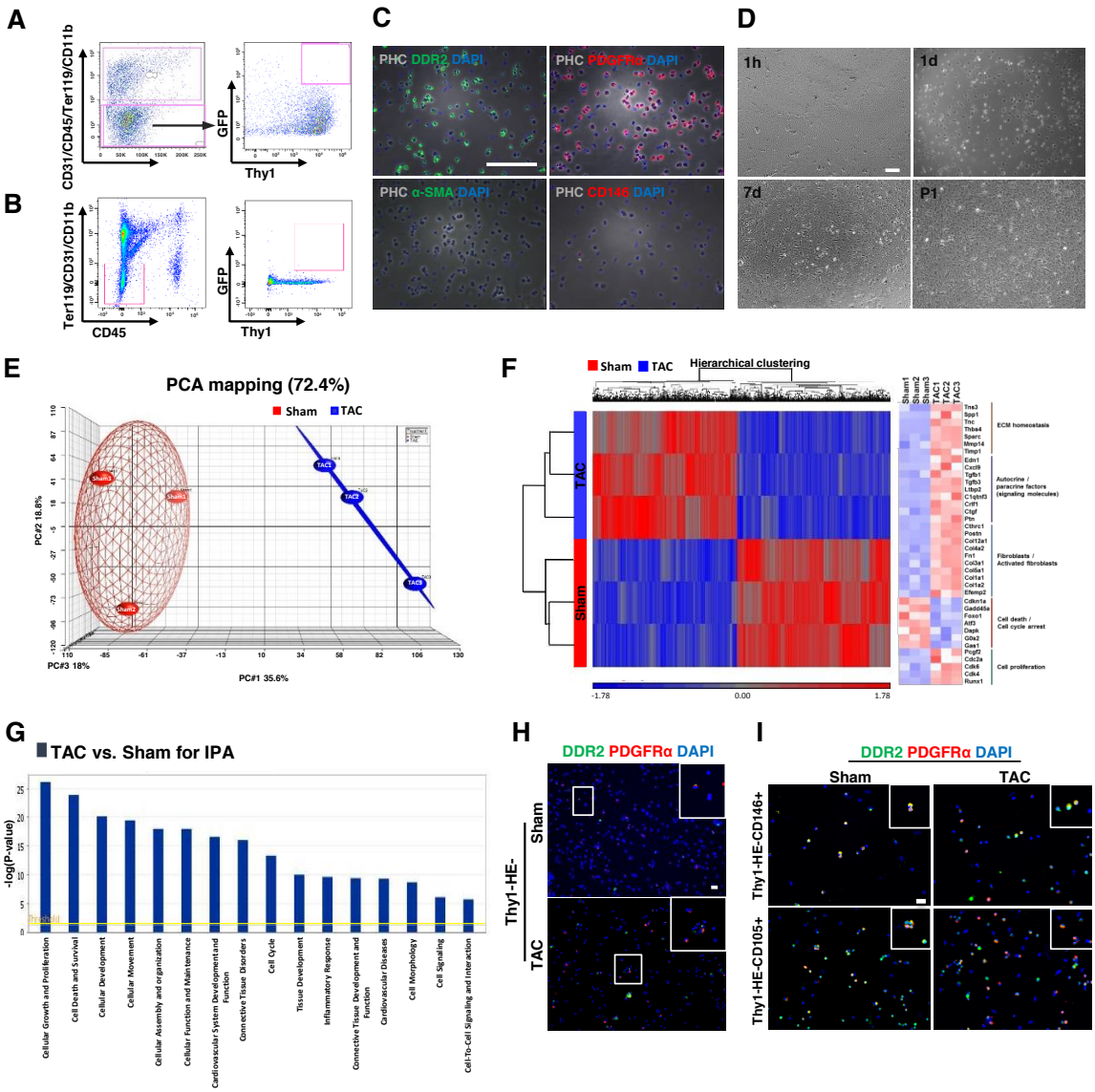

Online Figure I. Characterization of Thy1+HE- cells. (A-B) Flow cytometry of Myh6-GFP (n=3) **(A)** and Myh11Cre-eGFP (n=3) **(B)** hearts for Thy1+HE- cells. **(C)** Immunofluorescence staining of 50,000 cytospun Thy1+HE- cells isolated from freshly digested hearts. These cells express PDGFRα and DDR2, but rarely express CD146 or α-SMA. **(D)** Sorted Thy1+HE- cells were plated and observed at various time points. Scale bar: 200 μm. **(E)** Principal component analysis (PCA) of RNAseq data (performed on Thy1+HE- cells isolated from sham and TAC mice (n=3 each) 7 days after the operations) demonstrates reproducibility between biological replicates of the samples. **(F)** Heat map of RNA-seq data shows 1973 differentially expressed genes (using hierarchical clustering) between the two groups. Red indicates up-regulated genes and blue indicates down-regulated genes. There is increased expression of genes associated with ECM regulation, signaling pathways, fibroblasts function and activation, and cell cycle progression and decreased expression of cell-death and cell cycle arrest proteins in TAC (using fold change >1.5, $p<0.05$ as cut-off). **(G)** A listing of the top 16 bio-function terms enriched in TAC relative to sham. Analysis of differentially-expressed genes between Thy1+HE- cells from TAC (n=3) and sham (n = 3) at day 7 after TAC operation was performed using Ingenuity Pathway Analysis software. The y-axis is the log-transformed p value. p=0.05 is equivalent to y value of 1.3 (yellow line). **(H)** After isolation from sham and TAC hearts 7 days after the operation, some cytospun Thy1-HE- cells co-express PDGFRα and DDR2. **(I)** A fraction of Thy1-HE-CD146+ and Thy1-HE-CD105+ cells isolated from sham and TAC hearts 7 days after surgery express either DDR2 or PDGFRα; few cells express both. Scale bar: 50μm.

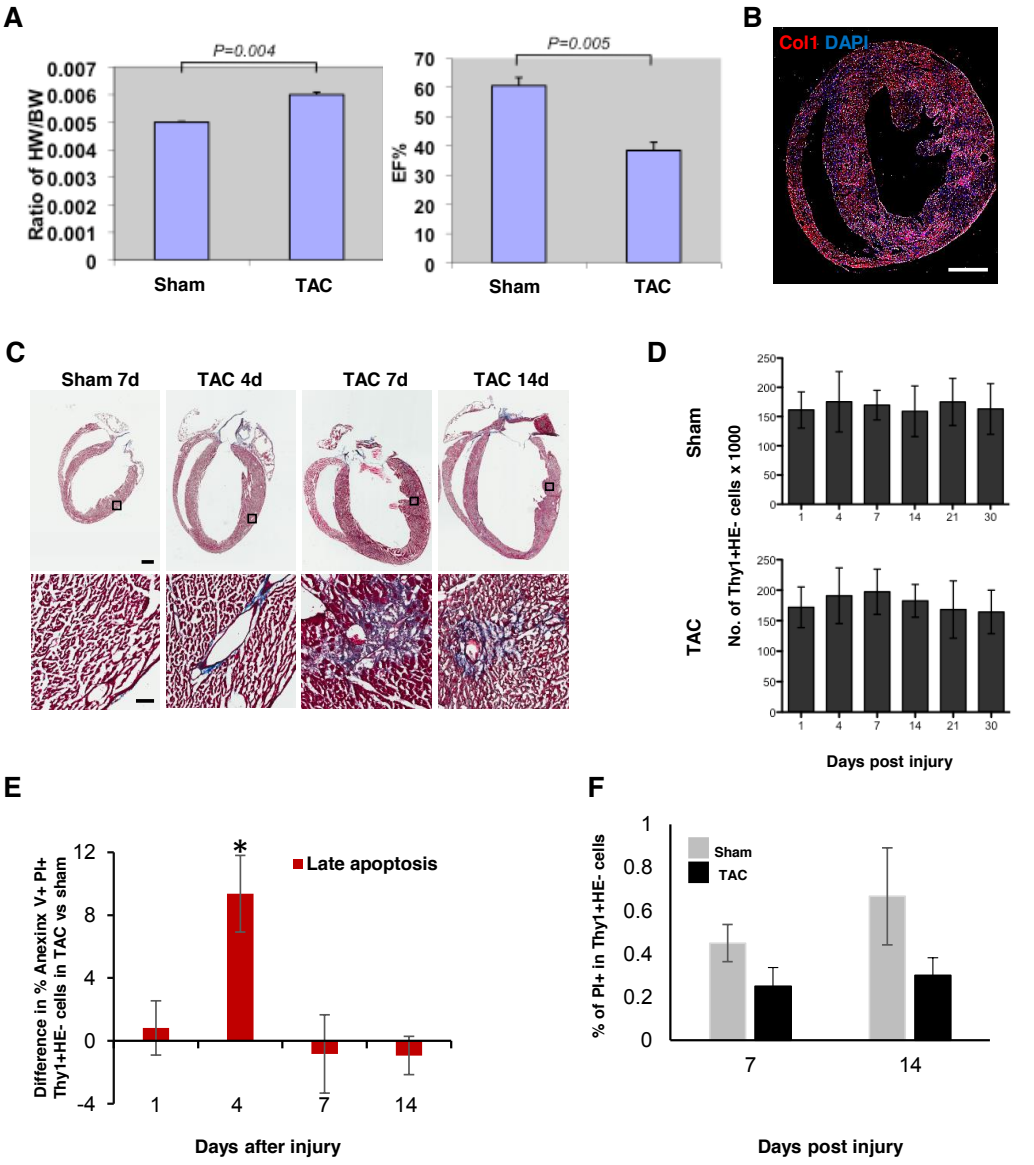

Online Figure II. Characterization of TAC injury and resultant Thy1+HE cell death. (A) TAC surgery consistently resulted in cardiac hypertrophy as evident by increased ratio of heart weight/body weight. The surgery also resulted in a reduction of the ejection fraction to approximately 35-45% by echocardiography (n=3 hearts/surgical group). **(B)** Immunostaining of gross heart sections with Col1 antibody showed diffused fibrosis 7 days after TAC injury. Scale bar: 1 mm. **(C)** Masson's trichrome staining of sham and TAC hearts at 4, 7, and 14 days post-injury. Scale bar, top: 1 mm, bottom: 100 μm. **(D)** The total number of Thy1+HE- cells slightly increases after injury in sham and TAC models, and a plateaus after the first week in the TAC model. **(E)** The number of late apoptotic (Annexin V+/PI+) cells in the Thy1+HE- population was higher 4 days after TAC operation than the sham surgery ($p<0.05$). **(F)** Necrotic cells (PI+) are rare among Thy1+HE- fibroblasts in both sham and TAC hearts at 7 and 14 days following the operation ($p>0.05$). All error bars represent s.e.m.

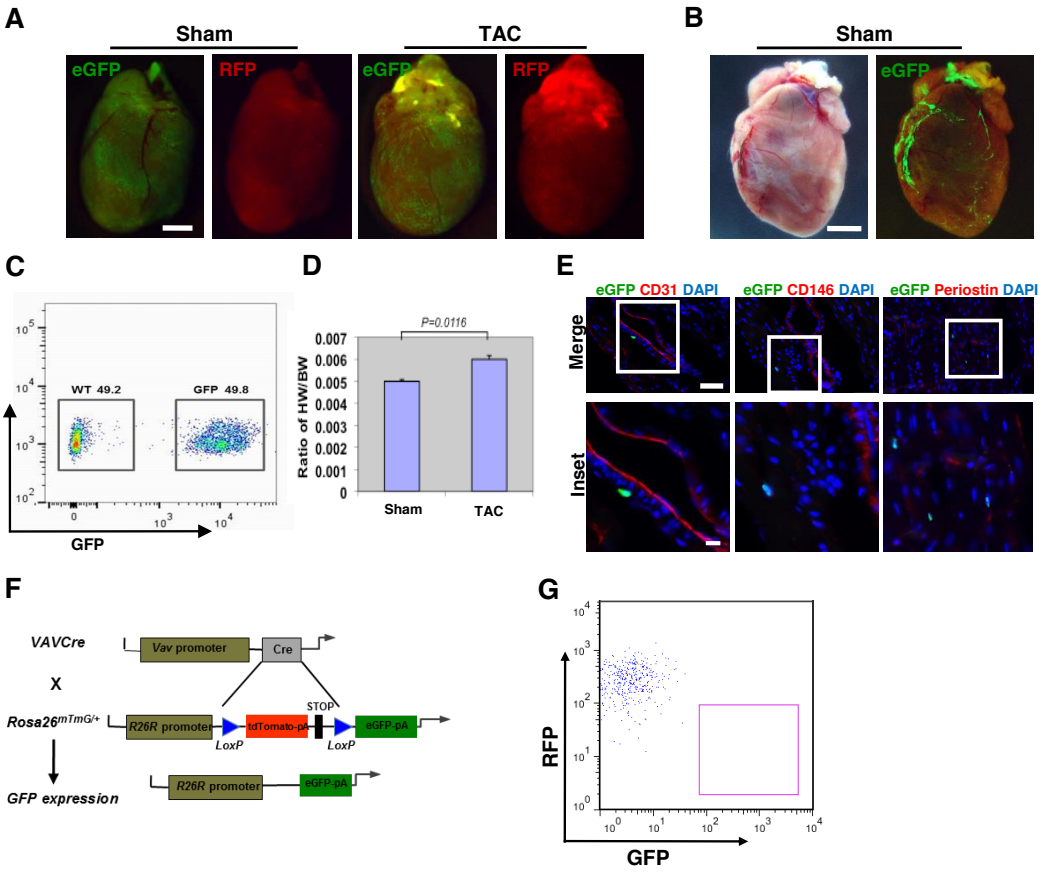

Online Figure III. Bone marrow and parabiosis models do not reveal hematopoietic contribution to cardiac fibroblasts. (A) Gross images of sham and TAC hearts in (GFP-labeled and RFP-labeled BM) BMT-recipient mice show transplanted cells in the heart. Scale bar: 2 mm. **(B)** Gross images of parabiosed wild-type singleton heart show GFP-labeled circulating cells in the vasculature. Scale bar: 2 mm. **(C)** Blood chimerism is achieved in parabiont pairs, analyzed 4 weeks after surgery. **(D)** Shared circulation in parabiotic mice does not alter loading of the TAC'ed heart. The TAC'ed heart showed an expected increase in heart weight-to-body weight ratio at the end of the study when the parabiont pair was separated (n=3 hearts/surgical group). **(E)** IHC of the wild-type heart in the parabiont pair with CD31, CD146, and Periostin. **(F)** Schematic representation of the VavCre/+;R26RmTmG/+. **(G)** Flow cytometry of Thy1+HE- cells for GFP and RFP (n=3 hearts/surgical group). Scale bar: 50 μm for merged panel and 12.5 μm for the inset. All error bars represent s.e.m.

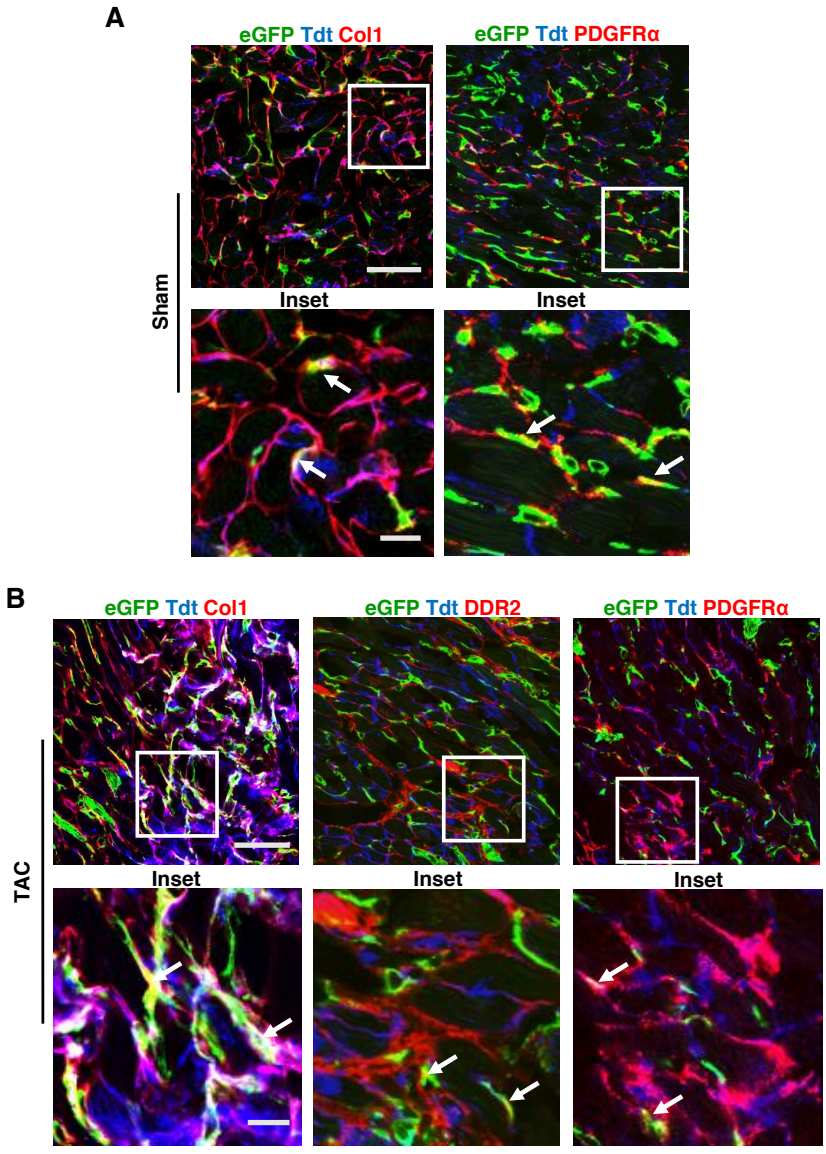

Online Figure IV. Confocal characterization of Tie2-derived cardiac fibroblasts. (A) Representative sections of $Tie2^{Cre/+}$;$R26R^{mT/mG}$ sham hearts stained with Col1 and PDGFRα. **(B)** TAC sections stained for DDR2, Col1, and PDFGRα. (Arrows indicate GFP+ Tbx18-derived cells that co-stain for the marker in red). Scale bar: 50 μm for merged panel and 12.5 μm for the inset.

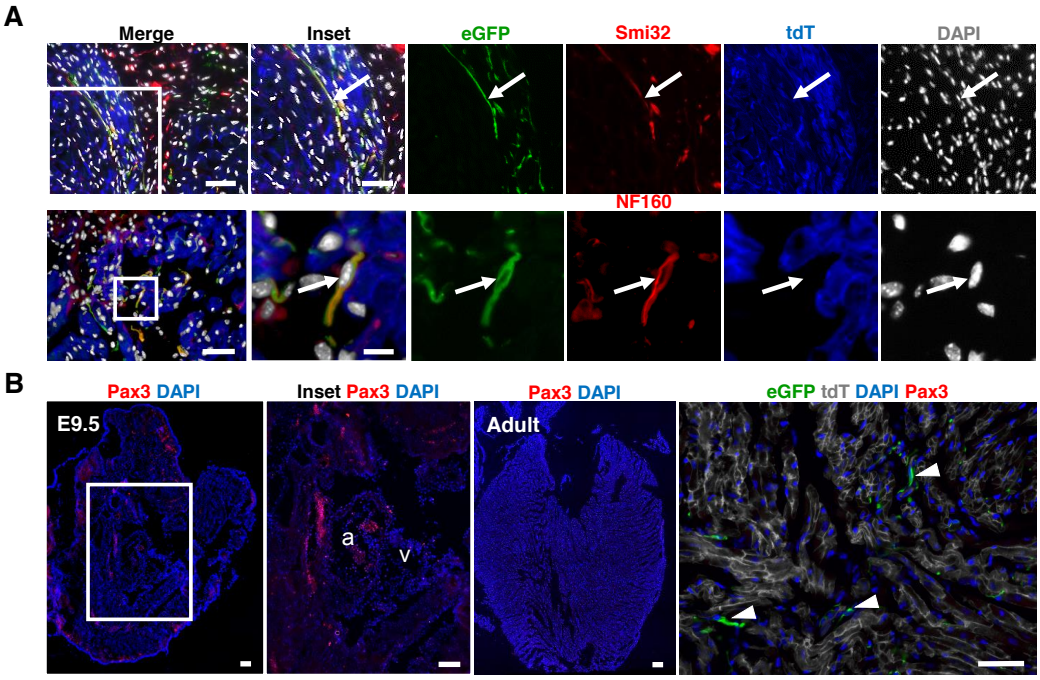

Online Figure V. Characterization of Pax3-derived cells. (A) Tissue sections stained for Smi32 and NF160, markers of neural tissue. **(B)** IHC of wild-type E9.5, wild-type adult heart, and adult Pax3Cre/+;R26RmTmG/+ heart sections to detect Pax3 expression (a: atrium and v: ventricle). Arrows indicate GFP+ cells that co-stain for the marker in red, and arrowheads indicate GFP+ (i.e. Pax3-derived) cells that do not stain with the marker in red. Scale bar: 50μm for merged panel and 12.5 μm for the inset.

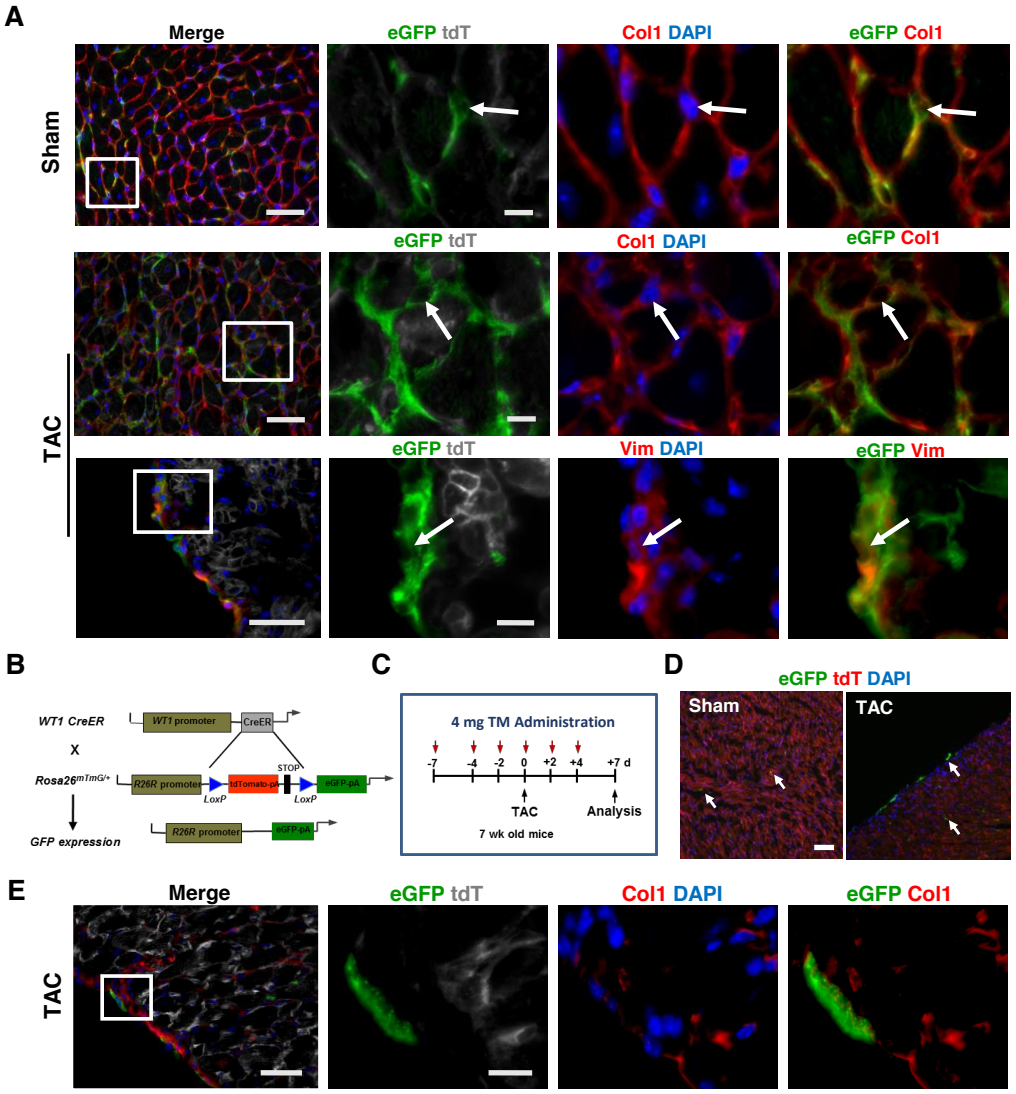

Online Figure VI. Epicardial contribution to cardiac fibroblasts. (A) Staining of Tbx18$^{Cre/+}$;R26R$^{mT/mG}$ with Col1 and Vim. (Arrows indicate GFP+ cells that co-stain for the marker in red). **(B)** Schematic of Wt1$^{CreERT2/+}$;R26R$^{mT/mG}$ model. **(C)** Schematic of TM administration strategy. **(D)** Labeled cells in sham and TAC hearts (n=4 per group). **(E)** IHC of TAC sections with Col1. Scale bar: 50 μm for merged panel and 12.5 μm for the inset.

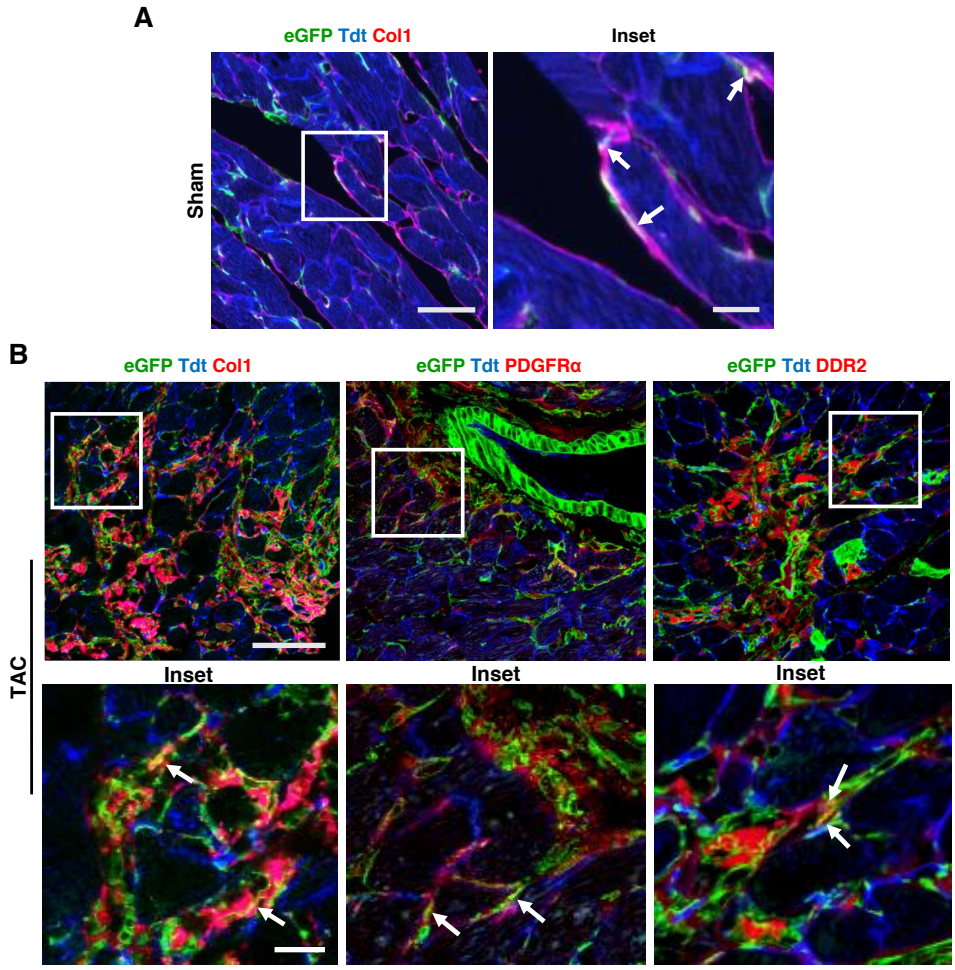

Online Figure VII. Confocal characterization of Tbx18-derived cardiac fibroblasts. (A) Immunohistochemistry of sham Tbx18Cre$^{mT/mG}$ sections with Col1. **(B)** Representative TAC sections were stained for Col1, DDR2, and PDGFRα. (Arrows indicate GFP+ cells that co-stain for the marker in red). Scale bar: 50 μm for merged panel and 12.5 μm for the inset.

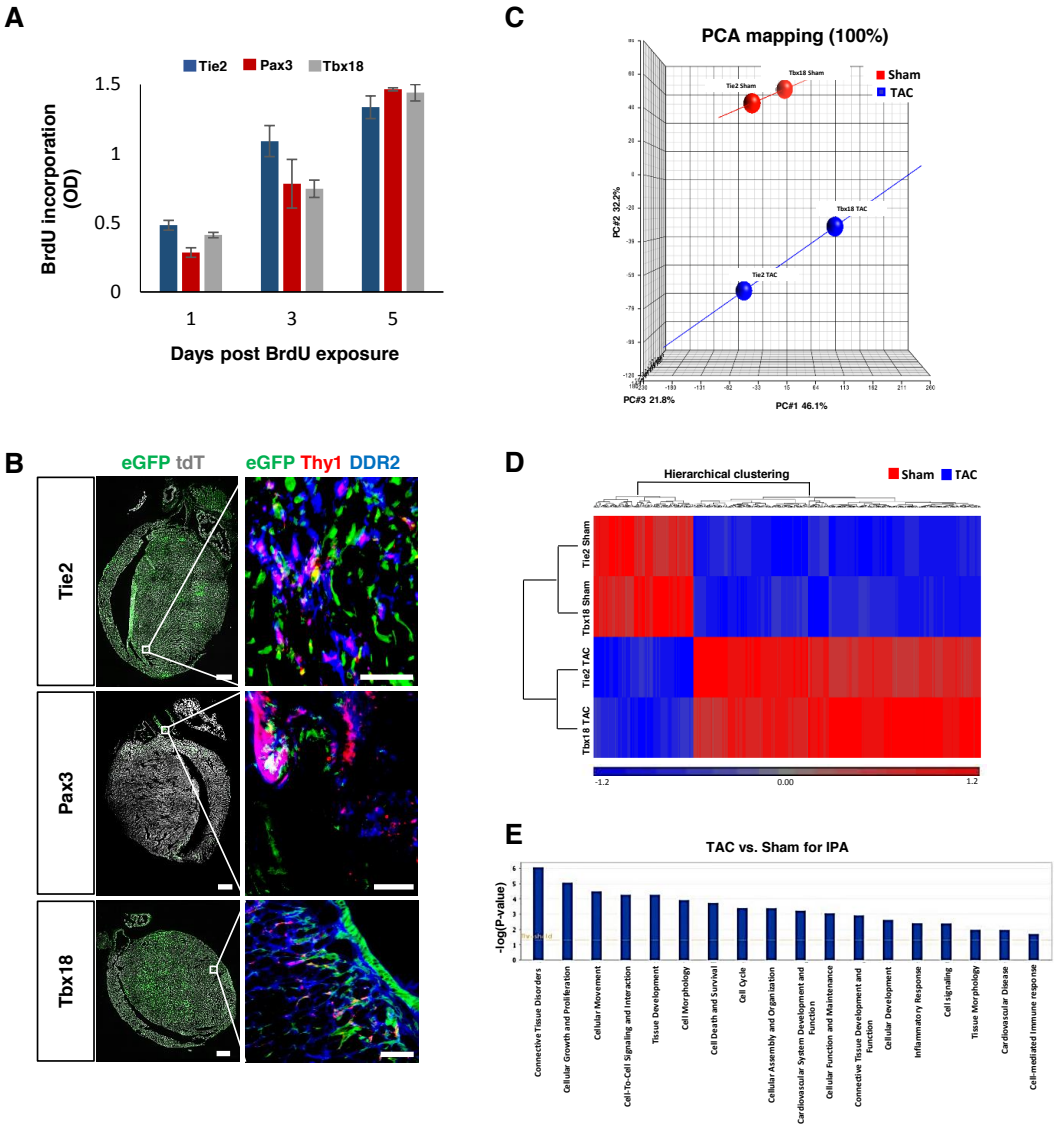

Online Figure VIII. Comparison of proliferation, localization and gene expression in Tbx18-, Tie2- and Pax3-derived fibroblasts. (A) No significant difference among relative BrdU incorporation in each lineage-derived fibroblasts at 1, 3 and 5 days post BrdU exposure. **(B)** Localization of Thy1+DDR2+ cells in each lineage-traced fibroblast subset. **(C)** PCA of RNA-seq data performed on GFP+Thy1+HE- cells isolated from Tie2 and Tbx18 mice 7 days after sham and TAC showed sham- and TAC-derived cells were clustered separately, confirming the similarity between Tie2 sham and Tbx18 sham, as well as between Tie2 TAC and Tbx18 TAC. Discrepancy between shams and TACs indicated different gene expression profile after TAC operation in Tie2 and Tbx18. **(D)** Heat map of the RNA-seq data shows differentially expressed genes (using hierarchical clustering) between the two groups (sham and TAC). Red indicates up-regulated genes and blue indicates down-regulated genes. **(E)** A listing of the top 18 bio-function terms enriched in TAC relative to sham mice. Analysis of differentially-expressed genes between Thy1+HE- cells from TAC and sham at day 7 after TAC operation was performed using Ingenuity Pathway Analysis software. The y-axis is the log-transformed p value. p=0.05 is equivalent to y value of 1.3 (yellow line). Scale bar: 50 μm.

1. Lang D, Lu MM, Huang L, Engleka KA, Zhang M, Chu EY, Lipner S, Skoultchi A, Millar SE, Epstein JA. Pax3 functions at a nodal point in melanocyte stem cell differentiation. *Nature*. 2005;433:884-887
2. Kisanuki YY, Hammer RE, Miyazaki J, Williams SC, Richardson JA, Yanagisawa M. Tie2-cre transgenic mice: A new model for endothelial cell-lineage analysis in vivo. *Developmental biology*. 2001;230:230-242
3. Zhou B, Ma Q, Rajagopal S, Wu SM, Domian I, Rivera-Feliciano J, Jiang D, von Gise A, Ikeda S, Chien KR, Pu WT. Epicardial progenitors contribute to the cardiomyocyte lineage in the developing heart. *Nature*. 2008;454:109-113
4. Xin HB, Deng KY, Rishniw M, Ji G, Kotlikoff MI. Smooth muscle expression of cre recombinase and egfp in transgenic mice. *Physiological genomics*. 2002;10:211-215
5. de Boer J, Williams A, Skavdis G, Harker N, Coles M, Tolaini M, Norton T, Williams K, Roderick K, Potocnik AJ, Kioussis D. Transgenic mice with hematopoietic and lymphoid specific expression of cre. *European journal of immunology*. 2003;33:314-325
6. Cai CL, Martin JC, Sun Y, Cui L, Wang L, Ouyang K, Yang L, Bu L, Liang X, Zhang X, Stallcup WB, Denton CP, McCulloch A, Chen J, Evans SM. A myocardial lineage derives from tbx18 epicardial cells. *Nature*. 2008;454:104-108
7. Ieda M, Fu JD, Delgado-Olguin P, Vedantham V, Hayashi Y, Bruneau BG, Srivastava D. Direct reprogramming of fibroblasts into functional cardiomyocytes by defined factors. *Cell*. 2010;142:375-386
8. Muzumdar MD, Tasic B, Miyamichi K, Li L, Luo L. A global double-fluorescent cre reporter mouse. *Genesis*. 2007;45:593-605

CHAPTER 3

The Cardiac Microenvironment Supersedes Developmental Origin for Fibroblast-to-Cardiomyocyte Reprogramming

Cardiac Microenvironment Supersedes Developmental Origin for Fibroblast-to-Cardiomyocyte Reprogramming

Sara Ranjbarvaziri[1,2,3], James L. Engel[1,2,3], Shuin Park[1,2,3], Ben Van Handel[4], Peng Zhao[1,2], Yichen Ding[1], Debashis Sahoo[5], Kevin Sung[6], Tzung K. Hsiai[1], Rajan P. Kulkami[6], Destaye M. Moore[2,7], Bennett G. Novitch[2,7], Young-Jae Nam[8], Reza Ardehali[1,2,3]

[1] Division of Cardiology, Department of Internal Medicine, David Geffen School of Medicine, University of California, Los Angeles, Los Angeles, CA 90095, USA

[2] Eli and Edythe Broad Center of Regenerative Medicine and Stem Cell Research, University of California, Los Angeles, Los Angeles, CA 90095

[3] Molecular, Cellular and Integrative Physiology Graduate Program, University of California, Los Angeles, Los Angeles, CA 90095, USA

[4] Department of Orthopedic Surgery, Keck School of Medicine of USC, University of Southern California, Los Angeles, CA, 90033, USA

[5] Departments of Pediatrics and Computer Science and Engineering, University of California, San Diego, La Jolla, CA 92093, USA

[6] Division of Dermatology, Department of Medicine, David Geffen School of Medicine, University of California, Los Angeles, Los Angeles, CA 90095, USA

[7] Department of Neurobiology, David Geffen School of Medicine at UCLA, Los Angeles, CA

[8] Department of Medicine, Division of Cardiovascular Medicine, Vanderbilt University School of Medicine, Nashville, TN

Corresponding author: RArdehali@mednet.ucla.edu

The authors have declared that no conflict of interest exists.

Abstract

Direct reprogramming of cardiac fibroblasts (CFbs) to cardiomyocytes is a promising strategy to regenerate damaged myocardium from endogenous fibroblasts and potentially minimize fibrotic tissue. Several studies have reported the remarkable tendency of fibroblasts to be reprogrammed more efficiently to induced cardiomyocytes (iCMs) *in vivo*, particularly in the context of cardiac injury, when compared to *in vitro* reprogramming. Despite the therapeutic promises of direct reprogramming, questions remain regarding how the heterogeneity of CFbs may influence cardiac reprogramming efficiency. It is not entirely known whether there exists a distinct subset of CFbs *in vivo* with a predisposition towards reprogramming to cardiomyocytes. Furthermore, it is possible that injury may induce cues in a subpopulation of CFbs that would make them more susceptible to conversion to iCMs. Herein, we employed genetic fate-mapping and transplantation studies to show that the majority of CFbs originate from a shared mesodermal ancestor as cardiomyocytes while a minority emerge from neural crest-derived precursors. Using a combination of the CLARITY technique and light-sheet microscopy, we demonstrated that developmental heterogeneity of CFbs partially influences their anatomical distribution within the heart. We provide compelling evidence that, regardless of their developmental origin, CFbs are able to be successfully converted to beating iCMs through *in vitro* direct reprogramming. However, when compared to fibroblasts of extra-cardiac organs of identical developmental origin, CFbs generated iCMs with higher efficiency, emphasizing the importance of the physiological microenvironment on cell fate conversion more so than their embryonic origin. Finally, we show that despite invoking similar levels of proliferation and activation, cardiac injury induces a temporary re-expression of early developmental genes in CFbs that is dependent on their developmental origin. These data underscore the importance of the developmental heterogeneity of CFbs when it comes to their direct reprogramming to iCMs during the injury. This in turn may be crucial for the development of targeted therapies to promote cardiac repair.

knowledge is essential to elucidate molecular mechanisms that efficiently drive *in vivo* CFb reprogramming to cardiomyocytes in the setting of cardiac injury.

Herein, we employed genetic fate-mapping techniques and demonstrated that multipotent progenitors expressing Mesp1 contribute to the majority of the cardiac cells, including CFbs. However, RNA sequencing and lineage tracing studies revealed that there also exists a small population of CFbs derived from the neural crest origin. To determine if functional differences exist among these developmentally distinct CFbs, we evaluated whether mesoderm-derived CFbs are more prone to direct reprogramming into induced cardiomyocytes (iCMs) because of their common ancestral origin. We provide direct evidence that, regardless of their developmental origin, CFbs are able to be successfully converted to functional iCMs through *in vitro* direct reprogramming. However, when we compared the reprogramming efficiency of cardiac fibroblasts with fibroblasts of extra-cardiac origin, but derived from equivalent embryonic germ layer, CFbs generated iCMs with higher efficiency regardless of their developmental origin, suggesting a critical role of the physiological microenvironment on cell fate. Remarkably, cardiac injury induces a temporary re-expression of early developmental genes in CFbs according to their embryonic origin, as evidenced by RNA sequencing. Taken together, our findings provide insight into the effect of the developmental origin of fibroblasts and the microenvironment where they reside on their reprogramming efficiency and response to injury.

Results

Cardiac cells are predominantly of Mesp1 origin

We generated Mesp1$^{Cre/+}$;Rosa26$^{mTmG/+}$ transgenic mice in which expression of Mesp1 leads to indelible labeling of cells from tdTomato (tdT) to GFP in a Cre-dependent manner **(Figure 1A)**. To validate that the Mesp1$^{Cre/+}$;Rosa26$^{mTmG/+}$ mouse model can recapitulate endogenous expression of Mesp1, we sorted both GFP and tdT expressing cells from E7.5 transgenic embryos, the developmental stage when Mesp1 expression is high [Ref] **(Supplementary Figure 1A)**. As expected, qPCR analysis showed that, in comparison to tdT+ cells, GFP+ cells expressed significantly higher levels of Mesp1 **(Supplementary Figure 1B)**. Mesp1-expressing cells and their progeny first appear at the cardiac crescent stage around E7 and contribute to the majority of the cells in the heart from E9.5 to adulthood **(Figure 1B)**. Immunohistochemical analysis (IHC) of heart tissue sections from adult mice showed co-localization of Mesp-1 lineage derived cells (GFP+ cells) with markers for cardiomyocytes (α-Actinin), smooth muscle cells (α-SMA), endothelial cells (CD31) and fibroblasts (DDR2), indicating that all major cardiovascular cell types are derived from Mesp1-expressing progenitor cells **(Figure 1C)**. These results were further confirmed by qPCR analysis of sorted Mesp1-derived cells from the adult heart for genes associated with different cardiac lineages **(Figure 1D)**.

Multipotent Mesp1 progenitors differentiate to fibroblasts after transplantation

To establish whether Mesp1-expressing cardiac progenitors can differentiate into fibroblasts *in vivo*, we transplanted freshly isolated GFP+ cells from E7.5 Mesp1$^{Cre/+}$;Rosa26$^{mTmG/+}$ transgenic mice and transplanted them into chick embryos (~1,000 cell/embryo) at the same developmental stage (HH8-HH13; Hamburger–Hamilton stages) **(Figure 2A)**. At HH35, the transplanted cells were found in the left ventricle of the developing chick heart **(Figure 2B)** and differentiated to fibroblasts (Collagen1 [Col1] and DDR2) or α-SMA expressing cells as evidenced by IHC **(Figure 2C and Supplementary Figure 2A)**. To further confirm our results, GFP+ cells were isolated from E7.5 Mesp1$^{Cre/+}$;Rosa26$^{mTmG/+}$ transgenic mice and subsequently transplanted under the kidney capsule of adult NOD/SCID gamma

(NSG) mice **(Figure 2D)**. Four weeks following transplantation, engrafted GFP+ cells showed evidence of differentiation and stained positive for fibroblast and smooth muscle cell markers **(Figure 2E, F and Supplementary Figure 2B)**. These results suggest that cardiac progenitors expressing Mesp1 are multipotent and can generate fibroblasts upon transplantation in two independent models.

Mesp1-expressing cells are the main contributors to the CFb population

It has been widely reported that the majority of CFbs are derived from the epicardium; a transient structure developed from the pro-epicardium (PEO)[11]. To determine whether Mesp1-derived cells contribute to the PEO, we analyzed $Mesp1^{Cre/+}$;$Rosa26^{mTmG/+}$ E9.5 embryos when the PEO is present underneath the sinus venosus [11, 12]. We observed that the majority of the cells expressing the PEO/epicardium marker WT1 co-localized with GFP, indicating that the PEO is predominantly of Mesp1 origin[13] **(Supplementary Figure 3A)**. At E14.5, cells from the PEO migrated to the outer surface of the heart forming the fetal epicardium. At this developmental stage, the majority of WT1+ epicardial cells were also expressing GFP, implying their Mesp1 origin **(Supplementary Figure 3B)**. We then directly analyzed the contribution of Mesp1 cells to CFbs by using a previously established panel of surface markers[5] to label the majority of CFbs. This method excludes hematopoietic (CD45-, Ter119-), macrophage (CD11b-), and endothelial (CD31-) lineages followed by inclusion of a Thy1+ (CD90+) cells (hereafter referred to as Thy1+HE-) **(Supplementary Figure 4A)**. Flow cytometry analysis showed that in adult hearts ~80-85% of CFbs were Mesp1 derived while ~12-15% had non-Mesp1 origin. **(Supplementary Figure 4B)**.

A small subset of CFbs originates from the neural crest

Our data thus far indicates the presence of two developmentally distinct CFb subsets in adult mouse heart; one of Mesp1 origin and the other derived from a non-Mesp1 source. In an attempt to determine whether these two CFbs subsets exhibit distinct phenotypes *in vitro* and *in vivo*, we first isolated GFP+ and tdT+ CFbs from adult $Mesp1^{Cre/+}$;$Rosa26^{mTmG/+}$ mouse hearts and expanded them separately in

culture. Both Mesp1 derived (GFP+) and non-Mesp1 derived (tdT+) CFbs adopted a spindle-shaped morphology consistent with a mesenchymal cell phenotype, and stained positive for the fibroblast marker Col1 **(Supplementary Figure 5A)**. The expression of fibroblast associated genes in cultured CFbs was analyzed by qPCR and confirmed similarity between the two subsets **(Supplementary Figure 5B)**. Upon stimulation with transforming growth factor β1 (TGF-β1), both GFP+ and tdT+ fibroblasts expressed α-SMA, a marker for activated fibroblasts **(Supplementary Figure 5C)**. To delineate potential differences between the two developmentally discrete fibroblast populations at the gene expression level, we performed RNA-sequencing on sorted GFP+ and tdT+ CFbs from adult $Mesp1^{Cre/+}$;$Rosa26^{mTmG/+}$ transgenic mice. The overall gene expression profiles between the two populations were similar, however tdT+ CFbs were highly enriched in genes associated with neuronal development and neural crest **(Figure 3A)**. These findings suggest that perhaps a subset of non-Mesp1-derived CFbs (tdT+ CFbs) may be derived from neural crest progenitor cells during development. To test this hypothesis, we generated $Pax3^{Cre/+}$;$Rosa26^{mTmG/+}$ mice to mark neural crest-derived cells **(Figure 3B)**. We then sorted GFP+ CFbs derived from Pax3+ neural crest cells for RNA-sequencing. We compared the gene expression profiles of Mesp1- and non-Mesp1-derived CFbs with neural crest-derived CFbs. As shown in **Figure 3C**, Pax3-derived CFbs shared a set of upregulated genes with non-Mesp1-derived CFbs which were not expressed in Mesp1-derived CFbs. Gene ontology analysis demonstrated high enrichment of genes related to neuronal development and maturation **(Figure D).** Further transcriptome analysis confirmed that non-Mesp1-derived CFbs clustered closely with Pax3-derived CFbs and showed upregulation of genes associated with neurons **(Figure 3E)**. Collectively, these results illustrate that neural crest-derived CFbs constitute a subset of cells that are distinct from the rest of the cardiac fibroblasts, most of which originate from mesodermal precursors.

CFbs of discrete developmental origins exhibit specific distribution within the heart

Quantitative anatomical mapping of CFbs can be useful to define the heterogeneity of different subsets in normal cardiac physiology and in response to injury. To evaluate whether the developmental origin of CFbs can specify their anatomical distribution, we assessed how Mesp1- and Pax3-derived CFbs are dispersed within each cardiac compartment. We first dissected adult hearts into 5 zones (left and right atria, left and right ventricles, and sepal wall) and isolated lineage traced CFbs from each anatomical region **(Supplementary Figure 6A)**. Flow cytometry analysis showed that Mesp1-derived CFbs were proportionally distributed in all cardiac chambers, while the majority of Pax3-derived fibroblasts were localized in the right atrium **(Supplementary Figure 6B)**. To label lineage-derived fibroblasts in the heart without the need for immunostaining, we used Col1a1$^{GFP/+}$ reporter mice [14], which has been shown to label the majority of fibroblasts, in combination with Mesp1$^{Cre/+}$;Rosa26$^{tdT/+}$ or Pax3$^{Cre/+}$;Rosa26$^{tdT/+}$ reporter mice **(Figure 4A)**. As shown in **Figure 4B**, lineage-derived CFbs were marked by co-expression of GFP and tdT in the heart sections from the triple transgenic mice.

To further explore the spatial distribution of Mesp1- and Pax3-derived CFbs in the intact heart, we applied recent advances in optical microscopy and image analysis. For three-dimensional (3D) anatomical localization studies, we developed a modified CLARITY technique, in which the heart is transformed into an optically translucent but structurally-preserved organ[15] with subsequent imaging by light-sheet fluorescence microscopy (**Figure 4C and Supplementary Figure 6C)**. With this strategy, lineage-derived CFbs were clearly visible in the hearts from both Mesp1$^{Cre/+}$;Rosa26$^{tdT/+}$;Col1a1$^{GFP/+}$ **(Supplementary video 1)** and Pax3^{Cre}/+;Rosa26$^{tdT/+}$;Col1a1$^{GFP/+}$ mice **(Supplementary video 2)** at a single-cell resolution. Our combined 3D and 2D analyses showed an even distribution of Mesp1-derived CFbs throughout all cardiac chambers, while the majority of Pax3-derived CFbs were localized in the right ventricular outflow tract, the aortic wall and the right atrium **(Figure 4D and E, Supplementary Figure 6D and E)**. Additionally, fluorescence-activated cell sorting (FACS) analysis of enzymatically isolated lineage-derived Col1a1+ cells from the different heart compartments confirmed the results from our 3D and 2D analyses, with similar distribution patterns of lineage-derived CFb

subsets **(Figure 4F)**. These data suggest that the developmental origin of CFbs may partially determine their distribution within the cardiac chambers.

CFbs of different developmental origin have similar cardiac reprogramming efficiency

As previous studies have demonstrated that overexpression of core cardiac-specific transcription factors results in the direct conversion of fibroblasts to induced cardiomyocyte-like cells (iCMs), we asked whether the developmental origin of fibroblasts can affect the efficiency of cell fate conversion[16, 17]. We hypothesized that Mesp1-derived CFbs, which share a common developmental origin with cardiomyocytes, are more prone to generate iCMs compared to CFbs from neural crest origin. We first sorted all Col1a1+CFbs (including both lineage derived [tdT+GFP+] and non-lineage derived [tdT-GFP+] CFbs) from Mesp1Cre/+;Rosa26$^{tdT/+}$;Col1a1$^{GFP/+}$ and Pax3$^{Cre/+}$;Rosa26$^{tdT/+}$;Col1a1$^{GFP/+}$ mice and transduced the cells with retroviruses expressing Gata4, Mef2C and Tbx5 (GMT) **(Figure 5A)**. Four weeks after transduction, both CFb subsets generated iCMs as evidenced by well-organized sarcomere structures (α-Actinin+ and Troponin T+) **(Figure 5B)** and spontaneous contraction **(Supplementary Video 3 and 4 and Supplementary Figure 7A and B)**. Notably, the iCMs no longer expressed Col1a1, indicating their reprogramming fate toward cardiomyocyte while silencing their fibroblast gene programs **(Supplementary Figure 8A and B)**. We then quantified the efficiency of reprogramming in both CFb subsets by counting the number of lineage-derived CFbs that generated iCMs by expression of α-Actinin and Troponin T as well as by qPCR analysis. Our results revealed no significant differences between the efficiency of reprogramming in CFbs derived from Mesp1 or Pax3 origin. **(Figure 5C and D)**. Furthermore, we found no significant differences between the reprogramming efficiency of CFbs when lineage derived CFbs (tdT+GFP+) were initially sorted and then subjected to reprogramming when compared to isolation of bulk fibroblasts based on Col1 expression (i.e. inclusion of [tdT+GFP+] and [tdT-GFP+]) for reprogramming **(Supplementary Figure 9A, B and C)**.

The normal heart is composed of distinct, yet functionally interconnected atrial, ventricular and pacemaker cell types, making generation of all specific subtypes desirable for therapeutic purposes[18].

Since no differences in the reprogramming efficiency of the two CFb subsets was noted, we then assessed whether CFbs of different developmental origins can favorably generate specific cardiomyocyte subtypes. As previous studies suggested the requirement of Hand2 for the generation of pacemaker in addition to atrial and ventricular iCMs, we added this transcription factor to our previous reprogramming cocktail **(Supplementary Figure 10A)**. Four weeks after the initiation of direct reprogramming, immunocytochemistry (ICC) and qPCR results showed that both CFb subsets (Mesp1- and Pax3-derived CFbs) generated all cardiomyocyte-like subtypes including atrial (MYL7, Nappa), ventricular (MYL2) and pacemaker (HCN4) iCMs with no significant preferences toward a specific subtype **(Supplementary Figure 10B, C and D)**.

Previous studies have revealed that cardiac neurons which contribute to the innervation of the heart are embryonically derived from neuroectoderm[19, 20]. To complement our cardiomyocyte direct reprogramming experiments, we studied whether Pax3-derived CFbs of neuroectoderm origin are more susceptible to generate induced neurons (iN) in comparison to mesodermal-derived CFbs. To generate iNs from CFbs, we overexpressed previously reported transcription factors (*Ascl1, Brn2 and Myct1*) in a co-culture setting with primary glial cells [21] **(Supplementary Figure 11A)**. Our results revealed that, similar to cardiomyocyte reprogramming, CFbs of both subsets generated iN expressing pan-neuronal markers (TUJ1, MAP2 and NCAM1) with similar efficiency **(Supplementary Figure 11B, C and D).** Together these results confirmed that despite distinct developmental origins, both CFb subsets can similarly adopt other cell lineages through cellular reprogramming.

The myocardial environment determines cardiac reprogramming efficiency of fibroblasts

As the reprogramming potential of fibroblasts from various sources has been reported to differ substantially[18, 22, 23], we sought to determine whether fibroblasts from different organs but derived from identical embryonic germ layer display similar reprogramming efficiency. To address this question, we designed a set of experiments to assess the effect of cardiac microenvironment on direct

reprogramming of cardiac fibroblasts. We compared the reprogramming efficiency of cardiac fibroblast (that reside in a similar microenvironment as cardiomyocytes) to fibroblasts isolated from extra-cardiac tissues. First, we isolated Mesp1-derived cardiac and pulmonary fibroblasts, which are both of mesodermal origin, from Mesp1$^{Cre/+}$;Rosa26$^{tdT/+}$;Col1a1$^{GFP/+}$ mice **(Figure 6A and B)**. Similarly, Pax3-derived cardiac and dermal fibroblasts of ectodermal origin were obtained from Pax3$^{Cre/+}$;Rosa26$^{tdT/+}$;Col1a1$^{GFP/+}$ mice **(Figure 6A and B)**. Fibroblasts were then cultured and reprogrammed to iCMs using GMT retroviral transduction (**Figure 6A and C)**. Thirty days after reprogramming, both ICC and qPCR showed that, regardless of their developmental origin, fibroblasts residing in the heart generated significantly higher percentage of mature cardiac Troponin T+ cells, when compared to pulmonary or dermal fibroblasts **(Figure 6D and E)**. Taken together, these findings provide direct evidence that fibroblasts residing in the heart are more efficiently reprogrammed to iCMs as opposed to fibroblasts of identical developmental origin isolated from other organs.

CFbs of different developmental origin show unique responses to injury

To further evaluate the functional differences between the two developmentally distinct CFb subsets, we assessed their responses to pressure overload injury induced by transverse aortic constriction (TAC). We explored whether the developmental origin of CFbs affects their proliferation rate and activation in response to injury **(Supplementary Figure 12A and B)**. Compared to sham controls, TAC operated hearts showed significant increase in size, suggestive of pathologic cardiac hypertrophy. Using echocardiography, we observed a reduction in left ventricular function at 7 and 30 days post TAC **(Supplementary Figure 12C)**. Masson's trichrome staining of the respective tissue revealed diffuse global fibrosis at 7 days after TAC which persisted 4 weeks post-operation (**Supplementary Figure 12D)**.

For the proliferation studies, Bromo-deoxyuridine (BrdU) was administered to Mesp1$^{Cre/+}$;Rosa26$^{tdT/+}$;Col1a1$^{GFP/+}$ and Pax3$^{Cre/+}$;Rosa26$^{tdT/+}$;Col1a1$^{GFP/+}$ mice at the time of operation followed by BrdU in drinking water until the day of analysis (7day post-TAC) **(Figure 7A)**. As shown in

Figure 7B, the fraction of BrdU+tdT+GFP+ fibroblasts in Mesp1- and Pax3-derived CFbs were similar in sham and increased to the same extent at 7 days post-TAC injury. Next, we sought to determine whether CFbs of different developmental origins display distinct patterns of pathological activation after injury. Confocal images revealed the presence of Mesp1- and Pax3-derived activated CFbs, marked by α-SMA and Periostin, in both perivascular and interstitial regions of the injured myocardium **(Figure 7C, D and E)**. These findings suggest that both CFb subpopulations exhibit similar degree of proliferation and activation. Next, we compared the transcriptional profile of the two developmentally distinct CFb subsets under normal cardiac physiology and in response to pathological pressure overload stress. We performed RNA-seq analysis on FACS-sorted lineage-derived CFbs 7 and 30 days post-TAC or sham controls **(Supplementary Figure 13A and B)**. GO term analysis revealed a significant number of genes associated with cell cycle, fibroblast activation, and fibrosis upregulated in fibroblasts of both subsets 7 days post TAC **(Figure 7F and G)**. Remarkably, injury induced a temporal re-expression of early mesoderm and cardiovascular development genes in Mesp1-derived CFbs while early neuronal genes and brain development were highly enriched in Pax3-derived CFbs indicating possible retention of developmental memory **(Figure 7H and I)**. However, by 30 days after injury in both CFb subsets, expression of genes associated with either cell cycle or fibroblasts activation was markedly reduced **(Supplementary Figure 13C)**. Similarly, early cardiovascular genes and early neuronal genes were down regulated in Mesp1 and Pax3 derived CFbs, respectively **(Supplementary Figure 13D)**. The temporal activation of the early germ layer genes in each CFb subset mirroring their developmental origin suggests that perhaps the most dynamic period to promote fibroblast lineage conversion may be confined to the early injury interval. Together these data suggest that despite similar proliferation and activation level, CFbs originating from different germ layers show unique responses to pressure overload injury with distinct gene expression profiles that reflect their developmental origin.

Discussion/Conclusion

Our studies have revealed how the developmental origin and physiological environment of fibroblasts may influence their reprogramming efficiency to induced cardiomyocytes. Through *in vitro* cardiac

reprogramming we show that the cardiac environment plays an essential role in facilitating direc reprogramming of fibroblasts to iCMs. Following pressure overload injury, we also observed a temporar re-expression of specific genes in CFbs that closely resembled the transcriptome of their respective developmental origins. The findings from our study may be a major step toward deciphering the molecula mechanisms of cardiac reprogramming and, in turn, may provide hints for overcoming molecular roac blocks in cardiomyocyte generation through reprogramming.

Direct reprogramming of fibroblasts to cardiomyocyte-like cells holds promise for cardiac regeneratio after injury. A major limitation to the clinical translation of this technology is the exceptionally lov conversion rate of fibroblasts to iCM. Among the many causes, this may be partly due to the inheren heterogeneity of fibroblasts and the presence of epigenetic barriers that may impeded cell fate conversion[24]. It has been suggested that direct reprogramming may be more permissive in closely relatec cell types, because cells that are derived from a common progenitor likely share some epigeneti features[25]. Indeed, a recent study by the Rosenthal group suggested that a subpopulation of CFbs may be more amenable to cardiac reprogramming due to their expression of core cardiogenic genes which are mainly associated with cardiomyocyte ontogenesis[4]. However, the hierarchical ontogeny and ancestra relationship of CFbs to cardiomyocytes had not been fully investigated. We used a combination of fate mapping and transplantation studies to show that during development transient common cardiovascula progenitors, expressing Mesp1, give rise to the majority of fibroblasts in addition to cardiomyocytes Mesp1, is a bHLH transcription factor that was previously shown to be expressed in the embryonic hear during early cardiovascular development[13]. Using RNA-seq analysis and lineage tracing studies, we demonstrated that while the majority of CFbs are derived from Mesp1-expresing progenitors, neural cres cells expressing Pax3 contribute to a minor subpopulation of fibroblast pool in the heart. Furthermore these two CFb subsets showed a preferential anatomical distribution within the intact heart. The identification of developmentally distinct CFbs raised the question of whether the origin of fibroblasts coul predict overall reprogramming efficiency towards iCMs. We hypothesized that because Mesp1-derivec

CFbs share a common ancestor to cardiomyocytes, this subset would be more prone to direc reprogramming in comparison to CFbs derived from a neural crest origin. Nevertheless, our data demonstrated that CFbs from both mesoderm or neural crest origins can be converted to iCMs with simila efficiency, thus refuting the hypothesis that the developmental origin of CFbs influences their direc reprogramming *in vitro*. These findings prompted us to explore whether factors other than cell intrinsi differences influence cell fate conversion.

During embryogenesis, fibroblasts are derived from various developmental origins and migrate to differen organs. Depending on the organ in which these cells reside, they are exposed to specific cell-ce interactions and physiological cues that may contribute to their distinct characteristics, differentiating then from fibroblasts of the same embryonic origin residing in other organs. Hence, we investigated whethe local environment where fibroblasts are residing can promote or deter their cell fate conversion. We observed that fibroblasts from the heart generate iCMs more efficiently when compared to fibroblast derived from the identical embryonic origin but residing in other organs. These findings suggest that the tissue specific environment represents a determinant factor in cell fate conversion. It also emphasizes the importance of choosing the right source of cells to achieve optimal cell fate conversion through *in vitro* reprogramming.

Lineage conversion involves a transition between different epigenetic states. This can be achieved by introduction of exogenous factors that accomplish two major tasks: (i) stimulation of regulators to properly reactivate the epigenetically repressed state of the target cell genes and (ii) activation of regulatory networks of genes that promote reprogramming to the desired cell type[26]. However, another important factor in this process, which has been somewhat overlooked, is the homeostatic state of the starting cell and its microenvironment. The *in vivo* environment of the heart appears to enhance the efficiency of direct reprogramming, with even higher efficiency being achieved after injury[6-8]. It remains unclear how cardiac injury can facilitate the overcoming of epigenetic hurdles and potentially render the

cells to be more amenable to fate switch. One potential explanation is that injury causes the substantial expansion of CFbs, especially in the infarct zone[5]. Cell proliferation has been suggested to be an essential component for direct reprogramming due to the de-condensed chromatin state during mitosis which makes the genome more accessible to reprogramming factors[27]. However, a recent study by Qian group using single cell RNA sequencing showed that increased proliferation in fibroblasts suppressed iCM generation[28]. These observations encouraged us to explore whether injury evokes differential responses from the various CFb subtypes such that a specific CFb population may be more preferentially primed for cardiac reprogramming. Our data from pressure overload injury revealed a parallel upregulation of proliferation and activation in both subsets of CFbs. This finding was in line with our previous studies in which epicardial and endothelial/endocardial derived CFbs, both of mesoderm origin, showed parallel pathological proliferation and ECM synthesis in response to TAC[5]. Interestingly, we observed a unique gene expression pattern in which CFbs reactivate early embryonic genes that correspond to their developmental origin indicative of their retained epigenetic memory. These findings further raise the intriguing possibility that Mesp1-derived CFbs may be more susceptible to be reprogrammed to iCMs *in vivo* due to the re-expression of early mesoderm and cardiac development genes after injury. On the other hand, Pax3-derived CFbs were enriched in early neuronal and brain development genes, suggesting that they may not be the ideal candidate for *in vivo* cardiac reprogramming. Our gene expression data also supports the possibility that injury may revert adult CFbs back to their embryonic state, which may lead to a higher reprogramming efficiency[22]. Notably, transcriptional changes in cell cycle, fibrosis and early developmental genes were no longer observed 30 days after the injury implying that the first week after pressure overload injury may be the most dynamic period for cellular reprogramming. These intriguing findings suggest that there exists a discrete temporal period in which the injury milieu of the heart may allow for endogenous cells to overcome epigenetic barriers that hinder the early stages of reprogramming. Identification of these environmental cues from the injured heart may enhance the efficiency of fibroblast to cardiomyocyte conversion.

In summary, our studies have demonstrated that the majority of CFbs originate from a shared ancestor as cardiomyocytes while a minority emerge from neural crest-derived origin. Through *in vitro* reprogramming, we revealed the determinant role of the endogenous environment on fibroblasts cell fate conversion. The changes in the transcriptome of CFbs that occur immediately after injury, in addition to the distinct cardiac environment may facilitate overcoming the epigenetic barriers *in vivo* and result in efficient reprogramming of CFbs within the scar tissue and promote cardiac repair. Further research to define the role of CFbs developmental heterogeneity in response to injury and direct reprograming to iCM is warranted.

Supplementary information for this article is available online.

SOURCES OF FUNDING

This work was supported by a grant from the NIH (DP2 HL127728), Eli & Edith Broad Center of Regenerative Medicine and Stem Cell Research Center at UCLA and Rose Hills Foundation Research Award (R.A.). S. R. was supported by the UCLA Graduate Programs in Bioscience (GPB).

AUTHOR CONTRIBUTIONS

S.R. and R.A. conceived the project and designed the experiments. S.R. performed the majority of the experiments and analyzed data from all experiments. S.R. prepared the figures. S.R. and R.A. wrote the manuscript. S.R., J.E. and Y.J.N. performed direct reprograming experiments. P.Z. performed the surgeries. B.V. and D.S. helped with RNA-seq analysis. D.M.M performed chick embryo transplantation. Y.D. performed light sheet microscopy imaging and all the image and video processing. S.R. had full access to all the data in the study and take responsibility for the integrity of the data and the accuracy of the data analysis. We are grateful for the expert technical assistance from the UCLA Broad Stem Cell Research Center (BSCRC) Flow Cytometry Core and Clinical Microarray Core. All authors reviewed the manuscript.

CONFLICT OF INTEREST

The authors declare no competing financial interests. Correspondence and requests for materials should be should be addressed to R.A. (RArdehali@mednet.ucla.edu).

1. Sanganalmath, S.K. & Bolli, R. Cell therapy for heart failure: a comprehensive overview of experimental and clinical studies, current challenges, and future directions. *Circ Res* **113**, 810-834 (2013).
2. Furtado, M.B. *et al.* Cardiogenic genes expressed in cardiac fibroblasts contribute to heart development and repair. *Circ Res* **114**, 1422-1434 (2014).
3. Morris, S.A. & Daley, G.Q. A blueprint for engineering cell fate: current technologies to reprogram cell identity. *Cell Res* **23**, 33-48 (2013).
4. Furtado, M.B., Nim, H.T., Boyd, S.E. & Rosenthal, N.A. View from the heart: cardiac fibroblasts in development, scarring and regeneration. *Development* **143**, 387-397 (2016).
5. Ali, S.R. *et al.* Developmental heterogeneity of cardiac fibroblasts does not predict pathological proliferation and activation. *Circ Res* **115**, 625-635 (2014).
6. Qian, L. *et al.* In vivo reprogramming of murine cardiac fibroblasts into induced cardiomyocytes. *Nature* **485**, 593-598 (2012).
7. Song, K. *et al.* Heart repair by reprogramming non-myocytes with cardiac transcription factors. *Nature* **485**, 599-604 (2012).
8. Jayawardena, T.M. *et al.* MicroRNA induced cardiac reprogramming in vivo: evidence for mature cardiac myocytes and improved cardiac function. *Circ Res* **116**, 418-424 (2015).
9. Mohamed, T.M.A. *et al.* Chemical Enhancement of In Vitro and In Vivo Direct Cardiac Reprogramming. *Circulation* (2016).
10. Fu, J.D. & Srivastava, D. Direct reprogramming of fibroblasts into cardiomyocytes for cardiac regenerative medicine. *Circ J* **79**, 245-254 (2015).
11. Ratajska, A., Czarnowska, E. & Ciszek, B. Embryonic development of the proepicardium and coronary vessels. *Int J Dev Biol* **52**, 229-236 (2008).
12. Katz, T.C. *et al.* Distinct compartments of the proepicardial organ give rise to coronary vascular endothelial cells. *Dev Cell* **22**, 639-650 (2012).
13. Saga, Y. *et al.* MesP1 is expressed in the heart precursor cells and required for the formation of a single heart tube. *Development (Cambridge, England)* **126**, 3437-3447 (1999).
14. Moore-Morris, T. *et al.* Resident fibroblast lineages mediate pressure overload-induced cardiac fibrosis. *J Clin Invest* **124**, 2921-2934 (2014).
15. Epp, J.R. *et al.* Optimization of CLARITY for Clearing Whole-Brain and Other Intact Organs(1,2,3). *eNeuro* **2** (2015).
16. Ieda, M. *et al.* Direct Reprogramming of Fibroblasts into Functional Cardiomyocytes by Defined Factors. *Cell* **142**, 375-386 (2010).
17. Song, K. *et al.* Heart repair by reprogramming non-myocytes with cardiac transcription factors. *Nature* **485**, 599-604 (2012).
18. Nam, Y.J. *et al.* Induction of diverse cardiac cell types by reprogramming fibroblasts with cardiac transcription factors. *Development* **141**, 4267-4278 (2014).
19. Hildreth, V., Anderson, R.H. & Henderson, D.J. Autonomic innervation of the developing heart: origins and function. *Clinical anatomy (New York, N.Y.)* **22**, 36-46 (2009).
20. Hildreth, V., Anderson, R.H. & Henderson, D.J. Autonomic innervation of the developing heart: Origins and function. *Clinical Anatomy* **22**, 36-46 (2009).
21. Vierbuchen, T. *et al.* Direct conversion of fibroblasts to functional neurons by defined factors. *Nature* **463**, 1035-1041 (2010).
22. Ieda, M. *et al.* Direct reprogramming of fibroblasts into functional cardiomyocytes by defined factors. *Cell* **142**, 375-386 (2010).

23. Doppler, S.A. *et al.* Cardiac fibroblasts: more than mechanical support. *J Thorac Dis* **9**, S36-S51 (2017).
24. Qian, L. & Srivastava, D. Direct cardiac reprogramming: from developmental biology to cardiac regeneration. *Circ Res* **113**, 915-921 (2013).
25. Vierbuchen, T. & Wernig, M. Molecular roadblocks for cellular reprogramming. *Molecular cell* **47**, 10.1016/j.molcel.2012.1009.1008 (2012).
26. Xu, J., Du, Y. & Deng, H. Direct Lineage Reprogramming: Strategies, Mechanisms, and Applications. *Cell Stem Cell* **16**, 119-134 (2015).
27. Gaspar-Maia, A., Alajem, A., Meshorer, E. & Ramalho-Santos, M. Open chromatin in pluripotency and reprogramming. *Nature reviews. Molecular cell biology* **12**, 36-47 (2011).
28. Liu, Z. *et al.* Single-cell transcriptomics reconstructs fate conversion from fibroblast to cardiomyocyte. *Nature* **551**, 100-104 (2017).
29. Moore-Morris, T. *et al.* Resident fibroblast lineages mediate pressure overload–induced cardiac fibrosis. *The Journal of Clinical Investigation* **124**, 2921-2934 (2014).
30. Engleka, K.A. *et al.* Insertion of Cre into the Pax3 locus creates a new allele of Splotch and identifies unexpected Pax3 derivatives. *Developmental Biology* **280**, 396-406 (2005).
31. Madisen, L. *et al.* A robust and high-throughput Cre reporting and characterization system for the whole mouse brain. *Nat Neurosci* **13**, 133-140 (2010).
32. Muzumdar, M.D., Tasic, B., Miyamichi, K., Li, L. & Luo, L. A global double-fluorescent Cre reporter mouse. *Genesis* **45**, 593-605 (2007).
33. Coughlan, A.M. *et al.* Myeloid Engraftment in Humanized Mice: Impact of Granulocyte-Colony Stimulating Factor Treatment and Transgenic Mouse Strain. *Stem Cells Dev* **25**, 530-541 (2016).
34. Adams, K.L., Rousso, D.L., Umbach, J.A. & Novitch, B.G. Foxp1-mediated programming of limb-innervating motor neurons from mouse and human embryonic stem cells. *Nat Commun* **6**, 6778 (2015).
35. Sung, K. *et al.* Simplified three-dimensional tissue clearing and incorporation of colorimetric phenotyping. *Sci. Rep.* **6**, 30736 (2016).
36. Ding, Y. *et al.* Light-sheet fluorescence imaging to localize cardiac lineage and protein distribution. *Sci. Rep.* **7**, 42209 (2017).
37. Fei, P. *et al.* Cardiac Light-Sheet Fluorescent Microscopy for Multi-Scale and Rapid Imaging of Architecture and Function. *Sci. Rep.* **6**, 22489 (2016).
38. Fehrenbach, J., Weiss, P. & Lorenzo, C. Variational algorithms to remove stationary noise: applications to microscopy imaging. *IEEE T. Image Proc.* **21**, 4420-4430 (2012).
39. Fehrenbach, J. & Weiss, P. Processing stationary noise: Model and parameter selection in variational methods. *SIAM J. Imag. Sci.* **7**, 613-640 (2014).
40. Otsu, N. A threshold selection method from gray-level histograms. *IEEE T. Systems Man Cybernetics* **9**, 62-66 (1979).
41. Ding, Y. *et al.* Light-sheet fluorescence imaging to localize cardiac lineage and protein distribution. *Scientific Reports* **7**, 42209 (2017).
42. Wu, J., Anczukow, O., Krainer, A.R., Zhang, M.Q. & Zhang, C. OLego: fast and sensitive mapping of spliced mRNA-Seq reads using small seeds. *Nucleic acids research* **41**, 5149-5163 (2013).
43. Liao, Y., Smyth, G.K. & Shi, W. featureCounts: an efficient general purpose program for assigning sequence reads to genomic features. *Bioinformatics (Oxford, England)* **30**, 923-930 (2014).

Mice

Mesp1$^{Cre/+13}$ and Col1a1$^{GFP/+29}$ mice were gifts from Dr. Mikkola from UCLA and Dr. Evans from UCSD. Pax3$^{Cre/+30}$, Rosa26$^{tdT/+31}$, Rosa26$^{mTmG/+32}$ and NSG (NOD/SCID gamma) mice[33] were obtained from the Jackson Laboratory and have been described previously. All procedures were carried out with the approval of the University of California, Los Angeles (UCLA) Animal Research Committee. Animal numbers and sample sizes reflected the minimal number needed for statistical significance based on power analysis and prior experience. Two operators blinded to the genotype and experimental design performed all animal surgeries, *in vivo* and *in vitro* analyses.

Genotyping

The following primers were used for genotyping:

Cre:

Forward: ATCCGAAAAGAAAACGTTGA

Reverse: ATCCAGGTTACGGATATAGT

mTmG:

Wild type Forward: CTCTGCTGCCTCCTGGCTTCT

Wild type Reverse: CGAGGCGGATCACAAGCAATA

Mutant Reverse: TCAATGGGCGGGGGTCGTT

tdT:

Wild type Forward: AAG GGA GCT GCA GTG GAG TA

Wild type Reverse: CCG AAA ATC TGT GGG AAG TC

Mutant Reverse GGC ATT AAA GCA GCG TAT CC

Mutant Forward CTG TTC CTG TAC GGC ATG G

Isolation of embryonic Mesp1 expressing progenitor cells

Embryos from timed mating of Mesp1$^{Cre/+}$;Rosa26$^{mTmG/+}$ transgenic mice were isolated at different embryonic days. GFP+ embryos were immediately digested with collagenase solution (collagenase A (10 mg/Ml) and B (10 mg/Ml) (Roche Diagnostics, Indianapolis, IN) in 10 mM Hank's_Balanced Salt Solution (HBSS) for 30 min at 37°C. GFP+ and tdT+ cells were sorted by FACS Aria II flow cytometer (BD Biosciences).

Chick Embryo Transplantation

Fertilized chicken eggs (McIntyre Poultry and Fertile Eggs) were incubated at 38 °C for ~60 h to Hamburger-Hamilton (HH) stage 14–17 prior to use. FACS-purified GFP+ cells from Mesp1$^{Cre/+}$;Rosa26$^{mTmG/+}$ embryos at embryonic day 7.5 (E7.5) were pooled with CFbs from wild type mice (1:1 ratio) and subsequently transplanted into the anterolateral plate mesoderm region of stage 8 or dorsomesocardial region of stage 13 chick embryos as previously described[34]. At stage 35, the heart and aortic arch region of chick embryos were harvested and fixed in 4% PFA for 1 hour and prepared for cryosections.

Kidney capsule Transplantation

Adult NSG mice (8-10 weeks old) were anesthetized with isoflurane and a transverse incision was made to expose the kidney. GFP+ cells were sorted from Mesp1$^{Cre/+}$;Rosa26$^{mTmG/+}$ embryos at E7.5 and after mixing with Matrigel (1:1 v/v), a suspension of 3×10^5 cell in 10-15 μL was injected directly underneath the capsular membrane of the kidney using a 26 gauge Hamilton syringe. The kidney was then gently repositioned into the abdominal cavity and the muscle and skin was sutured. Four weeks after transplantation the kidney was removed and processed for histology analysis.

Isolation, culture and characterization of fibroblasts

Before sacrifice, mice were injected with heparin, then the tissue of interest was dissected out and perfused with HBSS. For the dermal fibroblasts, we used the facial skins which originates from

neuroectoderm. The tissue was then cut into small pieces (~1mm) and digested with Liberase Blendzyme TH and TM (5mg/ml, Roche) in Medium 199 supplemented with DNAse I and polaxamer (10mg/ml) in 37°C for 1h. Cells were passed through a 70 μm cell strainer (BD Falcon) and centrifuged at 300 g for 5 min. The cell pellet was re-suspended in the staining buffer (3% FBS in HBSS) containing the relevant $Thy1^{+}HE^{-}$ surface marker antibodies [5] **(Supplementary Table 1)** for 30 min in the dark. No antibody was used for isolating fibroblasts from $Col1a1^{GFP/+}$ mice. Instead GFP+ cells were used to isolate lineage traced fibroblasts. Fibroblasts were sorted using a BD FACSAria II flow cytometer and then cultured on 0.1% gelatin-coated 12-well plates in DMEM supplemented with 15% FBS and antibiotics ($5x10^4$ cells per well). The medium was changed 24 hours after the initial culture, followed by changes every 48 hours. Cells were passaged upon 80% confluency. After the first passage, cells were washed and cultured in serum-free culture medium supplemented with 0.5 mg/mL insulin and 0.5 mg/mL transferrin. When confluent, cells were randomly treated either with 0 or 50 ng/mL TGF-β1. After 72 hours, untreated and TGF-β treated cells were washed, fixed in 4% paraformaldehyde and stained for expression of Col1 and α-SMA. Cell counting was performed on ImageJ using the 'Cell Counter' plug-in by two people blinded to the cell type and condition.

Flow cytometry analysis

Adult mouse hearts were cut into small pieces and digested using Liberase Blendzyme TH and TM (5mg/ml, Roche) in Medium 199 supplemented with DNAse I and polaxamer (10mg/ml) in 37°C for 1h. The digested cells were then suspended in staining buffer (3% FBS in HBSS) containing the relevant Thy1+HE- surface marker antibodies **(Supplementary Table 1)**. Cells were incubated in the dark for 30 minutes at room temperature. Cells were then washed with buffer and were analyzed after centrifugation.

BrdU detection by flow cytometry for in vivo proliferation studies

5-Bromo-2-deoxyuridine (BrdU) powder (Sigma) was dissolved in saline (10 mg/ml). BrdU was injected intraperitoneally right after aortic constriction surgery. Mice were supplied with BrdU in drinking water (1 mg/ml) until analysis (as described earlier). BrdU water was changed every two days. BrdU intracellular staining was performed according to instructions from the BD Pharmingen™ BrdU Flow Kit. In short, cells were fixed and permeabilized in Cytofix/Cytoperm Buffer (BD), followed by incubation in Cytoperm Permeabilization Buffer Plus and DNase treatment (both from BD) and exposure to fluorescent labeled anti-BrdU antibody. Cells were washed and re-suspended in staining buffer and analyzed using flow cytometry as described above.

Histological analysis (Trichrome staining, scar size measurement, Immunohistochemistry)

Heart tissues were fixed for 1 hour at 4°C in 4% paraformaldehyde (Electron Microscopy Sciences) in PBS (Fisher Scientific), washed in PBS, immersed in a solution of 30% sucrose (Sigma) in PBS at 4°C overnight, embedded in Tissue-Tek OCT Compound (Sakura), and transferred to a bath of 2-Methylbutane (Fisher Scientific) on dry ice. Frozen tissue sections were prepared at 7 µm thickness using a cryostat (Leica) and stored at -80°C. Masson's trichrome staining (Sigma) was performed according to manufacturer's instructions. For immunohistochemistry, slides were dried at room temperature for 20 minutes, washed 3 times for 10 minutes each in PBS, permeabilized in PBS containing 0.25% Triton X-100 (Fisher Scientific) for 10 minutes at room temperature followed by washing in PBS-T (PBS containing 0.05% Tween-20 (Fisher)) twice for 5 minutes. The tissue slides were incubated with blocking buffer (10% normal goat serum (Sigma) in PBS) for 30 minutes at room temperature. The tissue slides were then incubated with primary antibodies **(Supplementary Table 1)** diluted in blocking buffer overnight at 4 °C followed by 1 hour at room temperature. After washing three times for 10 minutes with PBS-T, the tissue slides were incubated with the secondary antibody **(Supplementary Table 1)** for 1 hour at room temperature, washed three times for 10 minutes with PBST, and then mounted with DAPI-containing mounting media (Vector). The immunostained slides were observed and analyzed using a Zeiss confocal microscope (LSM880) or Leica fluorescent

microscope (LEICACTR6500). Masson's trichrome staining (Sigma) was performed according to manufacturer's instructions and images were taken of the entire cross-section of the heart using bright-field microscopy (Leica). For assessment of the degree of cardiac fibrosis, NIH ImageJ software was used by a blinded operator to compare the area of tissue stained blue (collagen) to the total tissue area (6-10 randomly chosen sections per heart, n=6 hearts per strains).

CLARITY methods for cardiac clearing

Harvested embryonic hearts at E16.5, (the stage at which all 4 cardiac chambers are formed) were rinsed in PBS 3x for 10 minutes and then placed in 4% paraformaldehyde at 4°C for 4 hours. The hearts were then rinsed in PBS 3x for 10 minutes each and placed in a 4% acrylamide solution (Bio-Rad) along with 0.5% w/v of the photoinitiator 2,2'-Azobis[2- (2-imidazolin- 2-yl)propane]dihydrochloride (VA-044, Wako Chemicals USA). The tissues were incubated overnight at 4°C followed by incubation at 37°C for 3 hours to initiate polymerization of the acrylamide. After polymerization, the hearts were rinsed with PBS and then placed into a clearing solution comprised of 8% w/v sodium dodecyl sulfate (SDS, Sigma Aldrich) and 1.25% w/v boric acid (Fisher) (pH 8.5). The samples were incubated at 37°C until cleared. Tissues were then rinsed for one day in 1X PBS after clearing to remove residual SDS. After rinsing, cleared hearts were placed in refractive index matching solution (RIMS) for imaging and storage. The RIMS formulation is as follows: to make 30 mL RIMS, dissolve 40 grams of Histodenz (Sigma) in 0.02M Phosphate buffer (Sigma) with 0.05% w/v sodium azide (Sigma) and syringe filter through a 0.2 mm filter. The tissues can be stored at room temperature in RIMS until ready for imaging[35]. The fluorescence images were captured by the cardiac light-sheet fluorescence microscopy (LSFM)[36, 37]and were processed to remove stationary noise[38, 39]. To normalize the fluorescence intensity in various slices, we applied the Gaussian filter to acquire the distribution of photons in each image, and then we generated a processed image stack with the unified background. To accentuate co-localizations of GFP and tdTomato, we applied multi-level image thresholds based on Otsu's method[40] for segmenting the single slice in each fluorescent channel. Threshold levels for each channel were

manually chosen to extract the most accurate binary masks of each slice. Pixels defined with binary masks were merged together and visualized as overlapping regions, while the remaining regions were regarded as background. To reduce the artifacts of auto fluorescence induced by the residue hemoglobin, the area of overlapping region was pre-defined to range from 1 to 500 pixels, that is, from 4 to 2000 μm[41]. The contour of the 3-D digital heart was rendered by a user-defined intensity threshold, with pixel values above this threshold being shown in white with transparency. The image post-processing, segmentation and rendering were processed by MATLAB (Mathworks), ImageJ (NIH) and Amira 6.1 (FEI Software). The color-coded images were generated by a custom-made algorithm in MATLAB. We subjectively chose one region of interest and calculated the center of the region. Next, we calculated the distance from an arbitrary pixel to the center, and defined the distance with pseudo-color ranging from red to blue.

Transaortic Constriction **(TAC)**

Adult mice weighing 25+/-5 g were randomly divided into sham and TAC groups (n=4-6 per group; minimum n=4 to observe statistical significance, with more to account for possible animal death). Biological replicates were used, and the experiments were repeated 2-3 times. The number of animals used for each group was estimated based on mortality rate of 4-8% upon transaortic constriction, as well as in accordance with past studies using this injury model. Although there was a small variation in the severity and extent of cardiac fibrosis, there was a near-uniform degree of LV dysfunction. Animals were anesthetized by an i.p. injection of ketamine/xylazine (100 mg/10 mg/kg). Endotracheal intubation was performed using a blunt 20-gauge needle that was then connected to a volume-cycled rodent ventilator (SAR-830/P; CWE, Inc.) with a tidal volume of 0.2 ml and a respiratory rate of 120/min. The chest was entered in the second intercostal space at the top left aortic arch, the transverse aorta was isolated, and aortic constriction was performed by tying a 7-0 nylon suture ligature against a 27-gauge blunt needle. The needle was then removed to yield a constriction 0.4 mm in diameter. In sham-operated control mice, the entire procedure was identical except that aortic constriction was not

performed. The chest tube was used to evacuate the pneumothorax, and it was removed once negative pressure was re-established. The chest was closed in layers using 5-0 Vicryl sutures. Ventilation was maintained until sufficient spontaneous breathing occurred, followed by extubation and removal of the chest tube. The whole surgical procedure was performed under aseptic conditions. For post-operative analgesia, mice were injected with Buprenorphine (0.1 mg/kg) and Carprofen (5 mg/kg) intraperitoneally (2x a day for first 48h post operatively, minimum 4 doses). For analysis, animals were randomly divided to 1 and 4 weeks post-operation groups.

Echocardiography

Echocardiography was performed by a single operator who was blind to the mouse strains and treatment groups using the Vevo 770 high-resolution ECHO system equipped with a 35 MHz transducer. First, chest fur was removed using a depilatory lotion (Nair). Mice were lightly anesthetized with vaporized isoflurane (2.5% for induction, 1.0% for maintenance) in oxygen and lightly restrained in a supine position on a heated pad to maintain body temperature at 37° C. EKG leads were used to monitor their heart rate, which remained between 500 and 600 beats per minute. The probe was placed along the short axis of the left ventricle with the papillary muscles providing a guide for the proper depth. 2D images were captured to measure wall thicknesses and interdimensional space during both systole and diastole. Saved images were analyzed by a single operator who was blinded to the experimental design using the included Vevo 2100 software. The LV chamber dimensions and posterior wall thickness (PWT) were obtained from M- mode images; LV systolic function was also assessed from these measurements by calculating the fractional shortening and the ejection fraction (EF) and fractional shortening (FS).

Heart and body weight measurement

After 7 and 30 days post sham or TAC operation, mice (n=5 per operation) were sacrificed and their body weights were recorded. The heart was removed and, after PBS perfusion, weighed.

***RNA Extraction and Quantitative RT-PCR* (qPCR)**

Total RNA from tissue or cells was extracted using Trizol LS (Invitrogen) and RNeasy MinElute Cleanup Kit (Qiagen) according to manufacturer's instructions. The concentration and quality of extracted RNA were measured using a NanoDrop ND-1000 Spectrophotometer (Thermo Scientific). Complementary DNAs (cDNAs) was synthesized using the BioRad Reverse Transcriptase kit (BioRad). For qPCR, SYBR Green mix (BioRad) and primers (IDT DNA) targeting respective genes **(Sequences outlined in Supplementary Table2)** were added to the synthesized cDNA and run through a BioRad cell cycler (BioRad). We used the $\Delta\Delta$Ct method to analyze relative gene expressions. Technical replicates (n=3) and biological replicates (n=3) were performed. In all reprogramming experiments, gene expression values were normalized to cultured fibroblasts.

RNA Sequencing

Cells were isolated from sham- and TAC-operated hearts 7 and 30 days after operation (n=3 per group), and then sorted again directly into RTL buffer (Qiagen). Total RNA was extracted using RNeasy miniElute Cleanup Kit (Qiagen) according to manufacturer's instructions. The cDNA library was generated using the reagents provided in the SMARTer Stranded Total-RNA Seq kit Pico (Takara). The clustering was performed on a cBot cluster generation system using an Illumina HiSeq single read cluster generation kit (Illumina) according to the manufacturer's instructions. The amplified cDNA library was sequenced on an Illumina HiSeq 3000 for estimating transcript abundance (1X50 reads and >40 million reads/sample). The raw reads were generated by HiSeq 3000 sequencing control software and was mapped with OLego version 1.1.5[42]. and normalized by using TPM (Transcripts per millions) analysis. Total number of reads mapped to a known transcript annotation was estimated using feature Counts version v1.5.0-p2[43]. Expression levels for each transcript were determined by normalizing the counts returned by feature Counts using custom Perl scripts. Normalized expression levels for each transcript were determined by transforming the raw expression counts to TPM following log2 scaling.

Total number of reads mapped to the genome showed a bimodal distribution. This bimodal distribution separated high quality data and low-quality data. Clustering was performed using standard hierarchical agglomerative approach using Euclidian distance as a metric for complete linkage or centroid linkage; some clustering was performed using Cluster 3.0. Heat maps were generated using Java Treeview software. The statistical analyses were performed using Partek genomics Suite 6.6. Thresholds for selecting significant genes were set at >= 1.5-fold and $p<0.05$. Genes that met both criteria simultaneously were considered as significant changes.

Direct cardiac and neuronal Reprograming

To generate iCMs, fibroblasts were transduced with GMT or GMHT retroviruses as previously described[17]. In brief, isolated fibroblasts from the first passage were plated on gelatin (0.1%) coated dishes at 7500 cells/cm^2. 24 hours later media was changed and 0.5 μM A83-01 (Cayman Chemical) was added and kept throughout reprogramming. The next day fibroblasts were transduced for 24 hours with retroviruses containing 6 μg/ml polybrene (Sigma) then transferred to iCM media (10% FBS, 5% horse serum, 1% penicillin/streptomycin, 0.1 mm non-essential amino acids (Life Technologies), essential amino acids (Life Technologies), B-27 supplement (Life Technologies), insulin-selenium-transferrin (Life Technologies) and vitamin mixture (Sigma) in DMEM/M199 (4:1)). Media was changed every 2-3 days. After 4 weeks, reprogrammed cells were harvested for analyses.

Neuron-like cells were generated according to a previously described direct reprograming protocol[21]. Before reprogramming, glial cells were isolated from the brains of neonatal C57BL/6 mice (Post-natal day 1-5) followed by the protocol Neural Tissue Dissociation Kit (Miltenyi biotec). The cells were re-suspended in DMEM containing 500 mg/L glucose supplemented with 20% FBS, 200 mM L-glutamine, 100 U/ml penicillin, 0.1 mg/ml streptomycin and cultured in 75-cm2 flasks (10million cells/flask) for 10 days until the monolayers reached confluence. Media was changed every 2-3 day. The purity of the isolated glial cells was determined by ICC with glial specific marker, GFAP. After third passage, glial

cells were co-cultured with fibroblasts to increase the efficiency of neuronal reprogramming. First passage fibroblasts (7500 cells/cm^2) were transduced for 16-20 hours with retroviruses containing 8 µg/ml polybrene (Sigma). After replacing the media with fresh fibroblasts media (DMEM supplemented with 20% FBS and antibiotics) glial cells were added to the transduced plate of fibroblasts ($5X10^5$ glial cells/well). The next day, the media changed to N3 media (DMEM/F12 plus 1x N2 supplement, 10 ng/ml BDNF, 10 ng/ml CTNF, 10 ng/ml GDNF and 1 µg/ml puromycin) for additional 18 days before ICC and gene expression analyses. The media was changed every 2–3 days for the duration of the culture period.

Statistics

Statistical testing was performed with GraphPad Prism version 6. Results are presented as mean ± SEM and Student *t* test and 2 way-ANOVA are used for comparison analyses (significance was assigned for $P<0.05$). Biological replicates (n=5) were used. When representative FACS plots or IHC images are shown, at least three independent samples were analyzed from separate mice.

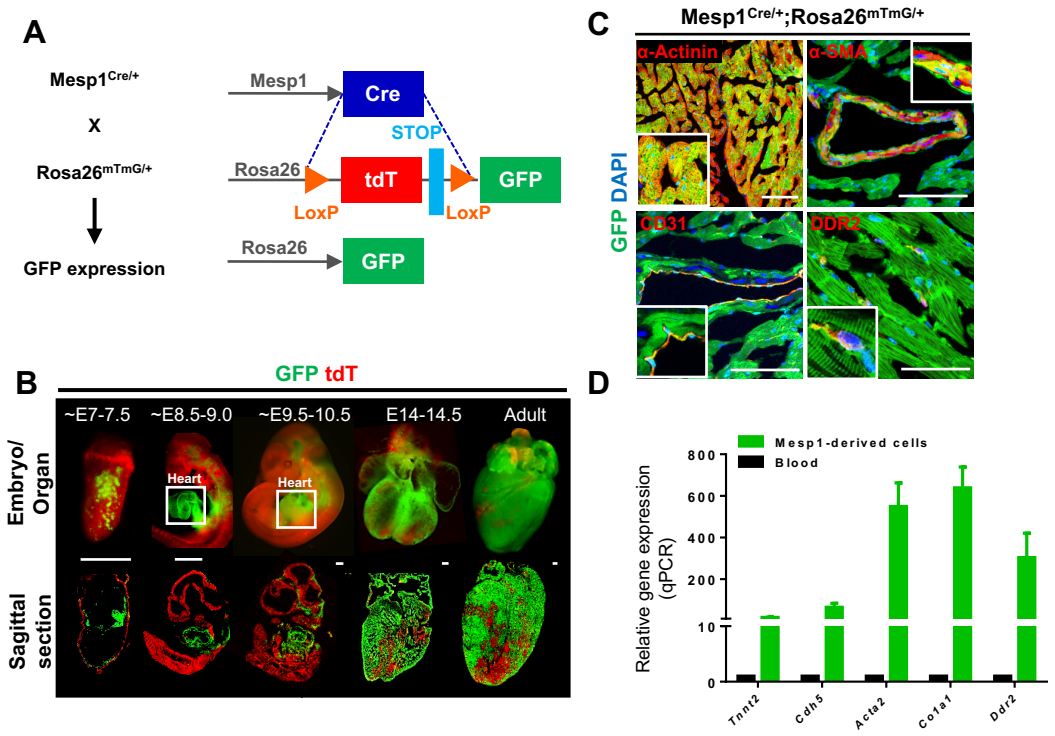

Figure 1. Lineage tracing of Mesp1 progenitors demonstrates contribution to the majority of cardiac cells including fibroblasts. (A) Schematic depiction of cell labeling by lineage tracing in the Mesp1$^{Cre/+}$;Rosa26$^{mTmG/+}$ model. **(B)** Lineage tracing of Mesp1-expressing cells at different stages of embryonic development to adulthood. **(C)** IF analysis of Mesp1$^{Cre/+;}$Rosa26$^{mTmG/+}$ adult mouse hearts stained with markers for cardiomyocytes (α-Actinin), smooth muscle cells (α-SMA), endothelial cells (CD31) and fibroblasts (DDR2). **(D)** The expression of different cardiac-specific genes was measured in Mesp1-derived cells from adult mouse heart in comparison to blood as control (n=5). Insets are the magnified images. Nuclei are stained with DAPI (blue). All error bars represent S.E.M. Scale bar: 100 μm. tdT: tdTomato, IF: Immunofluorescence, qPCR: quantitative PCR and DAPI: 4', 6-diamidino-2-phenylindole.

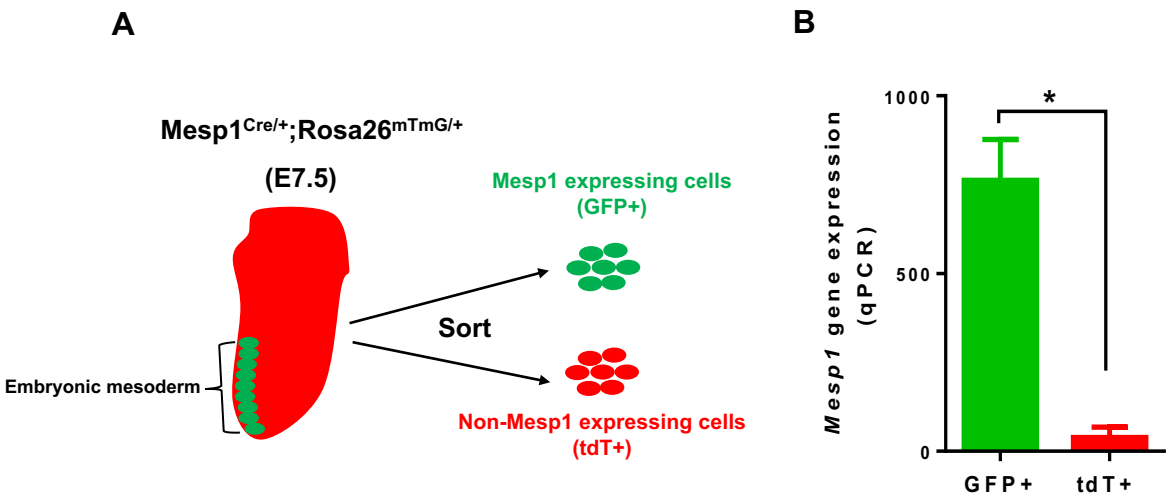

Supplementary Figure 1. Mesp1$^{Cre/+}$;Rosa26$^{mTmG/+}$ mouse model can be employed to isolate endogenous Mesp1-expressing cells during embryonic development. (A) Schematic showing that GFP and tdT expressing cells were sorted from E7.5 transgenic embryos using FACS. **(B)** The expression of *Mesp1* was measured in Mesp1-derived (GFP+) versus non-Mesp1 (tdT+)-derived cells from E7.5 embryos using qPCR. Whole hearts were used as reference. All error bars represent S.E.M. Unpaired T-test, * P<0.05. FACS: fluorescence activated cell sorting.

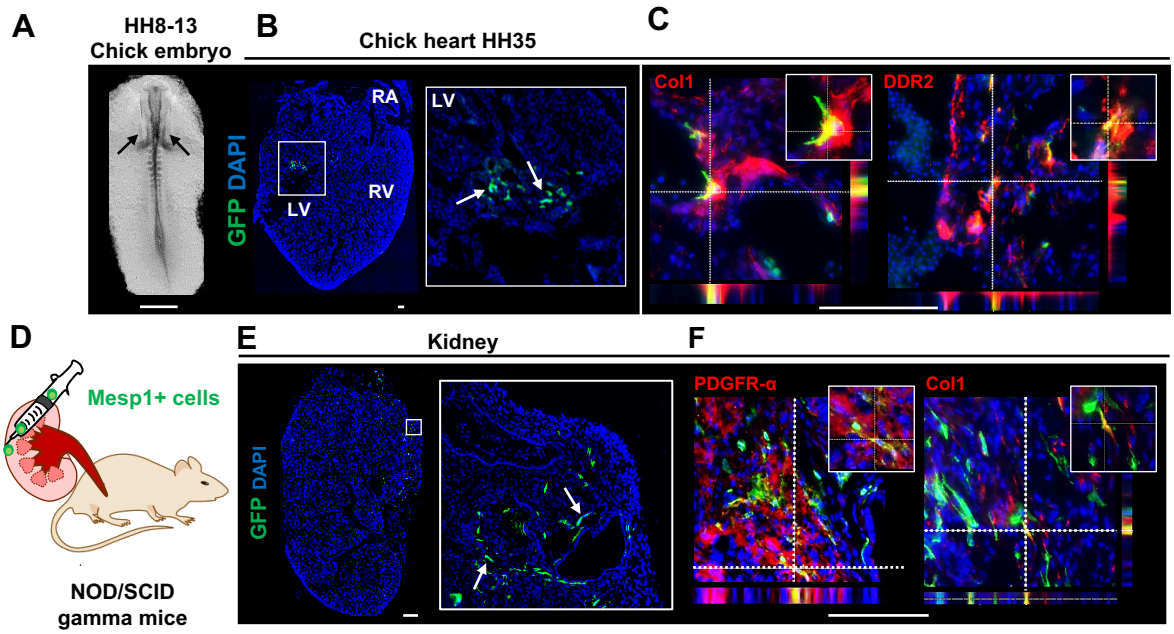

Figure 2. Mesp1-expressing cells generate fibroblasts after *in vivo* transplantation. (A) GFP+ cells from E7.5 Mesp1$^{Cre/+}$;Rosa26$^{mTmG/+}$ embryos were isolated and subsequently transplanted into the lateral plate mesoderm of chick embryos at HH stage 8-13 (black arrows, n=32 chick embryos). **(B and C)** GFP+ cells (white arrows) were observed in the left ventricle of the developing heart (stage HH35) and stained positive for fibroblast associated markers (Col1 and DDR2). Dashed lines indicate localization of the markers within eGFP+ Mesp1-derived cells. **(D)** Schematic depicts transplantation of Mesp1+ cells (isolated from E7.5 Mesp1$^{Cre/+}$;Rosa26$^{mTmG/+}$ embryos) into the kidney capsule of NOD/SCID gamma mice (n=5 mice). **(E)** Thirty days after injection, GFP+ cells were engrafted (white arrows) in the kidney capsule and stained positive for fibroblast markers (Col1 and PDGFRα). Insets are magnified images showing co-localization of GFP with fibroblast markers. Nuclei are stained with DAPI (blue). Scale bar: 500 μm (A, B and E), 100 μm (C and F). Col1: Collagen 1, HH: Hamburger Hamilton, RA: Right atrium, RV: Right ventricle and LV: Left ventricle.

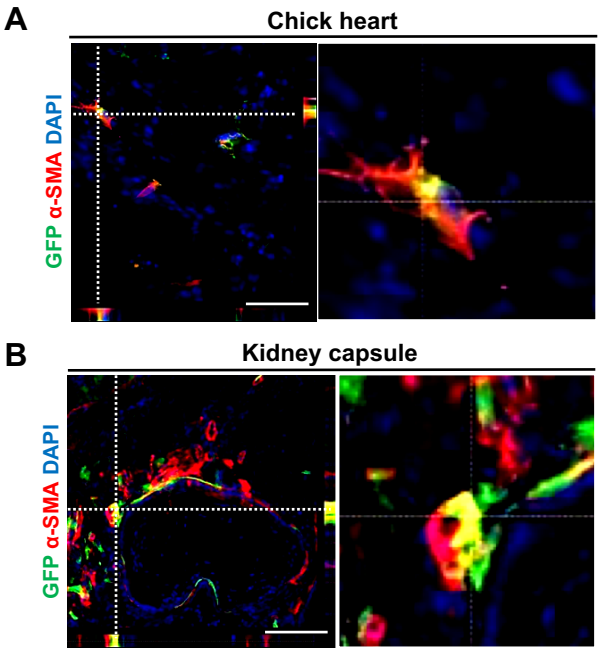

Supplementary Figure 2. Transplanted Mesp1-expressing progenitors generate α smooth muscle actin-expressing cells *in vivo*. GFP+ cells from E7.5 $Mesp1^{Cre/+}$;$Rosa26^{mTmG/+}$ embryos expressed α-SMA after transplantation into chick embryos (n=32 chick embryos) **(A)** and kidney capsule of NSG mice (n=8-10 mice). Insets are magnified z-stack images. Nuclei are stained with DAPI (blue). Scale bar = 100 μm.

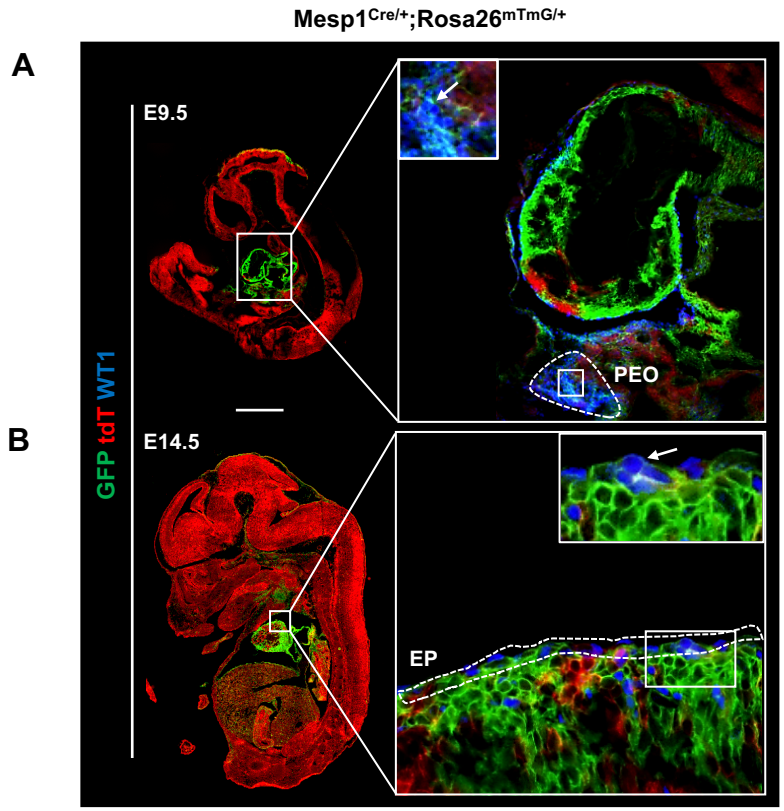

Supplementary Figure 3. Mesp1-derived cells contribute to the proepicardium (PEO) and epicardium (EP). Co-staining of Mesp1- (green) and non-Mesp1-derived (red) cells with WT1 (blue) on sections from E9.5 **(A)** and E14.5 **(B)** Mesp1$^{Cre/+}$;Rosa26$^{mTmG/+}$ embryos. Inset is the magnified area of the box. Arrows indicate lineage traced Mesp1 cells that express WT1. The dotted line encircles the in **(A)** and EP in **(B)**. n=10 embryos/time point. Scale bar: 1 mm. WT1: Wilms Tumor 1, PEO: Proepicardium, EP: Epicardium.

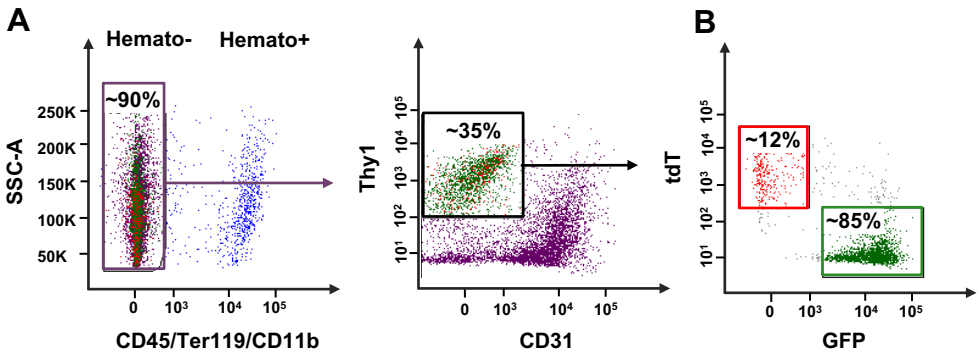

Supplementary Figure 4. Mesp1-derived cells contribute to the majority of CFbs in adult mouse hearts. After exclusion of hematopoietic cells (CD45+, Ter119+), macrophages (CD11b+), and endothelial cells (CD31+) **(A)**, the percentage of Thy1+GFP+ and Thy1+tdT+ cells were analyzed by flow cytometry **(B)**.

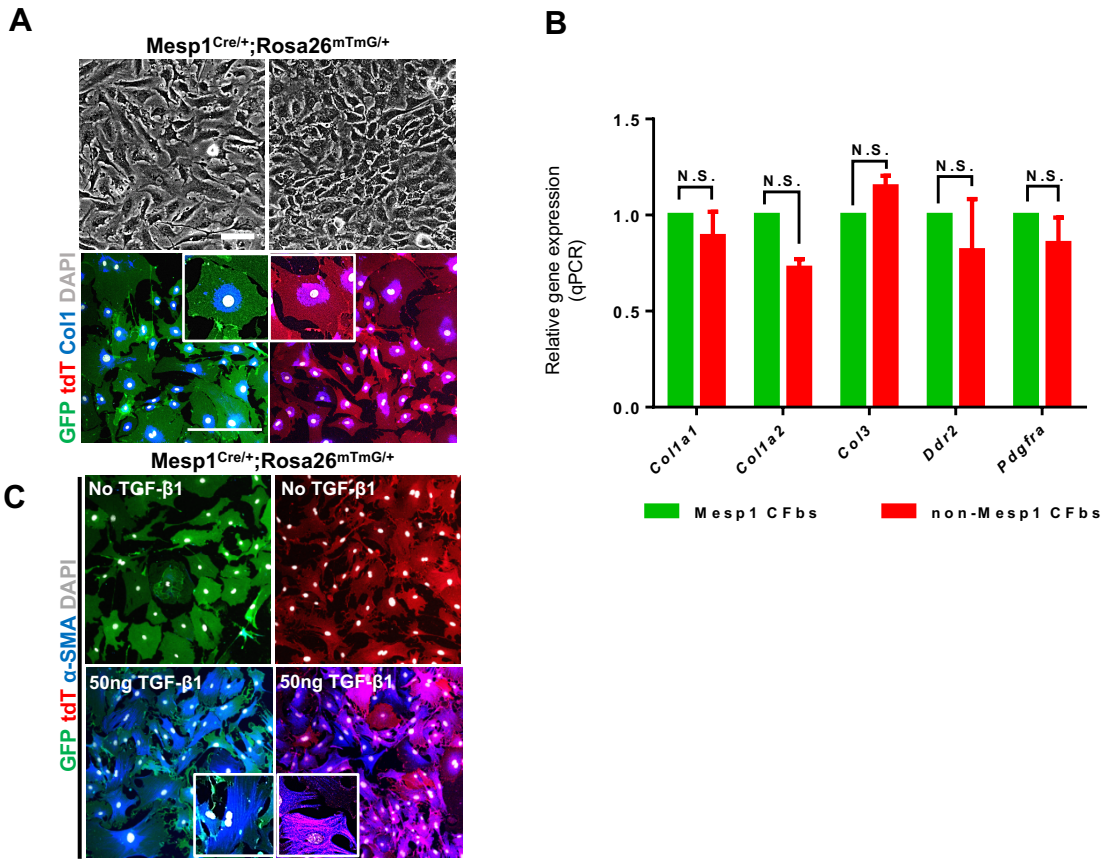

Supplementary Figure 5. Mesp1- and non-Mesp1-derived CFbs exhibit similar phenotypes *in vitro*. (A) After sorting, Mesp1-derived (GFP+) and non-Mesp1-derived (tdT+) CFbs from Mesp1$^{Cre/+}$;Rosa26$^{mTmG/+}$ mice showed spindle shaped morphology in culture and stained positive for the fibroblast marker Col1 (blue). **(B)** qPCR analysis of GFP+ and tdT+ CFbs for several genes associated with fibroblasts. **(C)** Exposure to TGF-β1 induced expression of α-SMA in both sub-populations of cultured CFbs. Scale bar = 100 μm. n=5 hearts. All error bars represent S.E.M. T-test, N.S. P>0.05. TGF-β1: transforming growth factor β1.

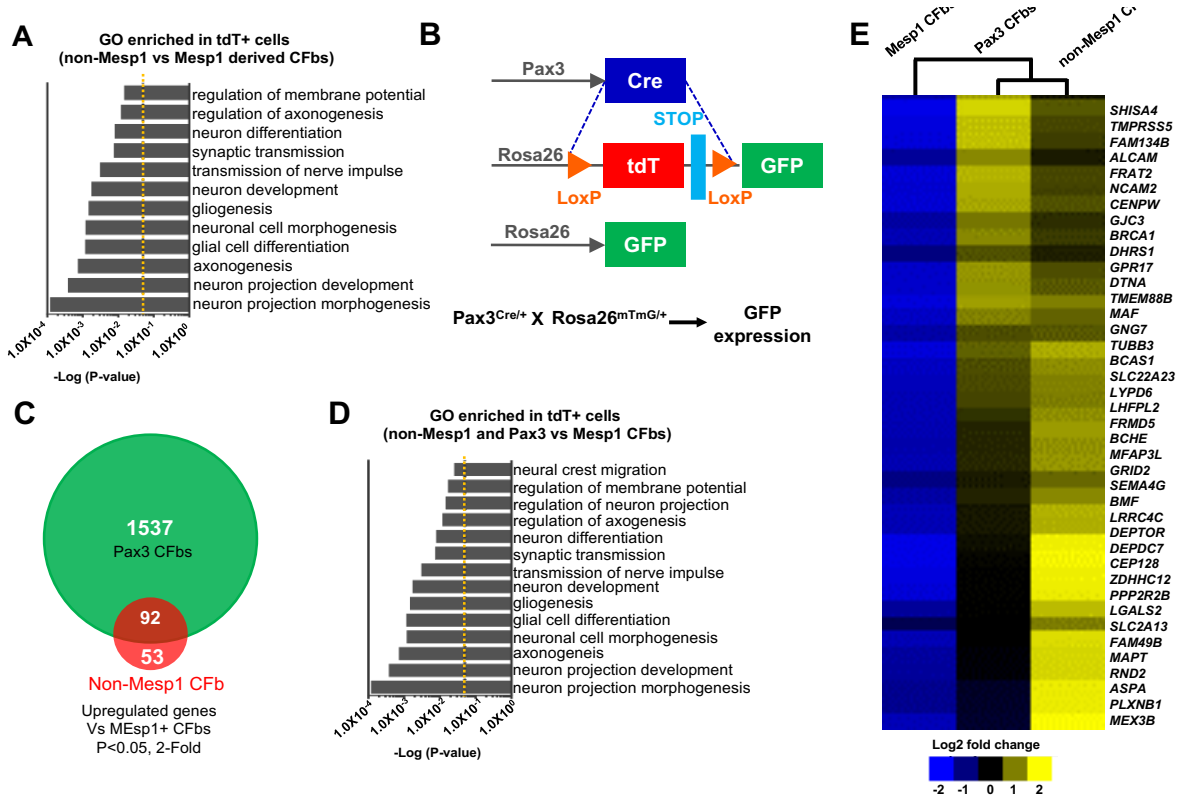

Figure 3. Non-Mesp1 derived CFbs are enriched in neuronal-associated genes and display similarities to Pax3 neural crest-derived CFbs. (A) Using a Mesp1$^{Cre/+;}$Rosa26$^{mTmG/+}$ mouse model, Mesp1- (GFP+) and non-Mesp1-derived (tdT+) CFbs were isolated for RNA-seq analysis. The top categories from GO analysis of upregulated genes in non-Mesp1-derived CFbs were associated with neuronal development and maturation. **(B)** Schematic depiction of cell labeling by lineage tracing in the Pax3$^{Cre/+}$;Rosa26$^{mTmG/+}$ model. **(C)** Venn diagram showing the overlap of upregulated genes between non-Mesp1- and Pax3-derived CFbs when compared to Mesp1-derived CFbs. **(D)** Selected categories from GO analysis of shared upregulated genes in non-Mesp1- and Pax3-derived CFbs compared to Mesp1-derived CFbs, which depicts pathways associated with neuronal development and regulation. **(E)** Heat map of selected shared, differentially expressed genes demonstrates that non-Mesp1-derived CFbs and Pax3-derived CFbs clustered together and were highly enriched in neuronal associated genes. n=2 per group. Dashed line indicates significance P<0.05. GO: Gene Ontology.

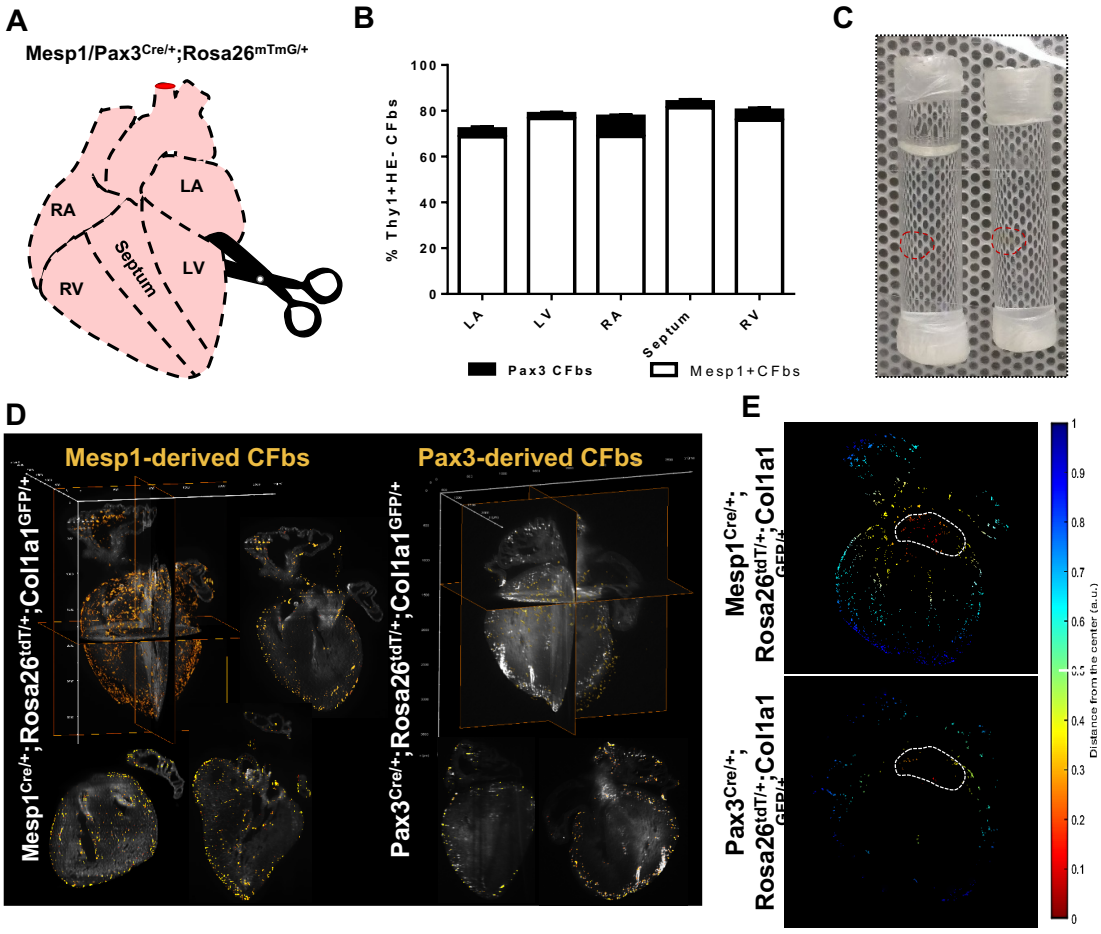

Supplementary Figure 6. Anatomical distribution of Mesp1- and Pax3-derived CFbs. (A) Adult hearts from Mesp1$^{Cre/+}$;Rosa26$^{mTmG/+}$ or Pax3$^{Cre/+}$;Rosa26$^{mTmG/+}$ mice were dissected into different compartments, representing right and left atria, right and left ventricles, and the septum. **(B)** Flow cytometry analysis showed the percentage of Mesp1- and Pax3-derived CFbs within different anatomical compartments (n=8-10 mice). **(C)** Embryonic hearts from embryos at E16.5 were made translucent using the CLARTY method. **(D)** 3D light-sheet microscopic images of cleared E16.5 Mesp1$^{Cre/+}$;Rosa26$^{tdT/+}$;Col1a1$^{GFP/+}$ and Pax3$^{Cre/+}$;Rosa26$^{tdT/+}$;Col1a1$^{GFP/+}$ hearts. Lineage-derived CFbs (gold) can be visualized at the single-cell resolution throughout the intact hearts. **(E)** The distance of arbitrary lineage-derived CFbs from the outflow tract region (dotted line area) were depicted by color, with red being the closest and sapphire being the furthest. Scale bar: 500 μm. All error bars represent S.E.M. LA: left atrium, LV: left ventricle, RA: right atrium and RV: right ventricle.

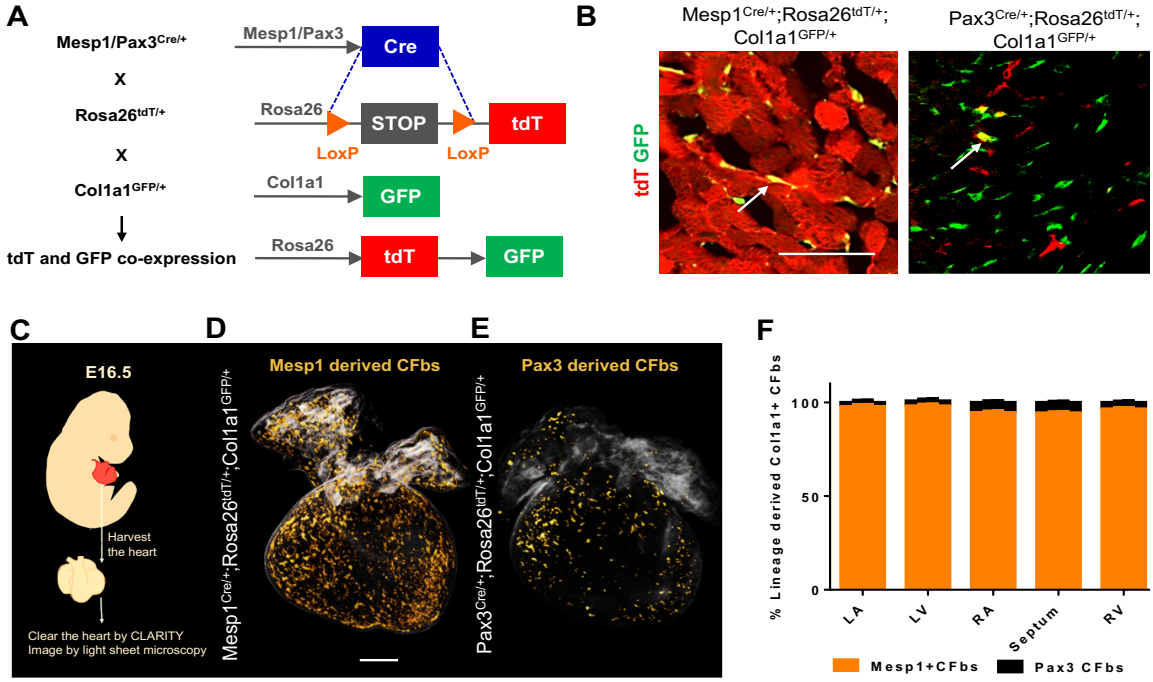

Figure 4. Mesp1- and Pax3-derived CFbs show distinct anatomical localization. (A) Schematic depiction for labeling and lineage tracing of CFbs by crossing Col1a1$^{GFP/+}$ with lineage-specific cre mice. **(B)** Confocal images of Mesp1- or Pax3-lineage-derived CFbs (tdT+GFP+, arrow). **(C)** Schematic showing sample preparation for CLARITY and light-sheet microscopy. 3D light-sheet microscopy of the cleared hearts (using CLARITY) shows distribution of Mesp1-derived **(D)** and Pax3-derived CFbs **(E)** within the intact heart**. (F)** Flow cytometry analysis of lineage derived CFbs in different heart compartments (n=5-6 hearts/lineage). Scale bar: 500μm. All error bars represent S.E.M. LA: left atrium, LV: left ventricle, RA: right atrium and RV: right ventricle.

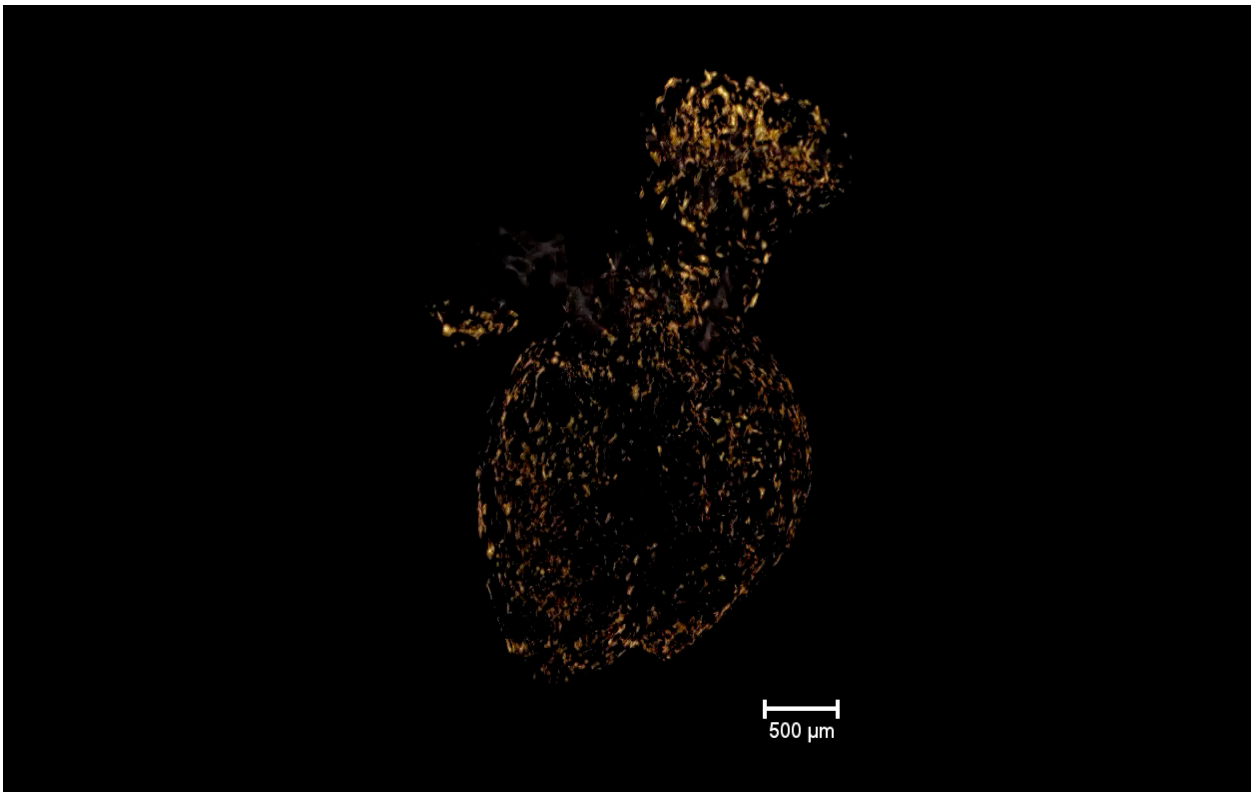

Supplementary video 1.

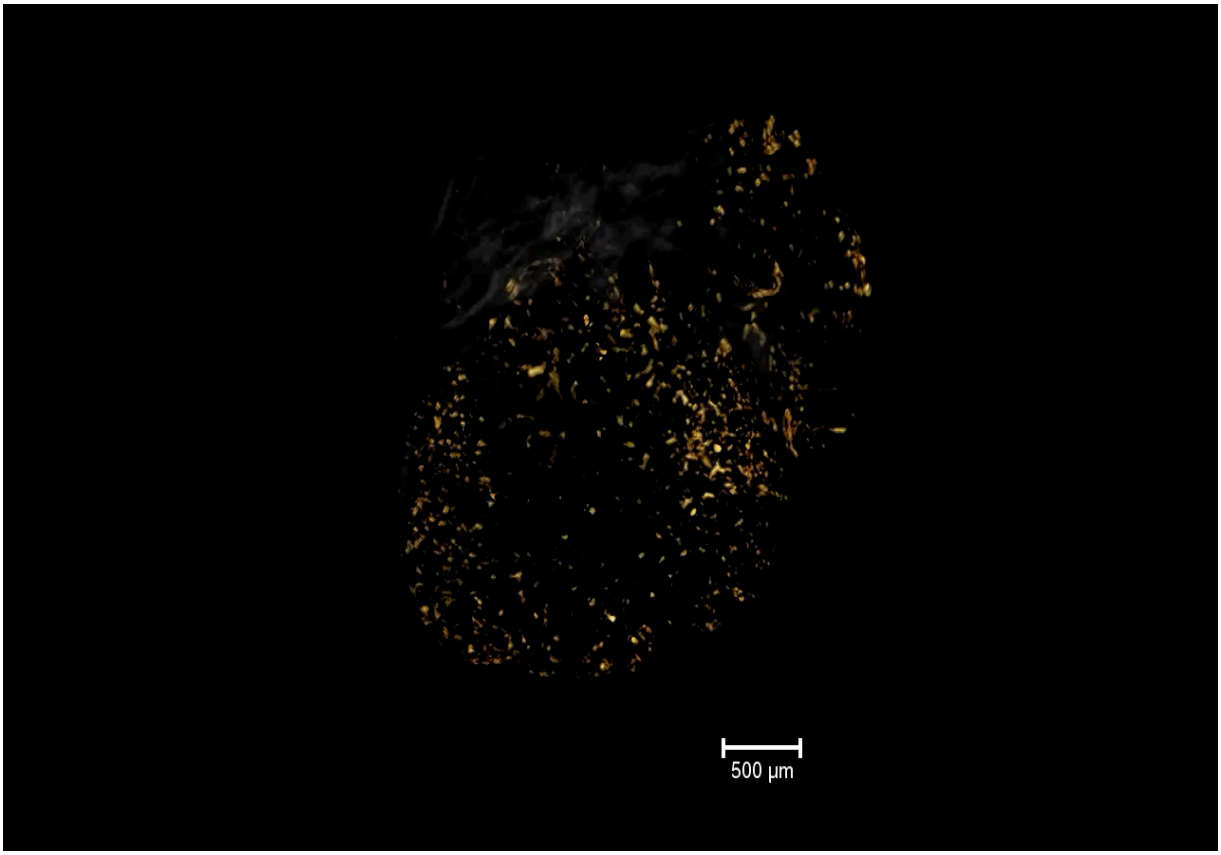

Supplementary video 2

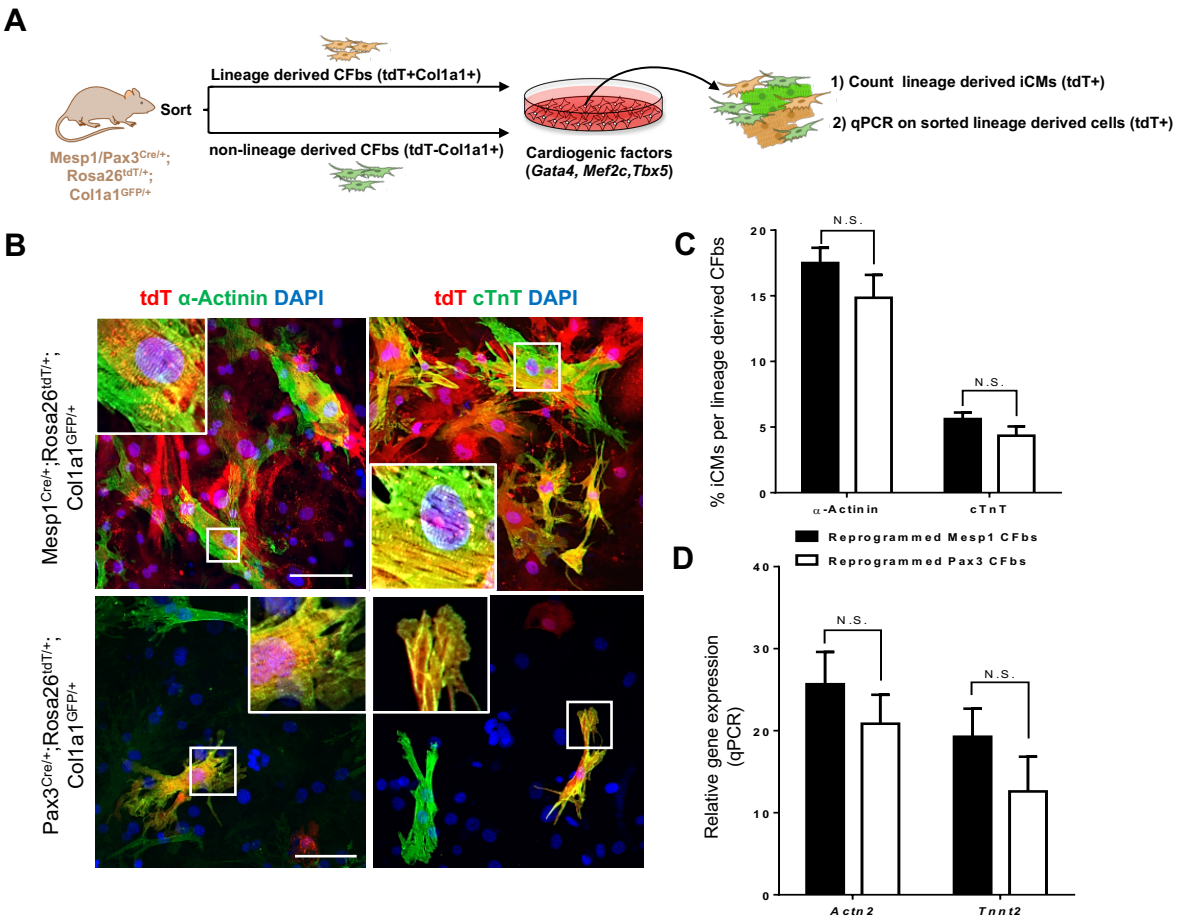

Figure 5. Mesp1- and Pax3-derived CFbs can be directly reprogrammed to generate iCMs. **(A)** Schematic of direct reprogramming approach to generate iCMs. **(B)** ICC analysis of lineage-derived cells stained for cardiomyocyte markers (green). **(C)** Quantitative comparison of the number of lineage-derived iCMs (tdT+α-Actinin+ or tdT+cTnT+) over the total number of lineage-derived cells (tdT+) (n=20 well/lineage). **(D)** qPCR analysis of cardiomyocyte-specific genes in the lineage-derived cells after sorting (n=10 well/lineage). Nuclei are stained with DAPI (blue). Scale bar: 100 μm. All error bars represent S.E.M. T-test, N.S. P>0.05. ICC: Immunocytochemistry, cTnT: cardiac troponin T and iCMs: induced cardiomyocytes.

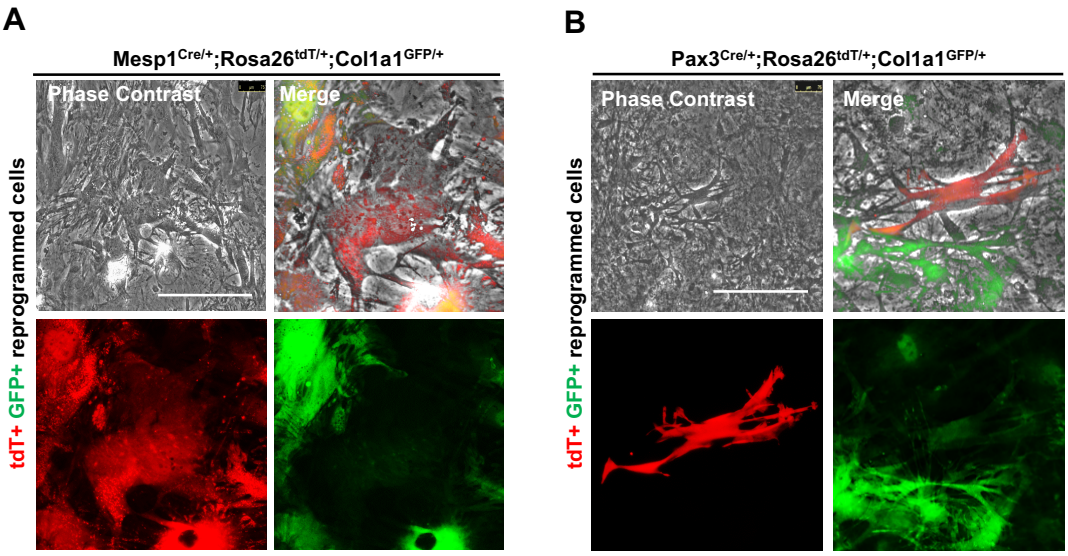

Supplementary figure 7. Spontaneous contraction of lineage-derived iCMs. iCMs from both Mesp1-derived CFbs **(A)** and Pax3-derived CFbs **(B)** demonstrated spontaneous contraction after 30 days of reprogramming.

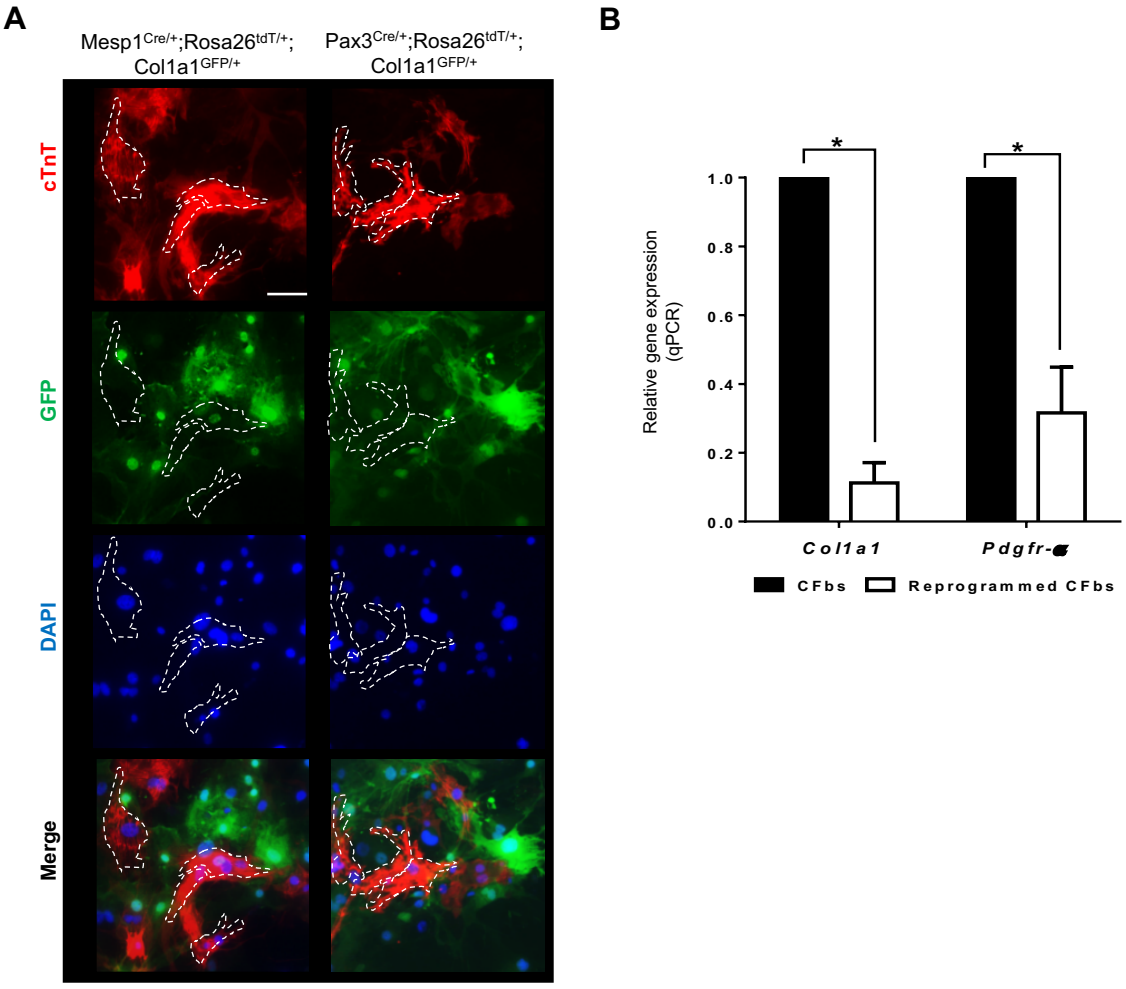

Supplementary Figure 8. iCMs downregulate expression of fibroblast markers. (A) Col1 expression was drastically reduced in reprogrammed iCMs. **(B)** qPCR analysis of genes associated with fibroblasts in reprogrammed CFbs (n=6 well/lineage). Nuclei are stained with DAPI. Scale bar: 100 μm. All error bars represent S.E.M. T-test, * P<0.05.

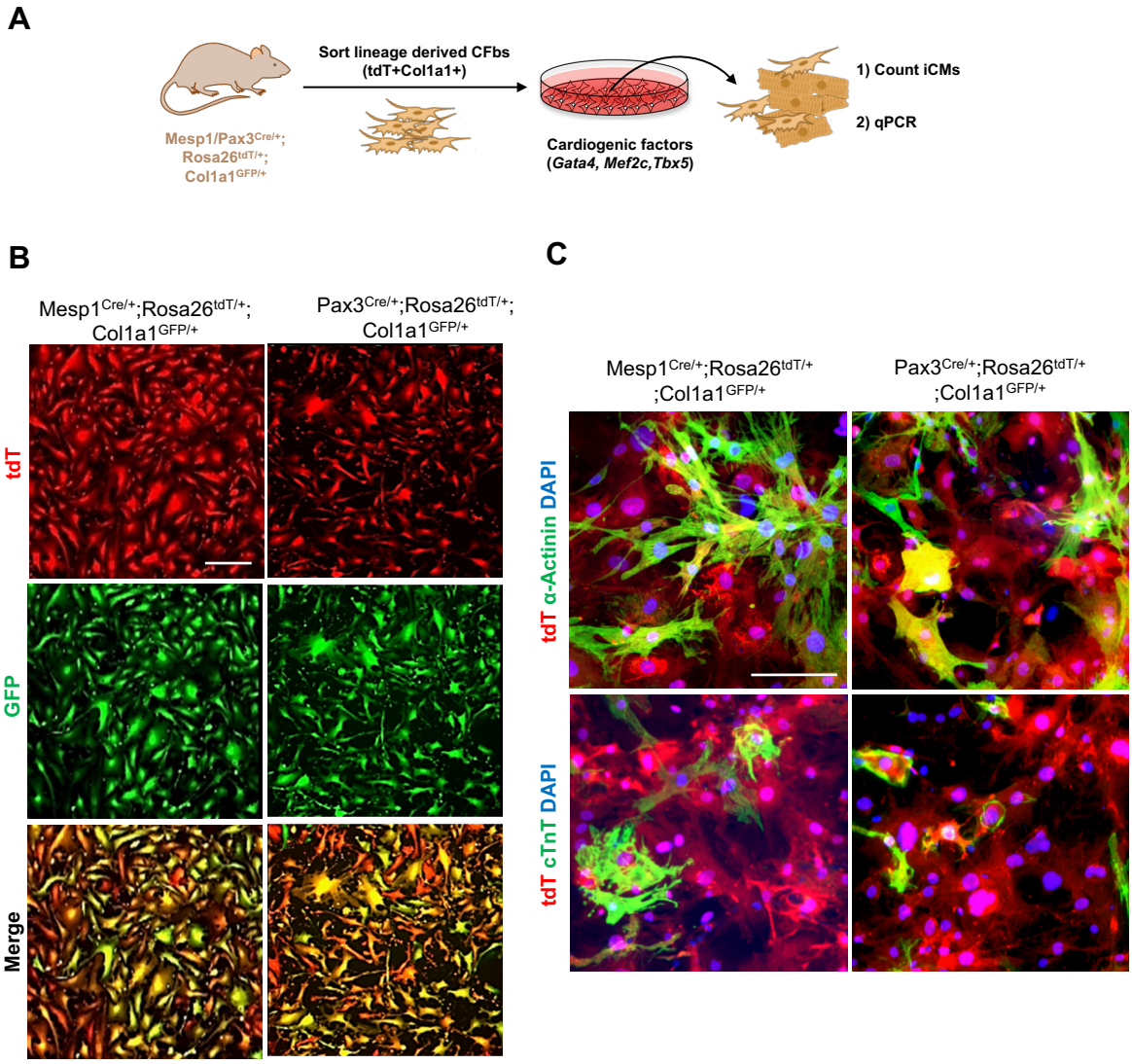

Supplementary Figure 9. Direct cardiac reprogramming of Mesp1- and Pax3-derived CFbs. (A) Schematic showing the experimental design where Mesp1- or Pax3-derived CFbs were isolated separately for reprogramming and subsequent analysis. **(B)** Lineage traced CFbs (tdT+GFP+) were sorted from Mesp1$^{Cre/+}$;Rosa26$^{tdT/+}$;Col1a1$^{GFP/+}$ or Pax3$^{Cre/+}$;Rosa26$^{tdT+/}$;Col1a1$^{GFP/+}$ mice (n=15 heart/lineage). Cultured cells retained their mesenchymal morphology after 3 passages. **(C)** ICC analysis of lineage-derived iCMs stained for cardiomyocyte markers after 30 days of direct reprogramming (α-Actinin and cTnT). Nuclei are stained with DAPI. Scale bar: 100 μm.

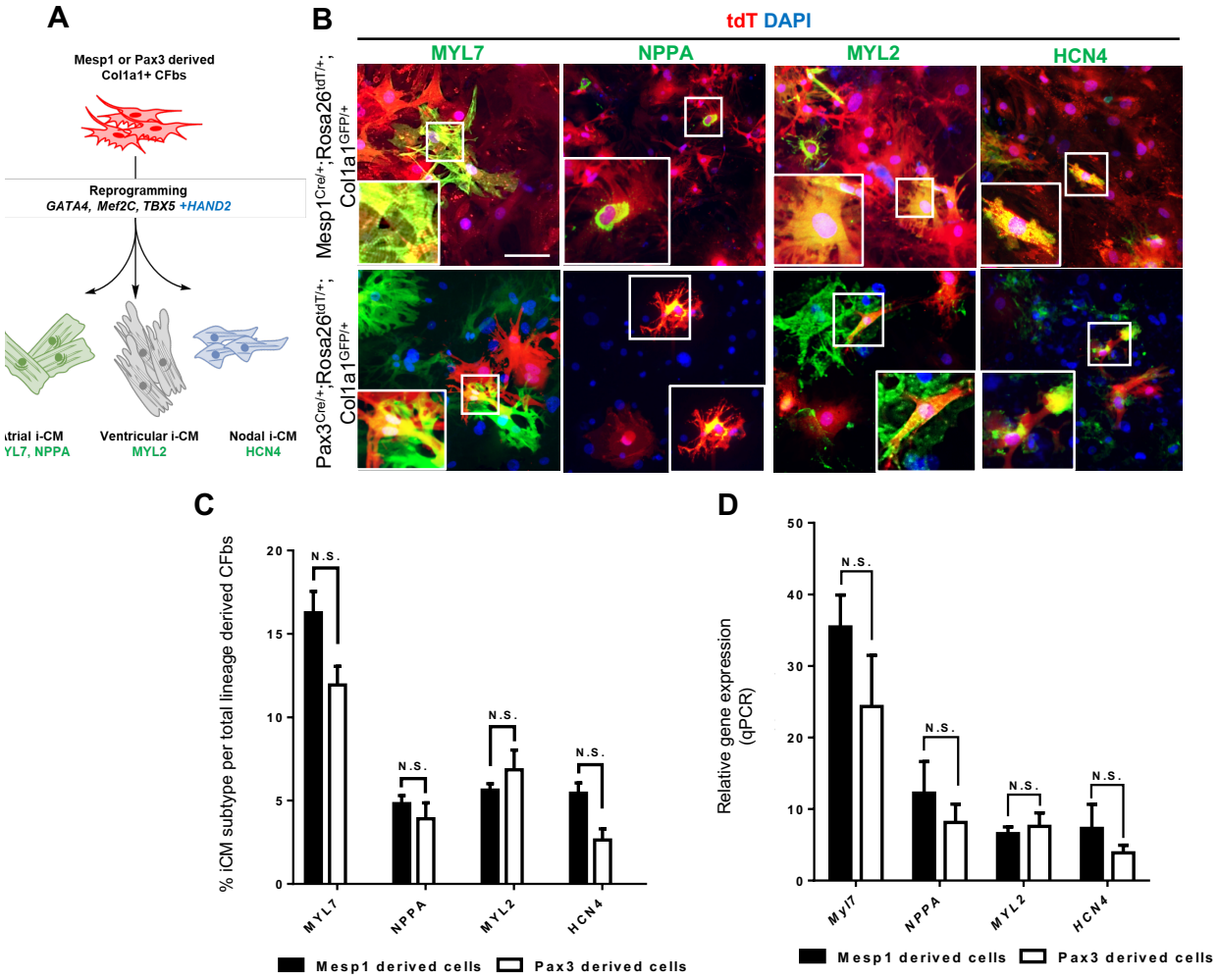

Supplementary Figure 10. Mesp1- and Pax3 -derived CFbs can be reprogrammed to generate different subtypes of iCMs. (A) Schematic of direct reprogramming approach to generate different iCMs subtypes. **(B)** ICC of reprogrammed Mesp1- or Pax3-derived CFbs with markers associated with atrial (MYL7 and NPPA), ventricular (MYL2) and nodal (HCN4) cardiomyocytes. Insets show boxed areas at higher magnification. **(C)** Quantitative comparison of the number of lineage-derived iCM subtypes over the total number of lineage derived cells (n=15 well/lineage/group). **(D)** qPCR analysis of genes associated with cardiomyocyte subsets in lineage derived cells after sorting (n=10 well/lineage). Nuclei are stained with DAPI. Scale bar: 100 μm. All error bars represent S.E.M. Two-way ANOVA, N.S. P>0.05.

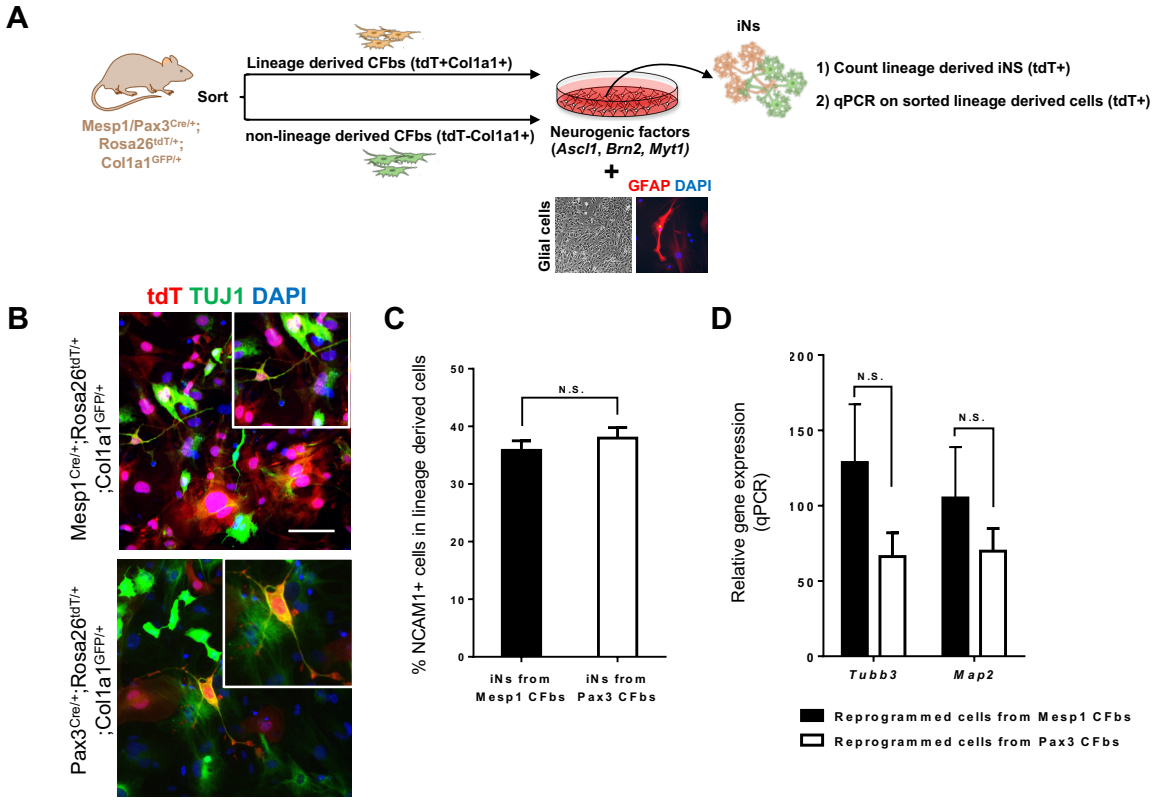

Supplementary Figure 11. Mesp1- and Pax3-derived CFbs generate iNs after direct reprogramming. **(A)** Schematic showing the direct reprogramming approach to generate induced neurons (iNs). **(B)** ICC analysis of lineage-derived iNs stained for a pan-neuronal marker, TUJ1 (green) (n=10 hearts/lineage). **(C)** Percentage of NCAM1+ iNs generated from Mesp1- or Pax3-derived CFbs, 21 days post-viral infection measured by flow cytometry (n=3 heart/lineage). **(D)** The efficiency of iN reprogramming was measured by qPCR analysis of neuronal markers in lineage-derived cells (n=4 hearts/lineage). Nuclei are stained with DAPI. Scale bar: 100 μm. All error bars represent S.E.M. T-test. N.S. P>0.05. iNs: induced neurons.

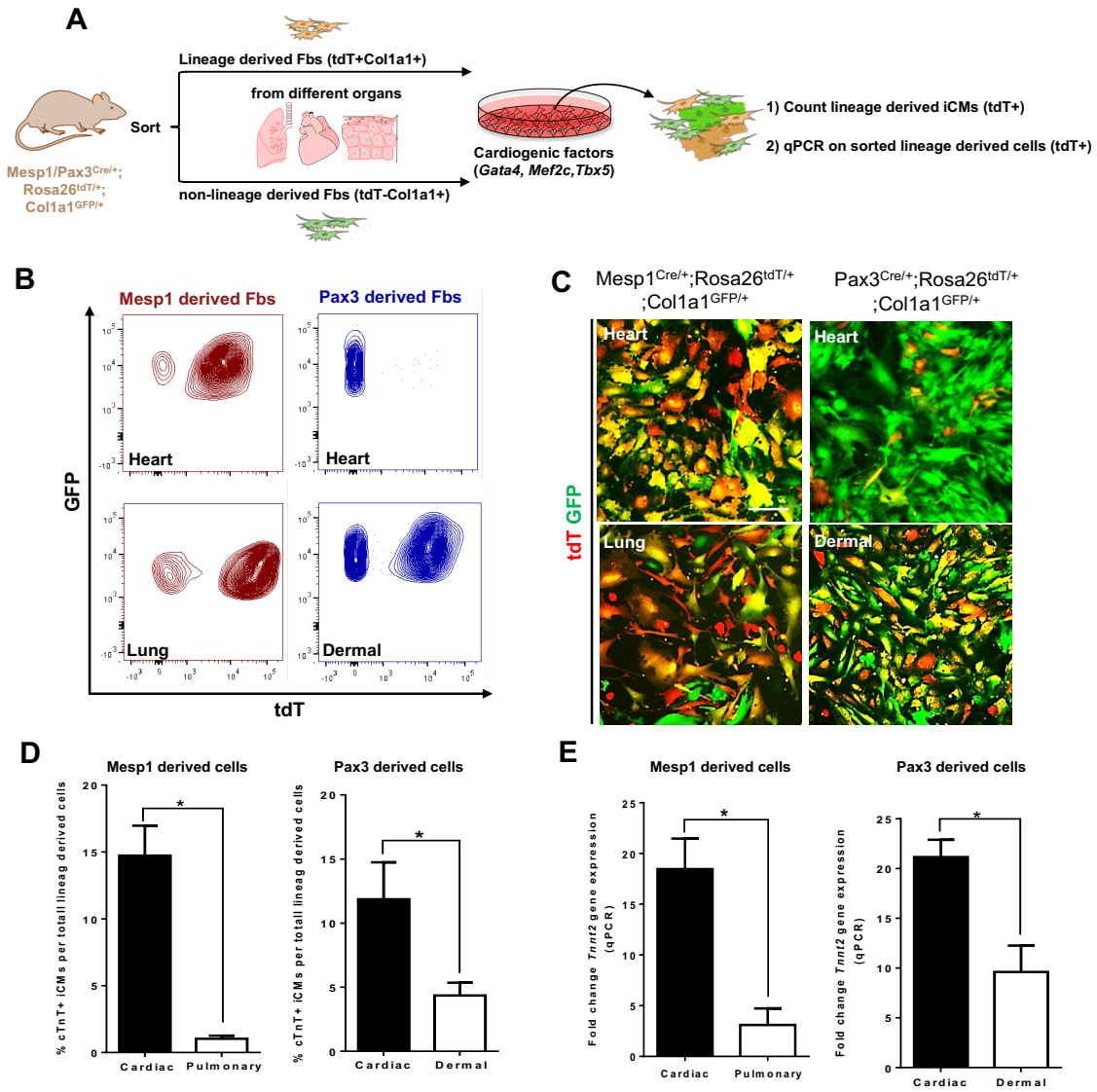

Figure 6. The efficiency of cardiac reprogramming mainly depends on the fibroblast organ of residence. (A) Schematic representation of the experimental design. **(B)** Flow cytometry analysis of lineage-derived fibroblasts isolated from different organs of Mesp1$^{Cre/+}$;Rosa26$^{tdT/+}$;Col1a1$^{GFP/+}$ or Pax3$^{Cre/+}$;Rosa26$^{tdT/+}$;Col1a1$^{GFP/+}$ mice (n=3-4 mice/lineage). **(C)** Freshly isolated Col1a1+ fibroblasts in culture were transduced after x days in culture without passaging them. **(D)** Quantitative comparison of lineage-derived cTnT+ iCMs over the total number of lineage derived cells (tdT+) (n=10 wells/organ). **(E)** The expression of *Tnnt2* gene in lineage derived cells (tdT+) was measured after sorting by qPCR (n=5 wells/organ). Scale bar: 100 μm. All error bars represent S.E.M. T-test. * P<0.05.

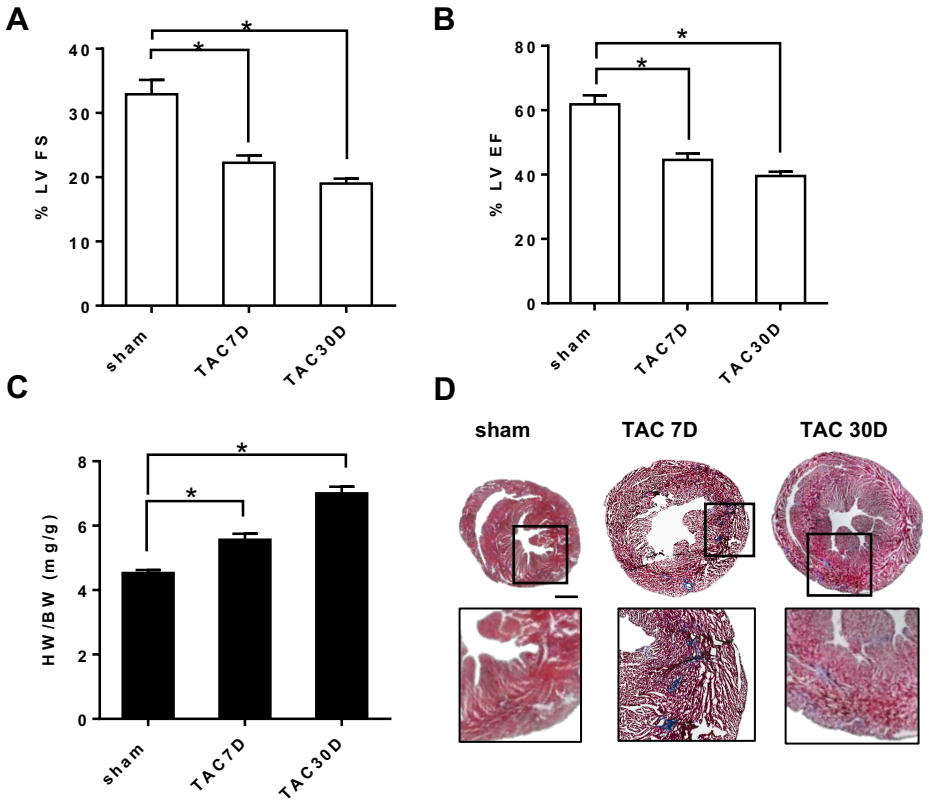

Supplementary Figure 12. Characterization of mice undergoing TAC injury. Fractional shortening **(A)** and ejection fraction **(B)** were measured by echocardiography. **(C)** The heart weight/body weight ratio in sham and TAC operated mice. **(D)** Masson's trichrome was used to visualize the extent of fibrosis. Scale bar: 1 mm. All error bars represent S.E.M., Two-way ANOVA, * $P<0.05$, n=6mice/surgical group. HW: heart weight, BW: body weight, EF: Ejection fraction and FS: Fractional shortening.

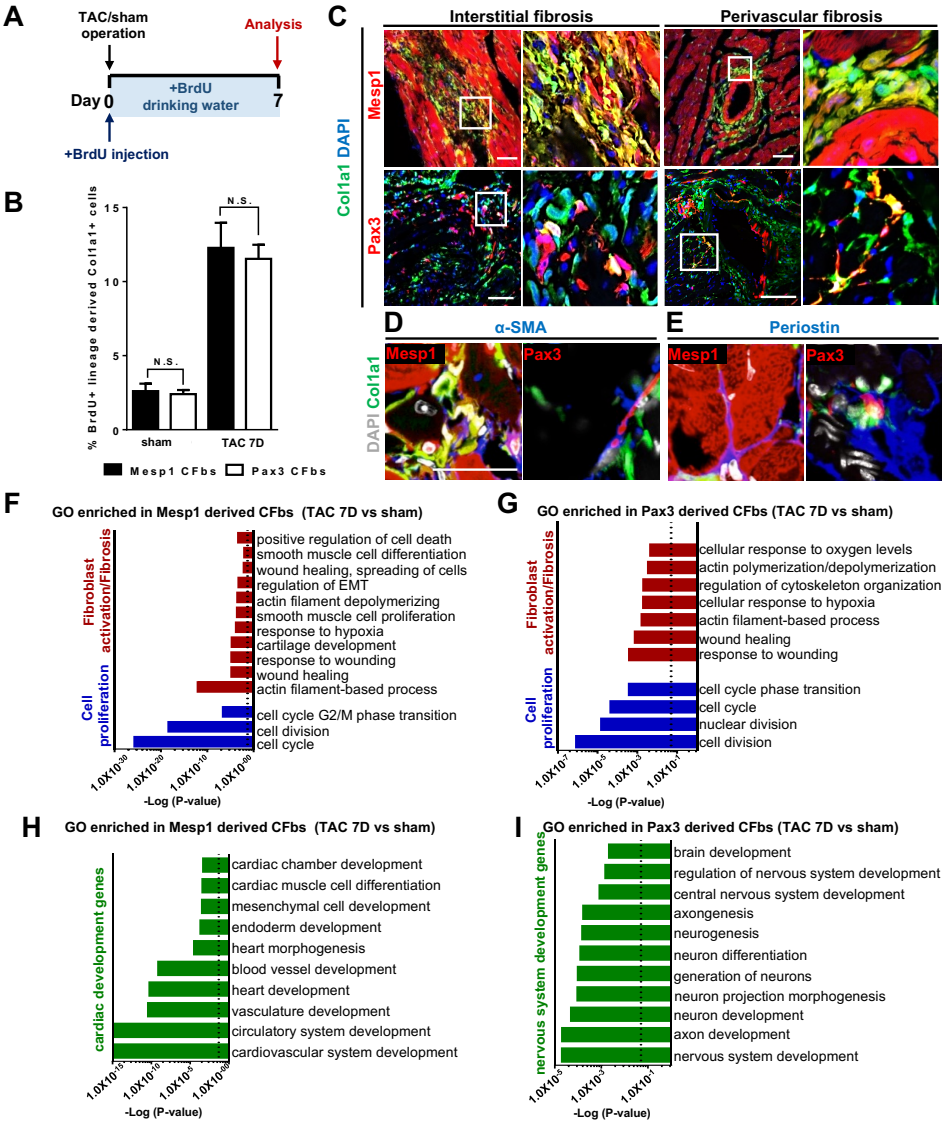

Figure 7. Mesp1- and Pax3-derived CFbs show unique re-expression of early developmental genes after TAC despite similar proliferation rates and contributions to scar formation. (A) Schematic representation outlining BrdU administration. **(B)** The percentage of BrdU+ Mesp1- and Pax3-derived CFbs similarly increased at 7 days post-TAC surgery (n=5-6 heart/lineage/surgical group). **(C)** Lineage traced CFbs were localized in both interstitial and perivascular fibrotic areas 7 days post-TAC and stained positive for markers associated with activated fibroblasts (α-SMA in **D** and Periostin in **E**). The top categories from GO analysis that were enriched in 7 days post-TAC relative to sham in Mesp1-derived CFbs **(F and H)** and Pax3-derived CFbs **(G and I)**, n=3-4 heart/lineage. Nuclei are stained with DAPI. Scale bar: 100 μm in C and 50 μm in D and E. All error bars represent S.E.M. Two-way ANOVA, N.S. P>0.05. Dashed line indicates significance P<0.05.

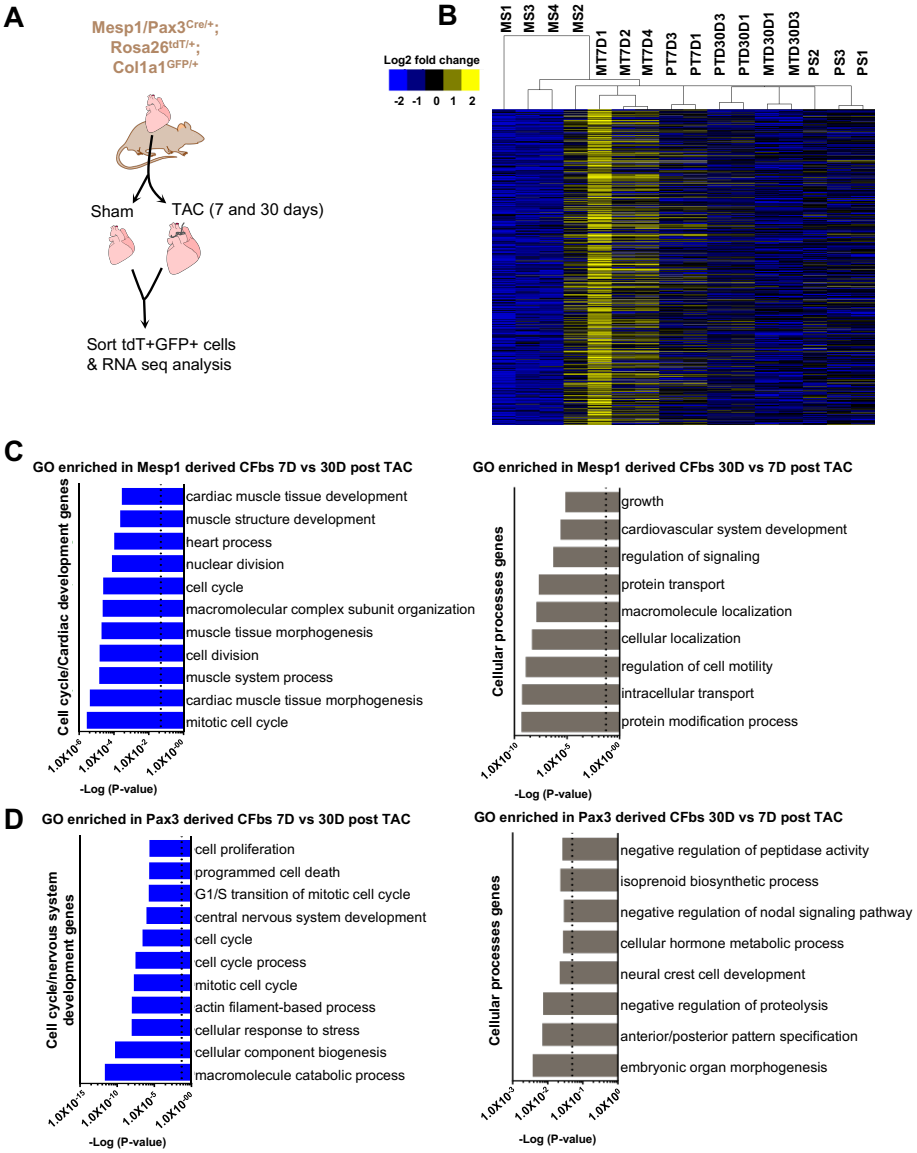

Supplementary Figure 13. Comparison of gene expression in Mesp1- and Pax3-derived CFBs 7 and 30 days after TAC. (A) Schematic representation of the RNA-seq experimental design. **(B)** Heat map and hierarchical clustering of genes expressed (TPM > 1.75 in at least 1 sample) of all groups (Mesp1- and Pax3-derived CFBs in sham, 7 days and 30 days post-TAC). Yellow indicates up-regulated genes and blue indicates down-regulated genes. The top categories from Gene Ontology (GO) analysis enriched in 7 and 30 days post-TAC operated hearts in Mesp1-derived CFBs **(C)** and Pax3-derived CFBs **(D)**. Dashed line indicates significance P<0.05. MS: Mesp1 sham, MT7D: Mesp1 TAC 7-day post TAC and MT30D: Mesp1 TAC 30-day post TAC.

Supplemental Table 1: Antibodies used for flow cytometry and immunostaining

Antibody	Catalog number	vendor
Collagen 1	Ab34710	Abcam
α-SMA	A2547	Sigma-Aldrich
PDGFR-α	Sc-338	Santa Cruz Biotechnology
Periostin	AF2955	R&D Systems
DDR2	MAB25381	R&D Systems
CD31	ab28364	Abcam
WT1	ab89901	Abcam
α-Actinin	A7811	Sigma-Aldrich
cTnT	MS-295-P0	Thermo Fisher Scientific
MYL7	17283-I-AP	Proteintech
NPPA	AP8534a	ABGENT
MYL2	10406-I-AP	Proteintech
HCN4	AB5808	Millipore
NCAM-1/CD56	FAB7820A	R&D Systems
GFAP	D1F4Q	Cell Signaling
TUJ1	ab78078	Abcam
Anti-Mouse CD 90.1 APC-eFluor 780	47-0900-82	eBioscience
Anti-Mouse CD 90.2 APC-eFluor 780	47-0900-82	eBioscience
Anti-Mouse CD31 PE-Cyanine7	25-0311-81	eBioscience
Anti-Mouse CD11b PE-Cyanine7	25-0112-81	eBioscience
Anti-Mouse CD45 PE-Cyanine5	48-0451-82	eBioscience
TER-119 PE-Cyanine7	25-5921-81	eBioscience
Donkey Anti-Rabbit Alexa Fluor 647	A-31573	Invitrogen
Rabbit Anti-Mouse Alexa Fluor 647	A-21239	Invitrogen
Chicken Anti-Rat Alexa Fluor 647	A-21472	Invitrogen
Goat Anti-Rabbit Alexa Fluor 594	A-11037	Invitrogen
Goat Anti-Rabbit Alexa Fluor 488	A-21206	Invitrogen
Goat Anti-Mouse Alexa Fluor 488	A-11001	Invitrogen
BD APC BrdU Flow Kit	BDB552598	BD Pharmigen

Supplemental Table 2: qPCR primers

Gene	Forward Primer	Reverse Primer
GAPDH	TTGTCTCCTGCGACTTCAAC	GTCATACCAGGAAATGAGCTTG
COL1A1	GCCAAGAAGACATCCCTGAAG	TGTGGCAGATACAGATCAAGC
COL1A2	GCCACCATTGATAGTCTCTCC	CACCCCAGCGAAGAACTCATA
COL3	TAGGACTGACCAAGGTGGCT	GGAACCTGGTTTCTTCTCACC
ACTA2	TGACGCTGAAGTATCCGATAGA	CGAAGCTCGTTATAGAAAGAGTGG
DDR2	CTGTGGGAGACCTTCACCTT	TAGATCTGCCTCCCTTGGTC
ACTN2	GACCATTATGATTCCCAGCAGAC	CGGAAGTCCTCTTCGATGTTCTC
PDGFR-α	GGACTTACCCTGGAGAAGTGAGAA	ACACCAGTTTGATGGATGGGA
TNNT2	GAAGTTCGACCTGCAGGAAA	TTCCCACGAGTTTTGGAGAC
MESP1	TGTACGCAGAAACAGCATCC	TTGTCCCCTCCACTCTTCAG
MYL7	GGCACAACGTGGCTCTTCTAA	TGCAGATGATCCCATCCCTGT
NPPA	GCTTCCAGGCCATATTGGAG	GGGGGCATGACCTCATCTT
MYL2	ATCGACAAGAATGACCTAAGGGA	ATCGACAAGAATGACCTAAGGGA
HCN4	TTGACTCGGAGGTCTACAAAAC	CAGGTCATAGGTCATGTGGAAG
TUBB3	TAGACCCCAGCGGCAACTAT	GTTCCAGGTTCCAAGTCCACC
MAP2	TTGGTGCCGAGTGAGAAGA	GTCTGGCAGTGGTTGGTTAA
CDH5	CAGCAACTTCACCCTCATAAAC	TCCCGATTAAACTGCCCATAC

CHAPTER 4

Genetic Regulation of Fibroblasts Activation and Proliferation in Fibrosis

Genetic Regulation of Fibroblast Activation and Proliferation in Cardiac Fibrosis

Sara Ranjbarvaziri, MS*, Shuin Park, BS*, Fides D. Lay, PhD, Peng Zhao, MD, PhD, Mark J. Miller, Xiuju Wu, PhD, Rong Qiao, MD, Justin M. Soffer, BS, Hanna K.A. Mikkola, MD, PhD, Aldons J. Lusis, PhD, Reza Ardehali, MD, PhD#

*These authors contributed equally to this article.

#corresponding author

Subject codes: cardiac fibroblasts, Hybrid Mouse Diversity Panel, isoproterenol, fibrosis

Short title: Genetic variability of fibroblasts in fibrosis

Author Information: The authors declare no competing financial interests. Correspondence and requests for materials should be addressed to R.A.: 675 Charles E. Young Drive S, Room 3645, Los Angeles, CA 90095-1760. Phone: 310-825-0819, Fax: 310-206-5777. Email: rardehali@mednet.ucla.edu

Word count: 4862

ABSTRACT

Background: Genetic diversity and the heterogeneous nature of cardiac fibroblasts (CFbs) have hindered characterization of the molecular mechanisms that regulate cardiac fibrosis. The Hybrid Mouse Diversity Panel (HMDP) offers a valuable tool to examine genetically diverse cardiac fibroblasts and their role in fibrosis.

Methods: Three strains of mice (C57BL/6J, C3H/HeJ, and KK/HlJ) were selected from HMDP and treated with either isoproterenol (ISO) or saline by an intraperitoneally implanted osmotic pump. After 21 days, cardiac function and levels of fibrosis were measured by echocardiography and trichrome staining, respectively. Proliferation and activation of CFbs were measured by *in vitro* and *in vivo* assays under normal and injury conditions. RNA-sequencing was done on isolated CFbs from each strain and results were analyzed by Ingenuity Pathway Analysis (IPA) and validated by reverse transcription-qPCR, Western blot, and ELISA.

Results: ISO treatment in C57BL/6J, C3H/HeJ, and KK/HlJ mice resulted in minimal, moderate, and extensive levels of fibrosis, respectively (n = 20). Isolated CFbs treated with ISO exhibited strain-specific increases in the levels of activation but showed comparable levels of proliferation. Similar results were found *in vivo*, suggesting that fibroblast activation, and not proliferation, may account for the differential levels of cardiac fibrosis after ISO treatment. RNA-sequencing revealed that CFbs from each strain exhibit unique gene expression changes in response to ISO, including an increase in pro-survival/anti-fibrotic pathways in C57BL/6J mice compared to other strains. We identified *Ltbp2* as a commonly upregulated gene after ISO treatment. LTBP2 specifically localized in the fibrotic regions of the myocardium and was elevated in the plasma of heart failure patients compared to healthy individuals.

Conclusions: This study highlights the importance of genetic variation in cardiac fibrosis by using multiple inbred mouse strains to characterize CFbs and their response to ISO treatment. Our data suggest that fibroblast activation is a response that correlates with extent of scar formation while proliferation may not necessarily drive development of fibrosis. Additionally, by comparing CFbs from multiple strains, we were able to identify potential pathways as therapeutic targets and LTBP2 as a promising diagnostic marker for fibrosis, with relevance to patients with underlying myocardial fibrosis.

INTRODUCTION

Acute myocardial injury or elevated pressure in the heart results in a multitude of cardiac pathologies, particularly cardiac fibrosis. It has been reported that such injury leads to activation and proliferation of cardiac fibroblasts (CFbs), some of which deposit excessive extracellular matrix (ECM) components that compromise myocardial structure and function[1, 2]. Despite the significant role that CFbs play in injury response, characterization of this cell type has been challenging due to their heterogeneous nature and lack of fibroblast-specific markers[2, 3]. Furthermore, detailed knowledge is lacking in the molecular mechanisms that regulate their specific contributions to scar development.

The Hybrid Mouse Diversity Panel (HMDP) is a collection of over 100 genotyped inbred strains of mice that allow for identification of genetic factors that contribute to various common disease traits[4]. In a comprehensive study by Rau et al., mice within the HMDP were phenotypically characterized following chronic treatment with the β-adrenergic agonist isoproterenol (ISO). Excessive stimulation of β-adrenergic receptors in the heart has been linked to increased CFb proliferation and collagen synthesis[5]. Chronic treatment of the HMDP with ISO resulted in a wide range of severity in cardiac hypertrophy and associated fibrosis across the different strains. These findings support the hypothesis that genetic variation influences the development and progression of cardiac dysfunction and pathological fibrosis. However, these studies evaluated changes at the cardiac tissue level and did not delineate the roles of specific cell types to each strain's respective phenotype.

In the present study, we utilized several HMDP strains with varying responses to ISO treatment to investigate the mechanisms by which their respective CFbs may regulate the process of cardiac fibrosis. We demonstrated that CFbs respond to ISO treatment in a strain-specific manner both *in vitro* and *in vivo*. Notably, CFbs from all three strains exhibited significant

differences in levels of activation in response to ISO but had similar rates of proliferation. Additionally, we performed RNA-sequencing and explored differentially expressed and shared genes among CFbs from three strains under normal and injury conditions. We identified *Ltbp2* as a potential unique marker of fibrosis that can be applied to a genetically diverse population. Overall, our findings contribute to the understanding of cardiac fibroblast function in the context of ISO-induced cardiac fibrosis and further highlights the importance of genetic variation in various diseases and cellular functions.

METHODS

Mice

Female C57BL/6J, C3H/HeJ, and KK/HlJ strains of mice were obtained from the Jackson Laboratory. All procedures were carried out with the approval of the University of California, Los Angeles (UCLA) Animal Research Committee or the Institutional Animal Care. Two operators blinded to the experimental designs performed all animal surgeries, *in vitro* and *in vivo* analyses.

ISO treatment

Isoproterenol (ISO) treatment was performed by implantation of Alzet osmotic pumps (Cupertino, CA) in adult female mice (8-10 weeks, n=20) of each strain (C57BL/6J, C3H/HeJ, KK/HIJ). Pumps were filled with ISO (Sigma, CA) (30mg/kg body weight/per day) and implanted in the abdominal cavity under anesthesia with isoflurane. Mice were treated pre- and postoperatively with Sulfamethoxazole and Trimethoprim oral suspension (Hi.Tech Pharmacal, NY). Mice in control groups were implanted with pumps filled with saline. Mice were sacrificed and hearts were harvested 21 days post-implantation for further analysis (n=40).

Cell Isolation, Culture, and Characterization

Mice were injected with heparin (SAGENT Pharmaceuticals) prior to being euthanized. After euthanization, the hearts were dissected and perfused with Hanks' Balanced Salt Solution (HBSS). They were cut into small pieces and digested with Liberase Blendzyme TH and TM (Roche) in Medium 199 with DNAse I (Invitrogen) and polaxamer in 37°C for 1h. Cells were passed through a 70μm cell strainer (BD Falcon) and centrifuged. The cell pellet was re-suspended in staining buffer (3% FBS in HBSS) containing the relevant $Thy1^{+}HE^{-}$ surface marker antibodies **(Supplementary Table I)** and incubated in the dark for 30 minutes at room temperature. After sorting (BD FACSAria II flow cytometer), $Thy1^{+}HE^{-}$ cells were cultured on 0.1% gelatin-coated 12-well plates in DMEM supplemented with 15% FBS and antibiotics ($5x10^{4}$ cells per well). The medium was changed 24 hours after the primary culture, followed by changes every 48 hours. Cells were passaged upon 80% confluency. After the first passage, cells were washed and cultured in serum-free culture medium supplemented with 0.5 mg/mL insulin and 0.5 mg/mL transferrin. At confluence, cells were treated with 100μm/L ISO (Sigma). After 72 hours, both untreated and treated cells were washed, fixed in 4% paraformaldehyde, and stained for expression of Col1, αSMA and pHH3. Cell counts were performed on ImageJ using the 'Cell Counter' plug-in and performed by two people who were blind to the cell type and condition.

RNA sequencing

$Thy1^{+}HE^{-}$ cells were isolated from saline and ISO-treated hearts 21 days after pump implantation (n=3 per strain/condition), and then sorted directly into TRIzol® LS Reagent (Ambion). Total RNA was extracted using the RNeasy miniElute Cleanup Kit (Qiagen), according to manufacturer's instructions. The complementary DNA (cDNA) library was generated using reagents provided in the KAPA Stranded RNA-seq kit. The amplified cDNA library was sequenced on an Illumina HiSeq 3000 according to manufacturer's instructions. Libraries were sequenced using 50 single-end read protocol, which yielded >20 million raw

reads per sample. Read quality was assessed using FastQC and reads were subsequently trimmed 5bp from the start of the reads up and 2 bp from the end of the reads. Alignment to the mm9 mouse genome were performed using Tophat v2.0.14 with -coverage-search option. Fragments Per Kilobase of transcript per Million mapped reads (FPKM) were then calculated using cuffdiff v2.2.1 using mm9 Refseq genes downloaded from the UCSC Genome Browser as the transcript annotation file. Further statistical analyses were performed using the cummeRbund package with thresholds for selecting significant genes set at ≥ 1.5-fold and $p<0.05$. Global functional analyses, network analyses and canonical pathway analyses were performed using Ingenuity Pathway Analysis (Ingenuity® Systems, www.ingenuity.com).

Plasma collection and Enzyme-linked immunosorbent assay (ELISA)

Blood was collected from mice after euthanasia from both saline and ISO-treated mice into Lithium Heparin Blood Collection Tubes (BD). Plasma was separated from blood using Ficoll-Paque PLUS (GE Healthcare) and following the manufacturer's instructions. ELISA was used to precisely measure the concentration of selected proteins in plasma samples from mouse and human. For ELISA we used commercially available kits (MyBioSource, **Supplementary Table II**) and followed the manufacturer's instructions. Briefly, 100 µL of standards or diluted plasma samples were loaded per well (antibody coated). After 2 hours of incubation at 37°C, the biotin-conjugated antibody was added to each well. Plates were then incubated for 1 hour at 37°C and after three washes, 100 µL of avidin conjugated to horseradish peroxidase was added. Wells were washed five times after 30 minutes of incubation at 37°C. Then 90 µL of 3,3′,5,5′-tetramethylbenzidine (TMB) was added followed by a 15 minute incubation in the dark. Results were read after adding 50 µL of top solution at an optical density of 450 nm using a plate reader (Molecular Devices). All samples were measured in duplicate and the calculated concentrations were multiplied by the dilution factor to determine the final concentration.

The study was approved by an IRB and participants gave written informed consent.

Statistical analysis

Statistical testing was performed with GraphPad Prism. Results are presented as mean ± SEM and were compared by using two-way ANOVA and student t-test (significance was assigned for $p<0.05$).

RESULTS

Pathological analysis of ISO-induced cardiac function and fibrosis in select mouse strains

The entire HMDP, consisting of 110 mouse strains were characterized at baseline and in response to ISO treatment to determine the extent of cardiac fibrosis **(Figure 1A)**. The survey revealed significant variations in cardiac structure and fibrosis under baseline conditions and in response to ISO administration[5, 6]. Based on this considerable variability, we selected three representative strains that exhibited distinct pathological phenotypes: C57BL/6J, C3H/HeJ, and KK/HIJ, showing minimal, moderate, and substantial myocardial fibrosis after ISO injury, respectively. Adult female mice (8-10 weeks, 20-28 grams) from each strain were intraperitoneally implanted with an Alzet micro-osmotic pump containing ISO (30 mg/kg/day) or saline for 21 days. As shown in **Supplementary Figure IA,** adult mice from all strains were of similar size and body weight (data not shown). After three weeks of saline or ISO treatment, animals were sacrificed and hearts were harvested for further analysis. To confirm the levels of cardiac fibrosis after treatment across the three strains, Masson's trichrome staining and ImageJ were used to visualize and quantify the fibrotic area. After saline treatment, there were minimal to no visible fibrotic areas across all three strains **(Figure 1B)**. After ISO treatment, both C3H/HeJ and KK/HIJ hearts exhibited clear fibrotic areas as demonstrated by staining for collagen deposition, while C57BL/6J hearts appeared to have minimal amounts of fibrosis. Consistent with the histological observations, quantitative analysis of the fibrotic areas showed

significant differences across the selected strains, with KK/HIJ hearts consistently exhibiting the greatest area of fibrosis in response to ISO **(Figure 1C)**. Additionally, with saline treatment, there were no significant differences in heart size between mice of different strains **(Supplementary Figure IB).** In response to ISO treatment, both KK/HIJ and C3H/HeJ strains showed observable increases in heart size **(Supplementary Figure IB)** and a significant increase in heart weight/tibia length ratios as compared to saline-treated hearts **(Supplementary Figure IC)**. In contrast, C57BL/6J mice showed minimal signs of cardiac hypertrophy in response to ISO.

Echocardiography demonstrated increased left ventricle end-diastolic dimension (LVEDD) and end-systolic dimension (LVESD) in the C3H/HeJ and KK/HIJ strains 21 days after ISO treatment **(Supplementary Figure ID)**. Furthermore, both C3H/HeJ and KK/HIJ mice exhibited significant decreases in ejection fraction **(Figure 1D)** and fractional shortening **(Supplementary Figure IE)** after ISO treatment. In contrast, C57BL/6J mice had preserved cardiac function with no significant changes in ejection fraction or fractional shortening in ISO-treated compared to saline-treated hearts **(Figure 1D and Supplementary Figure IE)**.

These results confirm that chronic β-adrenergic stimulation in different mouse strains (C57BL/6J, C3H/HeJ, and KK/HIJ) leads to varying severity of cardiac pathology. These phenotypical differences were used to further characterize the contributions of CFbs to isoproterenol-induced fibrosis.

***In vitro* characterization of strain-specific cardiac fibroblasts in response to ISO**

Based on the varying levels of fibrosis exhibited by the three selected strains, we focused on characterizing strain-specific CFbs and their potential role in generating the observed patterns of cardiac fibrosis. Initially, CFbs from each strain were isolated by FACS and cultured using an

established panel of surface markers: exclusion of hematopoietic ($CD45^-$, $Ter119^-$), macrophage ($CD11b^-$), and endothelial ($CD31^-$) lineages, followed by the inclusion of $Thy1^+$ cells (hereafter referred to as $Thy1^+HE^-$)[2]. Phase contrast images confirmed that CFbs from all strains exhibit similar mesenchymal morphology with a spindle-like phenotype **(Supplementary Figure IIA)**. Additionally, immunocytochemistry (ICC) demonstrated that these cells were positive for fibroblast markers collagen 1 (Col1) and PDGFRα, confirming the purity of our isolation method **(Supplementary Figure IIB and IIC)**. We then sought to determine whether these fibroblasts exhibited similar patterns of activation and proliferation in culture. CFbs were stained for the expression of α-smooth muscle actin (αSMA), a marker associated with activated fibroblasts[7], and phospho-Histone H3 (pHH3)[8], for proliferation analysis. We observed very low expression of αSMA within $Col1^+$ CFbs from all strains, indicating that these cells do not become activated without stimuli **(Supplementary Figure IID and IIE)**. Additionally, CFbs from all strains demonstrated similar rates of proliferation (%$pHH3^+$ nuclei) at the basal level **(Supplementary Figure IIF and IIG)**.

Given the observed variation in development of fibrosis in response to chronic β-adrenergic stimulation in mice, we compared how strain-specific CFbs may respond to ISO *in vitro*. CFbs from each strain were treated with culture media containing ISO (100μM) for 72 hours **(Figure 2A)**. Cells were then fixed and characterized by phase contrast microscopy and ICC. After treatment, cells from all strains appeared morphologically larger, particularly CFbs from C3H/HeJ and KK/HlJ mice **(Figure 2B)**. A significant number of CFbs from C3H/HeJ and KK/HlJ began to co-express αSMA and Col1, while CFbs from C57BL/6J exhibited minimal αSMA expression in the presence of ISO **(Figure 2C and 2D)**. Importantly, immunostaining for pHH3 revealed that the rate of proliferation was significantly increased across all three strains to similar levels when compared to their respective untreated control groups **(Figure 2E and 2F)**.

Together, these data suggest that cultured CFbs respond to ISO in a strain-specific manner. While ISO treatment resulted in similar levels of proliferation in cultured CFbs, we observed that their levels of activation were vastly different. This *in vitro* activation of CFbs reflected the fibrotic phenotypes observed in the three mouse strains after ISO treatment.

Cardiac fibroblasts demonstrate strain-specific responses to ISO treatment *in vivo*

The *in vitro* assays revealed that despite the differences in the level of activation, CFbs from different strains appear to proliferate similarly across all three strains upon stimulation with ISO. While other studies have viewed fibroblast activation and proliferation to be conjoint responses to stimulation, our *in vitro* results suggest otherwise. To determine whether a similar behavior is also observed *in vivo*, we investigated how CFbs proliferation and activation are regulated after ISO injury in the three selected strains.

First, we observed the presence of activated fibroblasts in C57BL/6J, C3H/HeJ, and KK/HlJ mice in response to ISO treatment. Immunohistochemistry (IHC) was used to observe co-localization of Col1 with αSMA or periostin[9, 10] for the identification of activated CFbs. In control groups, which received saline, Col1 staining was mainly present around larger vessels and co-localization with αSMA was exceedingly rare in all three strains **(Figure 3A)**. However, after ISO treatment, there was an increase in Col1 staining, particularly in C3H/HeJ and KK/HlJ hearts **(Supplementary Figure IIIA)**. Many $Col1^+$ cells also co-expressed αSMA in both the perivascular and interstitial regions of myocardium in C3H/HeJ and KK/HlJ hearts, indicting the presence of activated CFbs **(Figure 3A)**. This increase was quantified as the regions containing $Col1^+αSMA^+$ cells normalized to the total area of each heart section **(Figure 3B)**. IHC for periostin also confirmed the differential levels of activated CFbs observed across the three strains **(Supplementary Figure IIIB)**. Consistent with our *in vitro* results, the levels of CFb activation corresponded with the amount of fibrosis seen within each strain.

Next, we sought to assess the proliferative behavior of CFbs *in vivo* after ISO injury by administering Bromodeoxyuridine (BrdU). Mice were injected with BrdU at the time of micro-osmotic pump implantation for ISO and exposed to BrdU diluted in drinking water throughout the 21 days of treatment **(Figure 3C)**. IHC of the control hearts demonstrated low levels of $BrdU^+$ proliferating CFbs throughout the myocardium. However, with ISO treatment, we observed a significantly higher number of $BrdU^+$ CFbs throughout the perivascular and interstitial regions in all three strains **(Figure 3D)**. Flow cytometry was used for confirmation and demonstrated similar percentages of $BrdU^+$ CFbs in the control groups for all three strains. The proportion of $BrdU^+$ CFbs significantly increased to a similar amount after ISO treatment in all three strains **(Figure 3E and Supplementary Figure IIIC)**. These results demonstrate that while a similar pattern of CFb proliferation was observed in all three strains after ISO treatment, mouse strains with greater extent of cardiac fibrosis contained more activated CFbs.

Strain-specific cardiac fibroblasts have unique transcriptional profiles in response to *in vivo* ISO treatment

The use of multiple genetic strains for transcriptome analysis allows for a comprehensive approach to determine potential genetic contributors of specific phenotypes. To further characterize CFbs within the three selected strains, we performed RNA-sequencing on isolated CFbs from C57BL/6J, C3H/HeJ, and KK/HlJ mice that had undergone saline or ISO treatment. Overall gene expression profiles of ISO-treated CFbs were compared to their respective controls and the differentially expressed genes are shown in **Supplementary Figure IVA**. The effects of ISO on each strain's transcriptome was unique, as seen by principal component analysis (PCA) and hierarchical clustering, further justifying the need to study strain-specific phenotypes **(Figure 4A and Supplementary Figure IVA)**. Based on the *in vitro* and *in vivo* results, we focused on genes mainly associated with fibrosis and proliferation. By harnessing

these datasets, we observed that genes related to fibroblast activation and fibrosis were highly upregulated in KK/HIJ CFbs in response to ISO compared to C3H/HeJ and C57BL/6J CFbs **(Figure 4B)**. In contrast, we observed comparable expression levels of select cell cycle and proliferation genes across the three strains **(Figure 4C)**. We then used Ingenuity Pathway Analysis (IPA) to identify enriched pathways which may be responsible for regulating the differences between the strains. Interestingly, we detected higher activation of anti-fibrosis/pro-survival canonical pathways, such as Relaxin and Nitric Oxide signaling, in C57BL/6J CFbs in response to ISO **(Supplementary Figure IVB)**. The relative expression of key regulatory genes from these pathways was quantified by reverse transcription-PCR (RT-qPCR) to validate the gene expression data **(Supplementary Figure IVC**). These results suggest that in addition to CFb activation, other pathways may also be involved in modulating the extent of fibrosis as observed in different strains. However, further exploration of these pathways is required to delineate the mechanisms by which they alter cardiac fibrosis.

***Ltbp2* is commonly upregulated in all select mouse strains in response to cardiac fibrosis**

Similar to genome-wide association studies (GWAS), the HMDP facilitates identification of unique genes that may be associated with complex phenotypic traits. To account for diversity seen in heart failure pathologies, we sought to identify genes that can be associated with fibrosis regardless of the genetic background. From the RNA-sequencing data, we focused on genes that were upregulated within each strain in response to ISO. Several of these genes overlapped across two strains, but the majority of the genes were unique to each strain **(Figure 5A)**. Within the commonly upregulated genes among the three strains, we decided to focus on genes encoding secreted factors to determine whether any would be indicative of a detectable circulatory marker for fibrosis. We found four genes that were either upregulated in both

C3H/HeJ and KK/HlJ (*Comp, Cilp,* and *Tnc*), or in all three strains (*Ltbp2*) in response to ISO. RT-qPCR for each gene within CFbs confirmed the trends seen within the RNA-sequencing data **(Figure 5B and Supplementary Figure VA)**.

Since the four genes of interest encode secreted proteins, we first sought to determine whether ISO treatment elevates their levels in circulation. Plasma was collected from all three strains of mice treated with saline or ISO. Western blotting and ELISA were used to measure the levels of each protein of interest. COMP **(Supplementary Figure VB and VC)** and CILP **(Supplementary Figure VD)**, despite showing an interesting upregulation in the RNA-sequencing data, did not exhibit any noticeable trends in the plasma of ISO versus saline treated mice. TNC was found to be upregulated in both C3H/HeJ and KK/HlJ, but not in C57BL/6J, after ISO **(Supplementary Figure VE)**. The pathological role of *Tnc* in fibrosis and its role in regulating the secretion of pro-inflammatory cytokines and ECM regulatory enzymes during cardiac remodeling have already been established by several groups[11]. Finally, we found that LTBP2 levels were increased in plasma after ISO treatment in all strains **(Figure 5C)**. This result was of particular interest because it suggests that *Ltbp2* may have a role in fibrosis that is applicable across different genetic backgrounds. To confirm the presence of the LTBP2 protein in fibrosis, we conducted IF staining for LTBP2 in cardiac sections from all three strains after ISO treatment. In saline hearts, there was minimal LTBP2 expression throughout the myocardium. However, in ISO-treated hearts, LTBP2 expression was significantly increased and specifically found in fibrotic regions where it co-localized with cells expressing DDR2, a fibroblast marker, and αSMA, a marker for activated fibroblasts **(Figure 5D)**. Even in C57BL/6J hearts, where there was very little fibrosis in response to ISO, LTBP2 staining was present strictly in the fibrotic regions.

To determine whether the upregulation of LTBP2 can be also detected in other injury models, we performed transverse aortic constriction (TAC) surgery on the three mouse strains. TAC surgery induces pressure overload-associated cardiac hypertrophy and development of diffuse interstitial fibrosis. We observed cardiac hypertrophy and the presence of myocardial fibrosis in the three strains after TAC (data not shown). In C57BL/6J mice, RNA-sequencing and RT-qPCR demonstrated significant increases in *Ltbp2* expression in CFbs 7 days after TAC surgery compared to sham **(Supplementary Figure VIA and VIB)**. Additionally, IHC showed that LTBP2 was upregulated in response to TAC in all mouse strains and was mainly localized in the fibrotic areas **(Figure 5D)**. The specificity of LTBP2 expression in fibrosis within three different mouse strains and two injury models suggests that the expression of LTBP2 may be indicative of the development of cardiac fibrosis.

LTBP2 is expressed in the fibrotic regions of human myocardium and its levels are upregulated in plasma of heart failure patients

Since LTBP2 was found to be upregulated in multiple mouse strains with different genetic backgrounds after induction of fibrosis, we investigated whether LTBP2 is also present across a diverse group of human subjects with underlying heart failure. We found that LTBP2 levels were significantly higher in patients with heart failure with reduced ejection fraction (HFrEF) when compared to healthy individuals. **(Figure 6A and Supplementary Table III)**. Furthermore, IHC staining of human myocardial tissue from heart failure patients revealed LTBP2 expression to be significantly increased compared to expression in the healthy human myocardium **(Figure 6B)**.

Taken together, our results suggest that LTBP2 may act as a potential marker for cardiac fibrosis and its specific role in fibrosis requires further exploration.

DISCUSSION

Despite the functional significance of CFbs in cardiovascular disease, the specific contributions of these cells to cardiac fibrosis are not completely understood. Previous studies revealed a wide spectrum of cardiac pathology across various inbred strains of mice when subjected to chronic β-adrenergic stimulation by ISO[5, 6]. We hypothesized that characterizing fibroblasts of multiple strains with different severities of cardiac fibrosis would allow us to dissect the molecular mechanisms that regulate the specific contributions of these cells to scar development. Our results show that fibroblast activation, not proliferation, may dictate the striking differences in fibrosis among the highly divergent strains. Moreover, comparisons of expression patterns across the strains revealed differences in underlying pathways and identified a potential marker of fibrosis.

While recent research has focused on how CFbs become activated and proliferate in response to injury[12], the mechanisms by which these processes dictate scar development have yet to be explored. Prior to this study, CFb activation and proliferation were generally considered as interconnected responses that contribute to fibrosis[12, 13]. In this study, we attempted to parse out the specific contributions that each of these responses may have on cardiac fibrosis, independent of each other. By comparing CFbs from three select strains of the HMDP; C57BL/6J, C3H/HeJ, and KK/HlJ, which exhibited varying levels of fibrosis in response to ISO injury, we were able to identify key differences and similarities which may be crucial for understanding the contribution of CFbs to cardiac fibrosis. We discovered that there is a direct correlation of CFb activation with the severity of fibrosis, while CFbs from all strains exhibited similar proliferative capacity in response to injury. These results suggest that CFb proliferation is an independent response from CFb activation and does not necessarily drive the formation of fibrotic scar tissue. It is possible that CFb proliferation is an indicator of CFb stimulation, but the functional roles of this phenomenon require further study.

Myocardial injury evokes multiple signaling pathways in cardiac fibroblasts that ultimately lead to the activation of genes that regulate cardiac fibrosis[14]. To delineate gene expression differences between CFbs from each select strain, we conducted RNA-sequencing on sorted CFbs after saline and ISO treatment. CFbs from each strain displayed unique transcriptomes after saline treatment, suggesting that fibroblasts isolated from mice with different genetic backgrounds have profound differences in their gene expression profiles, even under homeostatic conditions. After ISO treatment, CFbs from each strain responded with distinct changes in their gene expression profiles, with enrichment of fibroblast activation genes conforming to the extent of fibrosis observed in each strain but comparable upregulation of proliferation genes. Additionally, when pursuing differentially expressed genes across the three strains, we identified a subset of genes within anti-fibrotic/pro-survival pathways that were more enriched in C57BL/6J CFbs after ISO. Specifically, we found strong correlations with the Relaxin and Nitric Oxide (NO) signaling pathways. Relaxin has been found to improve cardiac function and ameliorate fibrosis, thus attenuating arrhythmias and LV dysfunction in heart failure patients[15]. Likewise, the production of NO is generally associated with the synthesis of pro-angiogenic factors but, when fibroblasts are under stress, NO synthase is downregulated[16, 17]. These findings raise questions regarding whether phenotypic and/or transcriptomic changes observed after cardiac injury within a single mouse strain can be applicable to other strains without taking into account their genetic background. Further studies of these anti-fibrotic/pro-survival pathways, along with regulators of CFb activation and proliferation, are necessary to elucidate the mechanisms that regulate the spectrum of fibrosis seen across our three strains.

Heart failure resulting from prolonged interstitial fibrosis is a highly heterogeneous disorder influenced by many environmental and genetic factors. The unbiased genome-wide association study (GWAS) was designed to identify genetic variations on complex traits such as heart

failure[18]. However, multiple large-scale GWAS studies have provided limited success in identifying genetic signals driving heart failure[19]. This is partly due to paucity of quantitative phenotypic data as well as diverse environmental factors. Therefore, there have been challenges in developing treatments for heart failure and cardiac fibrosis that are applicable for a diverse population. The efficacy of currently available therapies and detection strategies varies in accordance to different patient populations. The HMDP is a unique tool to mimic in mice the genetic variance and substantial diversity of heart failure development seen in humans. While previous studies have sought to identify genetic markers uniquely associated with heart failure in a specific genetic background, we sought to investigate common markers that are associated with cardiac fibrosis in a panel of genetically diverse mouse strains. Our results revealed *Ltbp2* to be upregulated in CFbs from all three strains and the expression of LTBP2 was primarily localized in the fibrotic regions. LTBP2 is part of the Latent TGFβ1-Binding Protein family, which have been shown to participate in the regulation of TGFβ signaling and display high affinity binding sites for extracellular matrix proteins. However, while the functions of LTBP1[20], LTBP3[21], and LTBP4[22] in disease have been extensively characterized, the role of LTBP2 in cardiac injury is still unclear. Our results in both mice and human heart failure patients not only suggest that LTBP2 plays a key role in scar tissue development, but raises the possibility of LTBP2 being used as a diagnostic marker for fibrosis that can be used across a genetically diverse population. Whether LTBP2 is merely a surrogate for cardiac fibrosis or is involved in its pathogenesis is not entirely known. Nonetheless, it is important to interrogate this pathway to gain insight into mechanisms of CFb activation, explore how cardiac fibrosis is regulated and perhaps design novel anti-fibrotic therapies.

Our data demonstrates the importance of considering genetic backgrounds when conducting studies on CFbs that reflect changes in cardiac phenotype in response to injury. CFbs from three different mouse strains displayed unique behavioral and molecular changes that ultimately

contributed to their respective injury phenotypes. The comparisons conducted between the strains allowed for a unique approach in associating CFbs with a spectrum of fibrosis, rather than just the presence of fibrosis itself. This form of analysis allowed us to determine significant factors that directly correlate with the development of scar tissue, which may have not been recognized if the study was done within a single strain. This multiple-strain approach, when combined with molecular and cell-based characterizations, serves as an important tool for future work delineating the functions of not only CFbs, but of a variety of cardiac cell types.

AUTHOR CONTRIBUTIONS

S.R., S.P., and R.A. conceived the project and designed the experiments. X.W. and A.L. assisted with the initial design of the project. S.R. and S.P. performed all experiments, analyzed data and prepared the figures. S.R. and S.P. had full access to all the data in the study and take responsibility for the integrity of the data and the accuracy of the data analysis. S.P., S.R., and R.A. wrote the manuscript. F.L. helped with the analysis of RNA-sequencing data. M.J.M., R.Q., and J.M.S. assisted with immunostainings and trichrome staining. P.Z. performed all surgeries. All authors reviewed the manuscript. We acknowledge Dr. Adriana Huertas-Vazquez for proving us with human plasma samples. All echocardiograms were performed in the lab of Dr. Yibin Wang. We would also like to acknowledge Shuxun Ren with his assistance in the initial surgeries. The LTBP2 antibody was a generous gift from Dr. Marko Hyytiäinen from the University of Helsinki, Finland. We are grateful for the expert technical assistance from the UCLA Broad Stem Cell Research Center (BSCRC) Flow Cytometry Core and Clinical Microarray Core. We acknowledge Ngoc B. Nguyen and James L. Engel for their critical reading of this article.

SOURCES OF FUNDING

This work was supported by a grant from the NIH (DP2 HL127728), Eli & Edith Broad Center of Regenerative Medicine and Stem Cell Research Center at UCLA and Rose Hills Foundation Research Award (R.A.). S. R. was supported by the UCLA Graduate Programs in Bioscience (GPB) and S.P. was supported by the Ruth L. Kirschstein National Research Service Award (T32HL69766).

DISCLOSURES

None

AFFILIATIONS

From Division of Cardiology, Department of Internal Medicine, David Geffen School of Medicine, University of California, Los Angeles (S.R., S.P., P.Z., M.J.M., X.W., R.Q., J.M.S., A.J.L., R.A.); Eli and Edythe Broad Center for Regenerative Medicine and Stem Cell Research, University of California, Los Angeles (S.R., S.P., F.D.L., P.Z., M.J.M., R.Q., J.M.S., H.K.A.M., R.A.); Molecular, Cellular and Integrative Physiology Graduate Program, University of California, Los Angeles, (S.R., S.P., R.A.); Molecular Biology Institute, University of California, Los Angeles (H.K.A.M., A.J.L.); Department of Human Genetics, University of California, Los Angeles (A.J.L.); and Department of Microbiology, Immunology and Molecular Genetics, University of California, Los Angeles (A.J.L.)

REFERENCES

1. Fan D, Takawale A, Lee J and Kassiri Z. Cardiac fibroblasts, fibrosis and extracellular matrix remodeling in heart disease. *Fibrogenesis Tissue Repair*. 2012;5:15.

2. Ali SR, Ranjbarvaziri S, Talkhabi M, Zhao P, Subat A, Hojjat A, Kamran P, Muller AM, Volz KS, Tang Z, Red-Horse K and Ardehali R. Developmental heterogeneity of cardiac fibroblasts does not predict pathological proliferation and activation. *Circ Res*. 2014;115:625-35.

3. Travers JG, Kamal FA, Robbins J, Yutzey KE and Blaxall BC. Cardiac Fibrosis: The Fibroblast Awakens. *Circ Res*. 2016;118:1021-40.

4. Lusis AJ, Seldin MM, Allayee H, Bennett BJ, Civelek M, Davis RC, Eskin E, Farber CR, Hui S, Mehrabian M, Norheim F, Pan C, Parks B, Rau CD, Smith DJ, Vallim T, Wang Y and Wang J. The Hybrid Mouse Diversity Panel: a resource for systems genetics analyses of metabolic and cardiovascular traits. *J Lipid Res*. 2016;57:925-42.

5. Rau CD, Wang J, Avetisyan R, Romay MC, Martin L, Ren S, Wang Y and Lusis AJ. Mapping genetic contributions to cardiac pathology induced by Beta-adrenergic stimulation in mice. *Circ Cardiovasc Genet*. 2015;8:40-9.

6. Wang JJ, Rau C, Avetisyan R, Ren S, Romay MC, Stolin G, Gong KW, Wang Y and Lusis AJ. Genetic Dissection of Cardiac Remodeling in an Isoproterenol-Induced Heart Failure Mouse Model. *PLoS Genet*. 2016;12:e1006038.

7. Baum J and Duffy HS. Fibroblasts and myofibroblasts: what are we talking about? *J Cardiovasc Pharmacol*. 2011;57:376-9.

8. Crosio C, Fimia GM, Loury R, Kimura M, Okano Y, Zhou H, Sen S, Allis CD and Sassone-Corsi P. Mitotic phosphorylation of histone H3: spatio-temporal regulation by mammalian Aurora kinases. *Mol Cell Biol*. 2002;22:874-85.

9. Kanisicak O, Khalil H, Ivey MJ, Karch J, Maliken BD, Correll RN, Brody MJ, SC JL, Aronow BJ, Tallquist MD and Molkentin JD. Genetic lineage tracing defines myofibroblast origin and function in the injured heart. *Nat Commun*. 2016;7:12260.

10. Snider P, Standley KN, Wang J, Azhar M, Doetschman T and Conway SJ. Origin of cardiac fibroblasts and the role of periostin. *Circ Res*. 2009;105:934-47.

11. Okamoto H and Imanaka-Yoshida K. Matricellular proteins: new molecular targets to prevent heart failure. *Cardiovasc Ther*. 2012;30:e198-209.

12. Chen W and Frangogiannis NG. Fibroblasts in post-infarction inflammation and cardiac repair. *Biochim Biophys Acta*. 2013;1833:945-53.

13. Midgley AC, Rogers M, Hallett MB, Clayton A, Bowen T, Phillips AO and Steadman R. Transforming growth factor-beta1 (TGF-beta1)-stimulated fibroblast to myofibroblast differentiation is mediated by hyaluronan (HA)-facilitated epidermal growth factor receptor (EGFR) and CD44 co-localization in lipid rafts. *J Biol Chem*. 2013;288:14824-38.

14. Manabe I, Shindo T and Nagai R. Gene expression in fibroblasts and fibrosis: involvement in cardiac hypertrophy. *Circ Res*. 2002;91:1103-13.

15. Zhou X, Chen X, Cai JJ, Chen LZ, Gong YS, Wang LX, Gao Z, Zhang HQ, Huang WJ and Zhou H. Relaxin inhibits cardiac fibrosis and endothelial-mesenchymal transition via the Notch pathway. *Drug Des Devel Ther*. 2015;9:4599-611.

16. Dulak J, Jozkowicz A, Dembinska-Kiec A, Guevara I, Zdzienicka A, Zmudzinska-Grochot D, Florek I, Wojtowicz A, Szuba A and Cooke JP. Nitric oxide induces the synthesis of vascular endothelial growth factor by rat vascular smooth muscle cells. *Arterioscler Thromb Vasc Biol*. 2000;20:659-66.

17. Wang R, Ghahary A, Shen YJ, Scott PG and Tredget EE. Nitric oxide synthase expression and nitric oxide production are reduced in hypertrophic scar tissue and fibroblasts. *J Invest Dermatol*. 1997;108:438-44.

18. Stranger BE, Stahl EA and Raj T. Progress and promise of genome-wide association studies for human complex trait genetics. *Genetics*. 2011;187:367-83.

19. Rau CD, Lusis AJ and Wang Y. Genetics of common forms of heart failure: challenges and potential solutions. *Curr Opin Cardiol*. 2015;30:222-7.

20. Dallas SL, Keene DR, Bruder SP, Saharinen J, Sakai LY, Mundy GR and Bonewald LF. Role of the latent transforming growth factor beta binding protein 1 in fibrillin-containing microfibrils in bone cells in vitro and in vivo. *J Bone Miner Res*. 2000;15:68-81.

21. Penttinen C, Saharinen J, Weikkolainen K, Hyytiainen M and Keski-Oja J. Secretion of human latent TGF-beta-binding protein-3 (LTBP-3) is dependent on co-expression of TGF-beta. *J Cell Sci*. 2002;115:3457-68.

22. Bultmann-Mellin I, Dinger K, Debuschewitz C, Loewe KMA, Melcher Y, Plum MTW, Appel S, Rappl G, Willenborg S, Schauss AC, Jungst C, Kruger M, Dressler S, Nakamura T, Wempe F, Alejandre Alcazar MA and Sterner-Kock A. Role of LTBP-4 in alveolarization, angiogenesis and fibrosis in lungs. *Am J Physiol Lung Cell Mol Physiol*. 2017:ajplung 00031 2017.

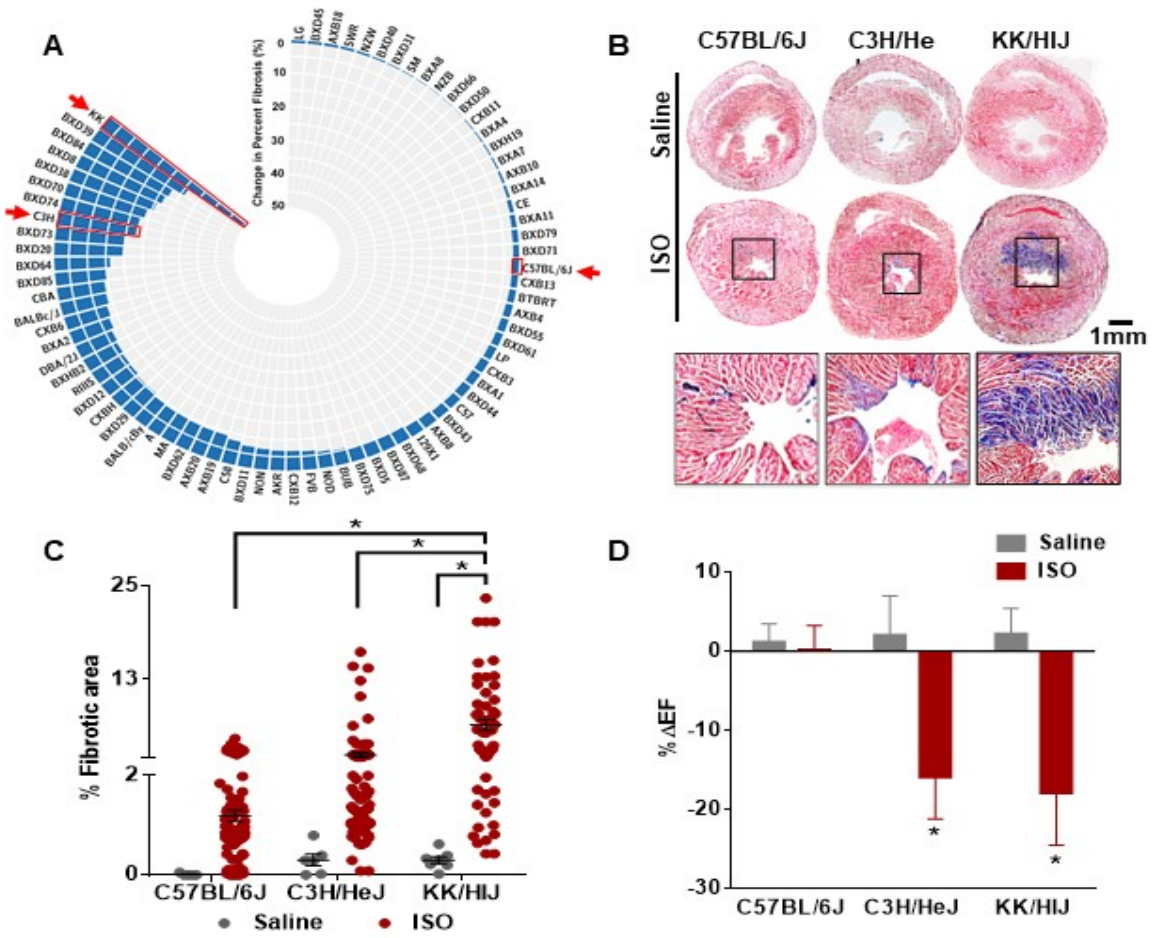

Figure 1. Severity of fibrosis varies across different mouse strains (C57BL/6J, C3H/HeJ, KK/HIJ) in response to ISO treatment. (A) Wide variation in percentage of fibrosis was observed between the strains of the hybrid mouse diversity panel (HMDP) after ISO treatment. **(B)** Masson's Trichrome stained sections of hearts from the three selected strains after 21 days of saline/ISO treatment (n=7-8 mice per condition). **(C)** Quantification of fibrotic area as a percentage of total section area (n=10-12 sections per heart, two-way ANOVA). **(D)** Left ventricular ejection fractions was measured by echocardiography in both saline- and ISO-treated groups across the different strains. (n=20 mice per strain). Data presented as mean ± SEM. Two-way ANOVA, *P < 0.05. Scale bar: 1mm

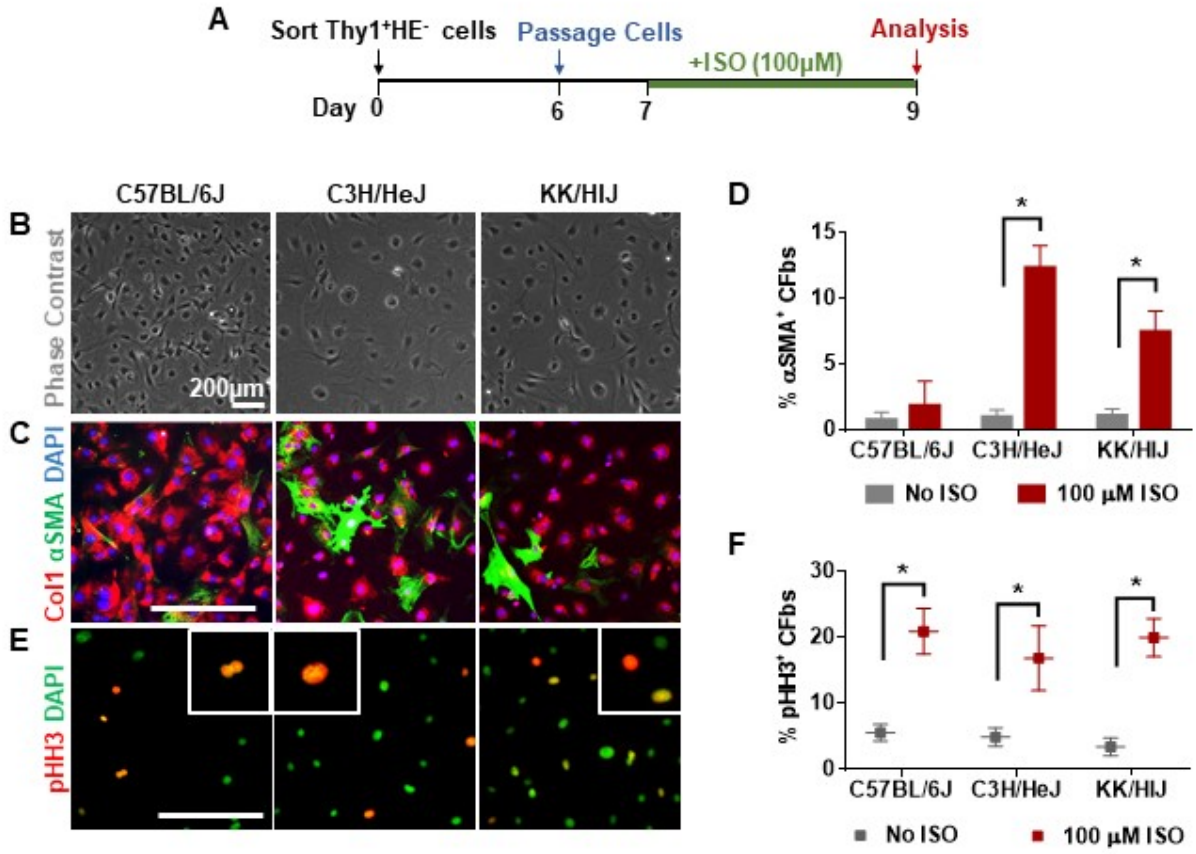

Figure 2. *In vitro* ISO treatment affects CFb activation and proliferation in a strain-specific manner. (A) Schematic diagram outlining the in vitro experiments. Cells were isolated by FACS, expanded, and passaged prior to exposure to ISO for 72 hours. **(B)** Phase contrast images of CFbs after ISO treatment. **(C)** Activated fibroblasts were identified by co-expression of Col1 (red) and αSMA (green) after ISO treatment. **(D)** Quantification of activated CFbs (Col1⁺αSMA⁺ cells) is shown as a percentage of double-positive cells relative to all fibroblasts (Col1⁺ cells) (n=5 wells/strain/condition). **(E)** The mitotic marker phospho-Histone H3 (pHH3) was used to identify proliferating CFs in response to ISO. **(F)** Proliferation of CFbs after ISO treatment was measured by comparing the number of pHH3⁺ nuclei relative to total nuclei (n=5 wells/strain/condition). DAPI was used to stain nuclei. Data presented as mean ± SEM. Multiple t-test, *P < 0.05. Scale bar: 200μm.

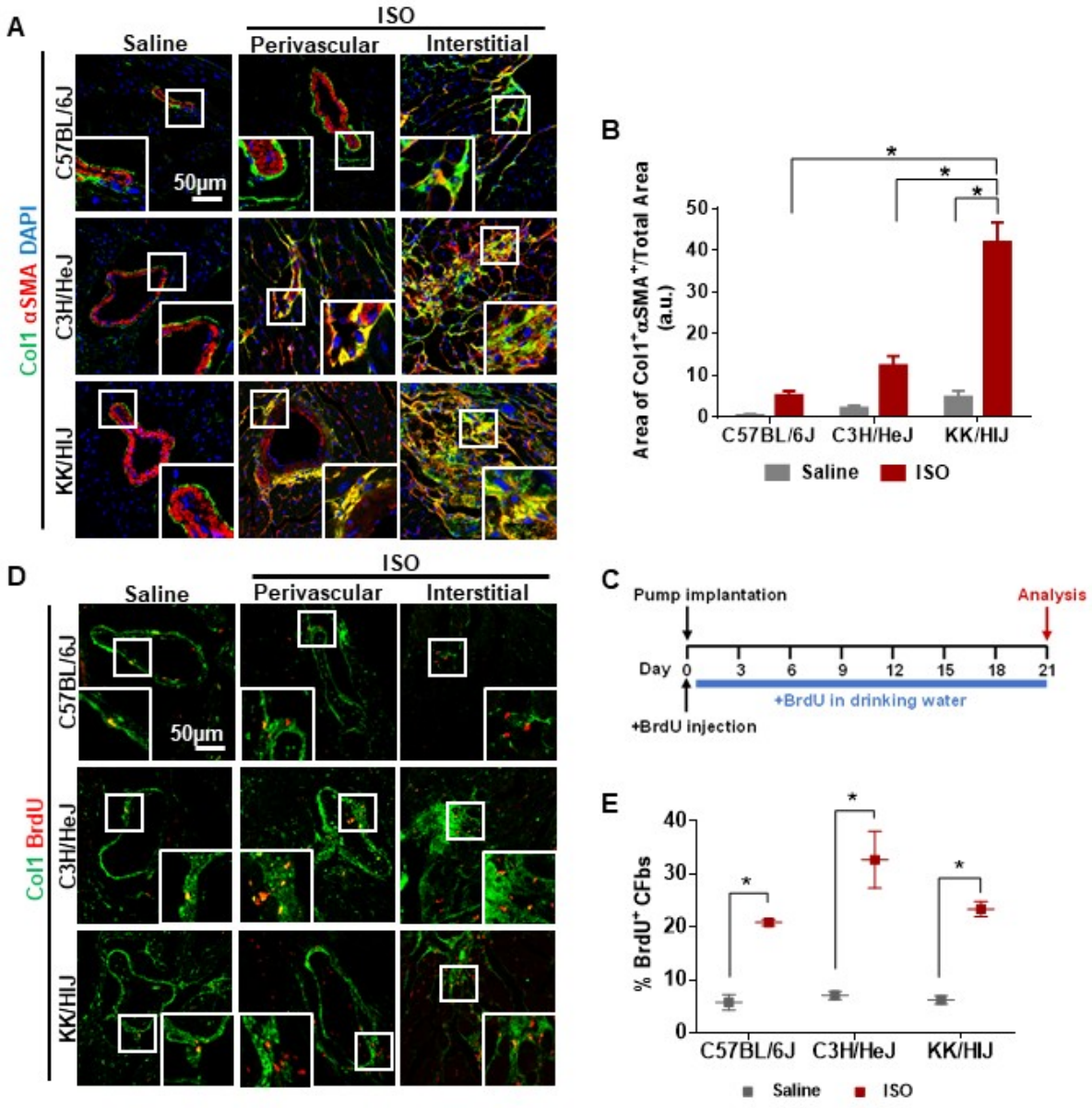

Figure 3. CFbs display a distinct pattern of activation and proliferation that is strain-specific after *in vivo* ISO treatment. **(A)** IHC of heart sections from different strains after treatment with saline or ISO stained for αSMA (red) and Col1 (green) in saline/ISO-treated hearts shows presence of activated fibroblasts in the perivascular and interstitial fibrotic areas. **(B)** Quantification of Col1^{+}αSMA^{+} co-localized areas as a percentage of total heart section area (n=3-4 heart per strain/condition). **(C)** Schematic of *in vivo* bromodeoxyuridine (BrdU) administration. **(D)** IHC of heart sections from different strains after treatment with saline or ISO shows BrdU^{+} cells within Col1^{+} perivascular and interstitial fibrotic regions. **(E)** The extent of CFb proliferation depicted as percentage of BrdU^{+} CFbs within the entire Thy^{+}HE^{-} population in each strain after saline or ISO treatment (n=12/strain/condition). DAPI was used to stain nuclei. Data presented as mean ± SEM. Two-way ANOVA, *P< 0.05. Scale bar: 50μm

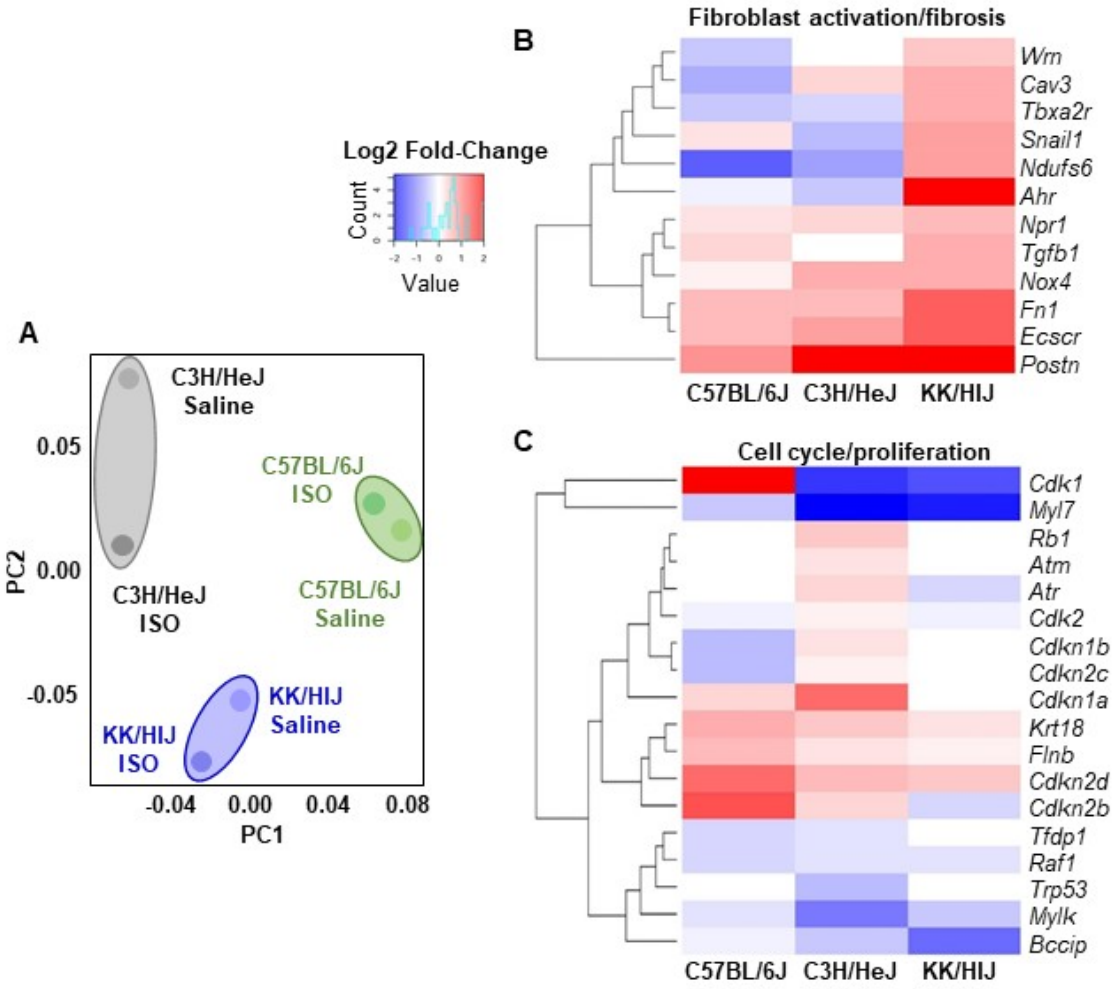

Figure 4. ISO treatment induces unique gene expression patterns in CFbs of different strains. **(A)** Principle component analysis (PCA) of RNA-sequencing data performed on strain-specific CFbs after saline or ISO treatment. **(B)** Heat map representing the log2 fold change value of select differentially expressed genes involved in fibroblast activation and fibrosis. **(C)** Heat map comparing expression changes of select genes involved in cell cycle and proliferation across the three strains.

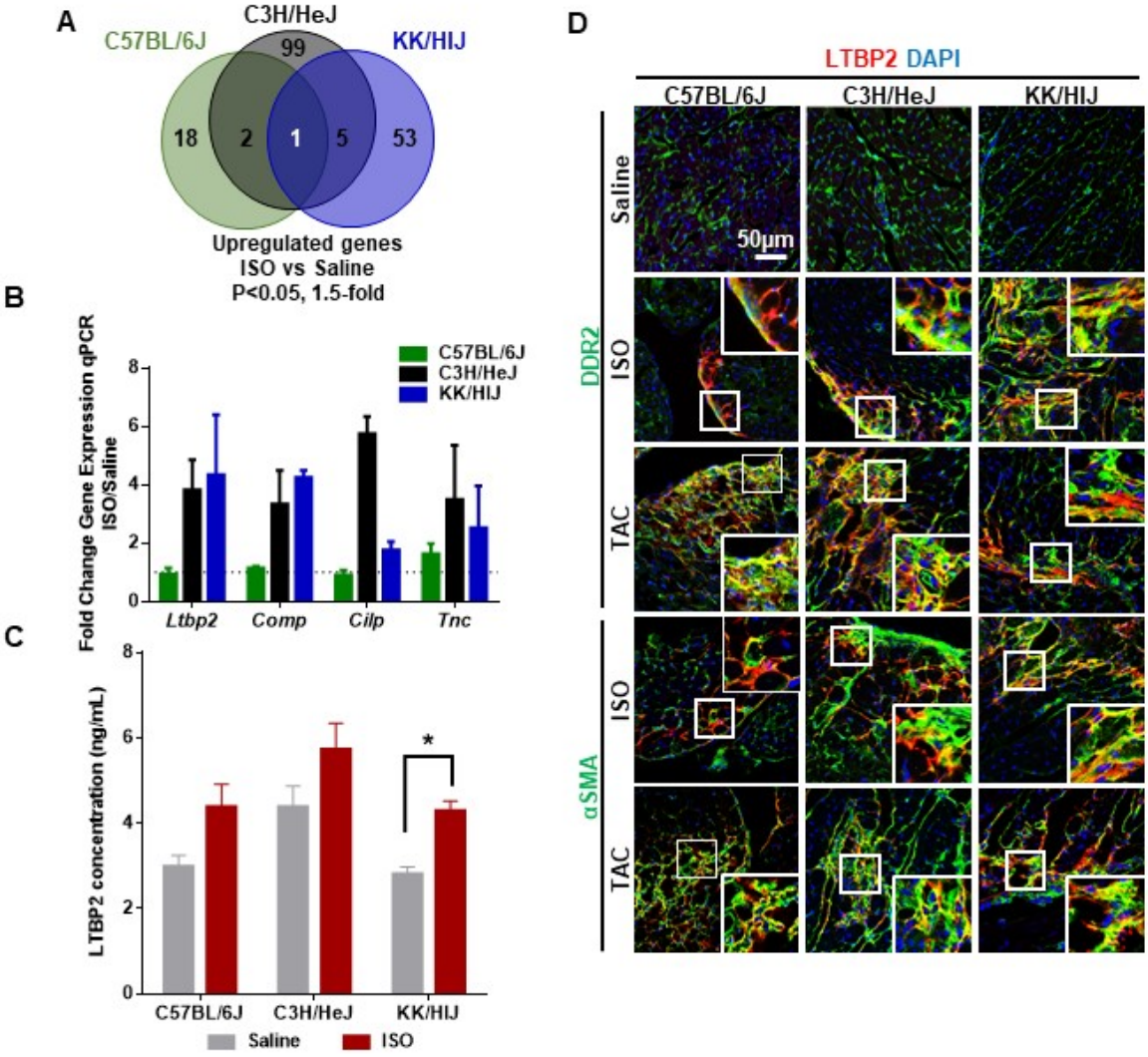

Figure 5. *Ltbp2* is upregulated in CFbs of all strains after stress. (A) Venn diagram depicting the number of overlapping upregulated genes across all three strains after ISO treatment. **(B)** RT-qPCR analysis of common genes which were differentially expressed between the strains after ISO treatment (n=3-4/strain/condition). **(C)** LTBP2 protein levels in mouse plasma samples after ISO treatment, measured by ELISA (n=3/strain/condition). **(D)** IHC of heart sections stained for LTBP2 (red) and DDR2 (green), to mark fibroblasts, after ISO treatment and TAC injury. DAPI was used to stain nuclei. Data presented as mean ± SEM. Two way ANOVA, *P < 0.05. Scale bar: 50μm

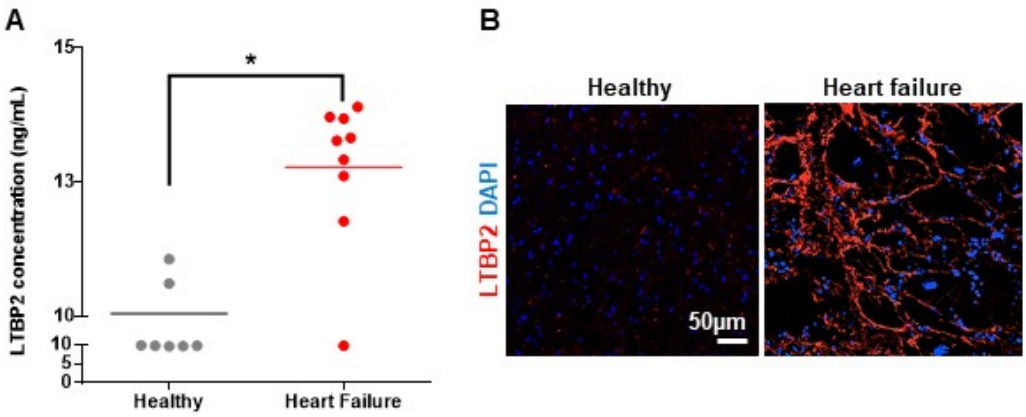

Figure 6. LTBP2 protein levels are upregulated in human heart failure patients. **(A)** Quantification of LTBP2 levels in plasma samples from healthy individuals and heart failure patients by ELISA. **(B)** IHC of heart sections from healthy and failing human hearts stained for LTBP2 (red). DAPI was used to stain nuclei. Data presented as mean ± SEM. T-test, *P < 0.05. Scale bar: 50µm.

SUPPLEMENTAL MATERIAL

METHODS

Echocardiography

Transthoracic echocardiography was performed on both saline and ISO treated mice before treatment and 21 days after pump implantation. Echocardiography was performed by a single operator who was blinded to the mouse strains and treatment groups using the Vevo 770 high-resolution ECHO system equipped with a 35 MHz transducer. First, chest fur was removed using a depilatory lotion (Nair). Mice were lightly anesthetized with vaporized isoflurane (2.5% for induction, 1.0% for maintenance) in oxygen and lightly restrained in a supine position on a heated pad to maintain body temperature at 37° C. Continuous EKG monitoring was done throughout the imaging studies and heart rates were maintained between 500 and 600 beats per minute. The probe was placed along the short axis of the left ventricle with the papillary muscles providing a guide for the proper depth. 2D images were captured to measure internal wall dimensions during both systole and diastole, as well as providing another measure of the heart rate. Saved images were analyzed by a single operator who was blinded to the experimental design using the Vevo 2100 software. The LV chamber dimensions and posterior wall thickness (PWT) were obtained from M-mode images; LV systolic function was also assessed from these measurements by calculating ejection fraction (EF) and fractional shortening (FS).

Heart weight, body weight, and tibia length collection

After 21 days of saline or isoproterenol treatment, mice from each strain (n=20 per strain) were sacrificed and their body weights were recorded. The heart was removed and, after PBS perfusion, weighed. Additionally, the right tibia of each mouse was removed and measured with a caliper.

Histological analyses (Trichrome staining, scar size measurement, immunohistochemistry)

Freshly isolated tissues were fixed in 4% paraformaldehyde (Electron Microscopy Sciences) in PBS (Fisher Scientific) overnight in 4°C. Afterwards, the tissues were washed with PBS and immersed in a 30% sucrose solution (Sigma) in PBS in 4°C overnight. The hearts were then embedded in Tissue- Tek OCT Compound (Sakura) and transferred to a bath of 2-Methylbutane (Fisher Scientific) on dry ice. Frozen tissues were sectioned at 7 µm thickness using a cryostat (Leica) and stored at -80°C.

Masson's trichrome staining (Sigma) was performed according to the manufacturer's instructions and images were taken of the entire cross-section of the heart using bright-field microscopy (Leica). To assess the degree of cardiac fibrosis, NIH ImageJ software was used by comparing the area of tissue stained blue (collagen) to the total tissue area (10-12 randomly chosen sections per heart, n=6 hearts per strains).

For immunohistochemistry, slides were dried at room temperature for 20 minutes, washed 3 times for 10 minutes each in PBS, permeabilized in PBS containing 0.25% Triton X-100 (Fisher Scientific) for 10 minutes at room temperature followed by washing in PBS-T (PBS containing 0.05% Tween-20 (Fisher)) twice for 5 minutes. The tissue slides were incubated with blocking buffer (10% normal goat serum (Sigma) in PBS-T) for 30 minutes at room temperature. The tissue slides were then incubated with primary antibodies **(Supplementary Table I)** diluted in blocking buffer overnight at 4 °C followed by 1 hour at room temperature. After washing three times for 10 minutes with PBS-T, the tissue slides were incubated with the secondary antibody **(Supplementary Table I)** for 1 hour at room temperature, washed three times for 10 minutes with PBS-T, and then mounted with DAPI-containing mounting media (Vector). The immunostained slides were observed and analyzed using a fluorescent microscope (LEICACTR6500, Leica) and a confocal microscope (LSM880, Zeiss).

BrdU detection by flow cytometry and immunohistochemistry

BrdU (10mg/mL) was injected intraperitoneally on the day of pump implantation. Mice were supplied BrdU in their drinking water (1 mg/mL) for 21 days. The water was changed every two days. Intracellular staining for BrdU was performed in accordance to the instructions of the BD Pharmingen™ BrdU Flow Kit. In short, cells were fixed and permeabilized in Cytofix/Cytoperm Buffer (BD), followed by incubation in Cytoperm Permeabilization Buffer plus (BD) and DNase treatment (BD). The cells were then exposed to fluorescent anti-BrdU antibody, washed, resuspended in staining buffer, and analyzed using a BD FACSAria II flow cytometer. For immunohistochemistry, slides were dried at room temperature for 20 minutes, washed 3 times for 10 minutes each in PBS, permeabilized in PBS containing 0.5% Triton X-100 (Fisher Scientific) for 10 minutes at room temperature, and pre-treated with 2M HCl for 30 minutes at 37°C. After brief washing with PBS, the slides were incubated with blocking buffer (10% normal goat serum (Sigma) in PBS) for 30 minutes at room temperature. The slides were then incubated with anti-BrdU antibody (Abcam) and primary antibodies to mark fibroblasts and activated fibroblasts **(Supplementary Table I)** in 4°C overnight, followed by 15 minutes in 37°C. After washing three times for 10 minutes with PBS-T, the tissue slides were incubated with the secondary antibody **(Supplementary Table I)** for 1 hour at room temperature, washed three times for 10 minutes with PBS-T, and then mounted with mounting media (Vector). The immunostained slides were then imaged by an LSM880 confocal microscope (Zeiss).

Quantitative RT-qPCR

Total RNA from $Thy1^{+}HE^{-}$ cells from control and ISO-treated hearts were extracted using TRIzol® LS Reagent (Ambion) and RNeasy MinElute Cleanup Kit (Qiagen) according to the manufacturers' instructions. The concentration and quality of extracted RNA were measured using a NanoDrop ND-1000 Spectrophotometer (Thermo Scientific). cDNA was synthesized using an *iScript*™ cDNA Synthesis Kit (Bio-Rad). For quantitative RT-qPCR, we used an *iTaq*™ *Universal SYBR® Green*

supermix (Bio-RAD), amplified cDNA and gene-specific primers **(Supplementary Table IV)** on a *CFX96 real-time* PCR detection system (Bio-Rad). PCR conditions included initial denaturation at 95°C for 2 minutes and 10 seconds, 39 cycles of denaturation at 95°C for 15 seconds, annealing at 60°C for 30 seconds, extension at 72 °C for 30 seconds, followed by a final extension at 72°C for 10 minutes. The mean cycle threshold (Ct) values from triplicate measurements were used to calculate relative gene expressions, with normalizations to GAPDH as an internal control. We used the ΔΔCT method to analyze relative gene expression in treated samples compared to non-treated samples. Technical replicates (n=3) and biological replicates (n=3) were performed for each strain.

Western Blotting

For western blots, albumin was removed from plasma using the AlbuSorb™ kit (Biotech Support Group #A185-1) and the concentration of total protein present afterwards was quantified using a Pierce™ BCA Protein Assay Kit (Thermo Scientific). Plasma was denatured and reduced in 1x Laemmli Sample Buffer (Bio-Rad) with 5% 2-Mercaptoethanol. 20µg of total protein was run on 4-15% Mini-PROTEAN® TGX™ Precast Gels first at 80V for 30 minutes and then 130V for another 45 minutes. The gels were transferred onto Amersham Hybond™ -P membranes by wet transferring for 1.5 hours at 70V. The membranes were then blocked with 5% non-fat milk and blotted with primary antibodies **(Supplementary Table I)** overnight at 4°C. After washing, secondary antibodies **(Supplementary Table I)** conjugated to horseradish peroxidase were added for 1 hour at room temperature. The membranes were developed using Pierce™ ECL Western Blotting Substrate (Thermo Scientific) and a Bio-rad Analyzer.

Transaortic Constriction (TAC)

Adult mice weighing 25±5 g were randomly divided into sham and TAC groups (n=4-6 per group) Animals were anesthetized by an intraperitoneal injection of ketamine/xylazine (100 mg/10

mg/kg). Endotracheal intubation was performed using a blunt 20-gauge needle that was then connected to a volume-cycled rodent ventilator (SAR-830/P; CWE, Inc.) with a tidal volume of 0.2 ml and a respiratory rate of 120/min. The chest was entered in the second intercostal space at the top left aortic arch, the transverse aorta was isolated, and aortic constriction was performed by tying a 7-0 nylon suture ligature against a 27-gauge blunt needle. The needle was then removed to yield a constriction 0.4 mm in diameter. In sham-operated control mice, the entire procedure was identical except that aortic constriction was not performed. The chest tube was used to evacuate the pneumothorax, and it was removed once negative pressure was re-established. The chest was closed in layers using 5-0 Vicryl sutures. Ventilation was maintained until sufficient spontaneous breathing occurred, followed by extubation and removal of the chest tube. The whole surgical procedure was performed under aseptic conditions.

Supplementary Table I: Antibodies used for flow cytometry, immunostaining and Western blot

Antibody	Catalog number	Vendor
Collagen 1	ab34710	Abcam
αSMA	A2547	Sigma-Aldrich
PDGFRα	Sc-338	Santa Cruz Biotechnology
Periostin	AF2955	R&D Systems
LTBP2	Gift from Dr. Marko Hyytiäinen from the University of Helsinki, Finland	
DDR2	MAB25381	R&D Systems
pHH3	ab47297	Abcam
BrdU	ab6326	Abcam
Anti-Mouse CD 90.1 APC-eFluor 780	47-0900-82	eBioscience
Anti-Mouse CD 90.2 APC-eFluor 780	47-0900-82	eBioscience
Anti-Mouse CD31 PE-Cyanine7	25-0311-81	eBioscience
Anti-Mouse CD11b PE-Cyanine7	25-0112-81	eBioscience
Anti-Mouse CD45 PE-Cyanine5	48-0451-82	eBioscience
TER-119 PE-Cyanine7	25-5921-81	eBioscience
Donkey Anti-Rabbit Alexa Fluor 647	A-31573	Invitrogen
Rabbit Anti-Mouse Alexa Fluor 647	A-21239	Invitrogen
Goat Anti-Rabbit Alexa Fluor 594	A-11037	Invitrogen
Goat Anti-Rabbit Alexa Fluor 488	A-21206	Invitrogen
Goat Anti-Mouse Alexa Fluor 488	A-11001	Invitrogen
TNC	OAAI00437	Aviva systems biology
CILP	OAEB01146	Aviva systems biology
COMP	Sc-25163	Santa Cruz Biotechnology

Supplementary Table II: ELISA kits

Marker	Species	Catalog number	vendor
LTBP2	Mouse	MBS2885029	MyBioSource
LTBP2	Human	MBS2882493	MyBioSource
TNC	Mouse	MBS2508432	MyBioSource
COMP	Mouse	MBS2886878	MyBioSource

Supplementary Table III: Characteristics of human subjects

	Age (year)	Gender	Etiology (%)	EF (%)	Median BNP (pg/ml)	DM	h/o HTN
Healthy individuals	50±10	50% M 50% F	N/A	55≥	NA	0%	0%
Heart failure patients	59±7	75% M 25% F	62.5 ischemic 37.5 non-ischemic	23 ± 4.5	713 (541-1719)	% 62.5 Y % 37.5 N	75% Y 25% N

Supplementary Table IV: RT-qPCR primers

Gene	Forward Primer	Reverse Primer
Gapdh	TTGTCTCCTGCGACTTCAAC	GTCATACCAGGAAATGAGCTTG
Ltbp2	AACAGCACCAACCACTGTATC	CCTGGCATTCTGAGGGTCAAA
Cilp	ATGGCAGCAATCAAGACTTGG	AGGCTGGACTCTTCTCACTGA
Comp	ACTGCCTGCGTTCTAGTGC	CGCCGCATTAGTCTCCTGAA
Tnc	GCAGTGAAAAGCGGTGTCC	CTTCTCCGGTATAGCCCTCGT
Vegfc	GAGGTCAAGGCTTTTGAAGGC	CTGTCCTGGTATTGAGGGTGG
Nos3	GGCTGGGTTTAGGGCTGTG	CTGAGGGTGTCGTAGGTGATG
Arg2	TCCTCCACGGGCAAATTCC	GCTGGACCATATTCCACTCCTA
Socs3	ATGGTCACCCACAGCAAGTTT	TCCAGTAGAATCCGCTCTCCT

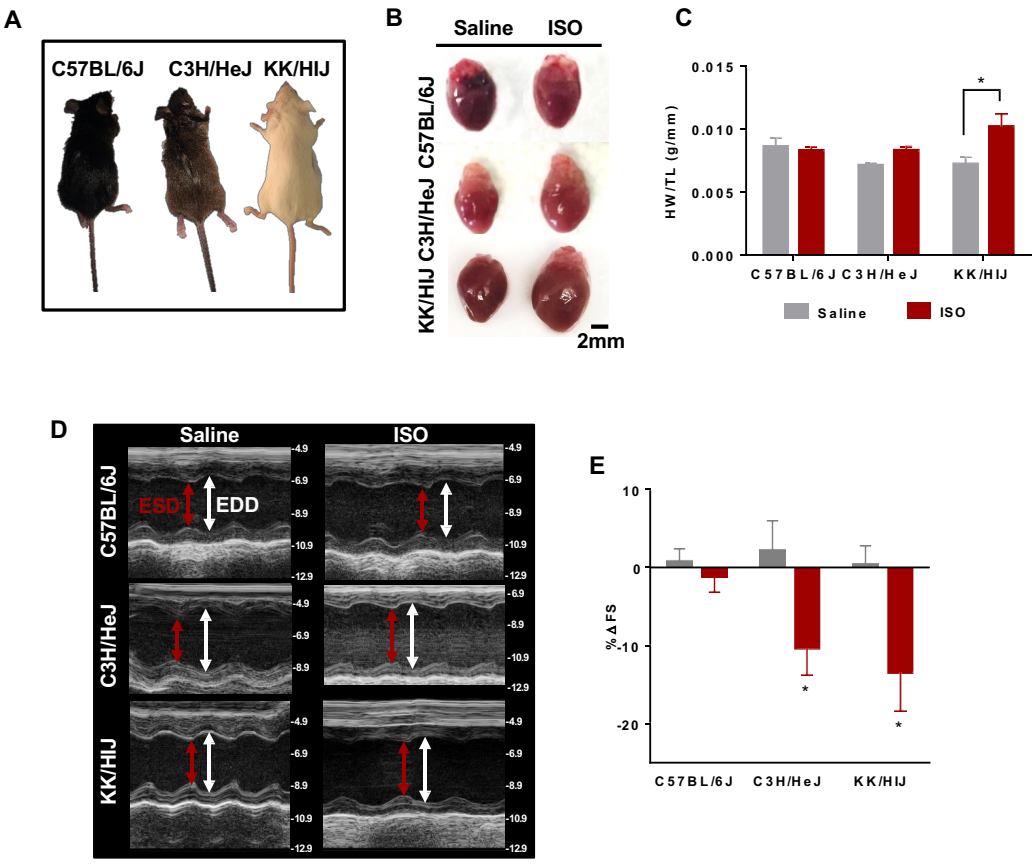

Supplementary Figure I. Severity of cardiac hypertrophy and cardiac dysfunction varies among select strains in response to ISO treatment. (A) Representative images of adult, female mice (8-12 weeks) from all three strains: C57BL/6J, C3H/HeJ, and KK/HIJ. **(B)** Whole heart images of the different strains after 21 days of saline/ISO treatment (n=6 mice/condition). **(C)** Heart weight/tibia length (HW/TL) ratio after treatment with saline or ISO (n=20 hearts/strain). **(D)** Representative M-mode echocardiographic images of hearts from animals following 21 days of saline or ISO treatment (n=20 mice/strain). **(E)** Fractional shortening was measured by echocardiography in both saline and ISO groups across the different strains (n=20 mice/strain). Data presented as mean ± SEM. Two-way ANOVA, *P < 0.05. Scale bar: 2mm.

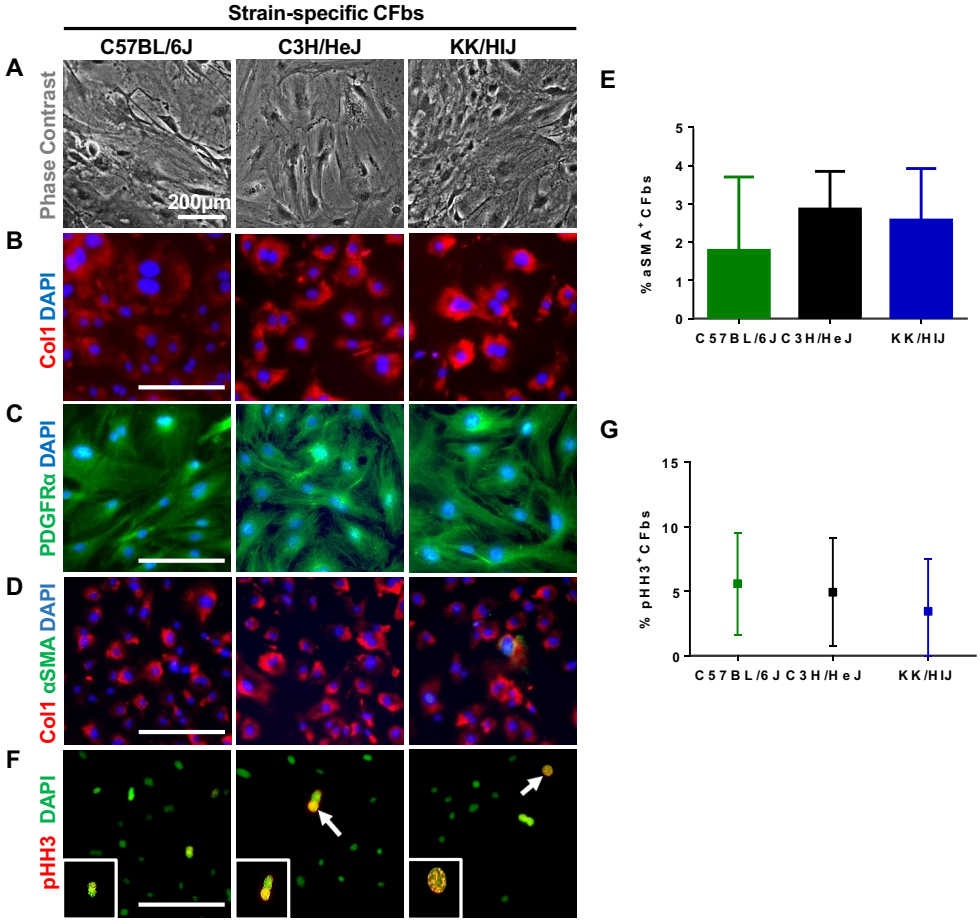

Supplementary Figure II. Strain-specific CFbs exhibit similar characteristics in culture. **(A)** Thy1+HE- cells from the hearts of the three strains were isolated by FACS and expanded in culture. **(B-C)** Cultured Thy1^{+}HE^{-} cells expressed fibroblast associated markers Collagen1 (Col1) (red) and PDGFRα (green). **(D-E)** Rare, activated CFbs were observed in the absence of any stimuli. Activated CFbs were marked by co-expression of αSMA (green) and Col1 (red). The bar graph demonstrates the percentage of Col1^{+}αSMA^{+} cells relative to all Col1^{+} cells (n=5 wells/strain/condition). **(F-G)** Proliferating CFbs were identified by nuclear staining for phospho-Histone H3 (pHH3) (red). The percentage of pHH3^{+} nuclei was measured relative to total nuclei (green) (n=5 wells/strain/condition). DAPI was used to stain nuclei. Data presented as mean ± SEM. T-test. Scale bar: 200μm.

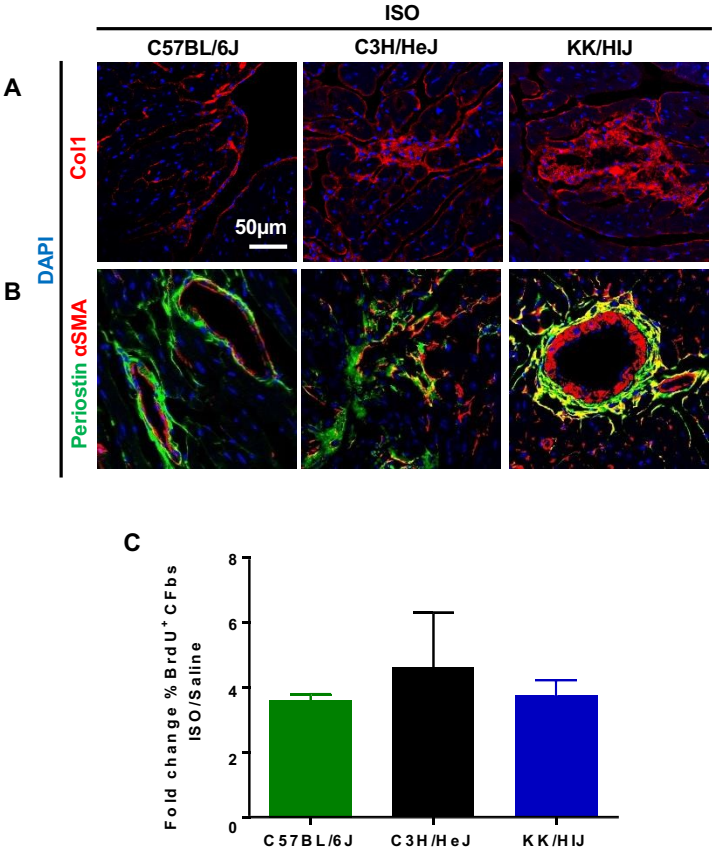

Supplementary Figure III. Levels of CFb activation after ISO treatment correlate with extent of collagen deposition, while CFb proliferation does not. (A) Heart sections after ISO treatment were stained for Col1 (red) to visualize extracellular matrix deposition. **(B)** IHC of ISO-treated heart sections stained for periostin (green) and αSMA (red), which both mark activated fibroblasts. **(C)** Fold change of proliferation rates in response to ISO were compared across the different strains. Each ISO-treated group was normalized to their respective control groups within each strain (n=12/strain/condition). DAPI was used to stain nuclei. Data presented as mean ± SEM. Two-way ANOVA, *P < 0.05. Scale bar: 50μm.

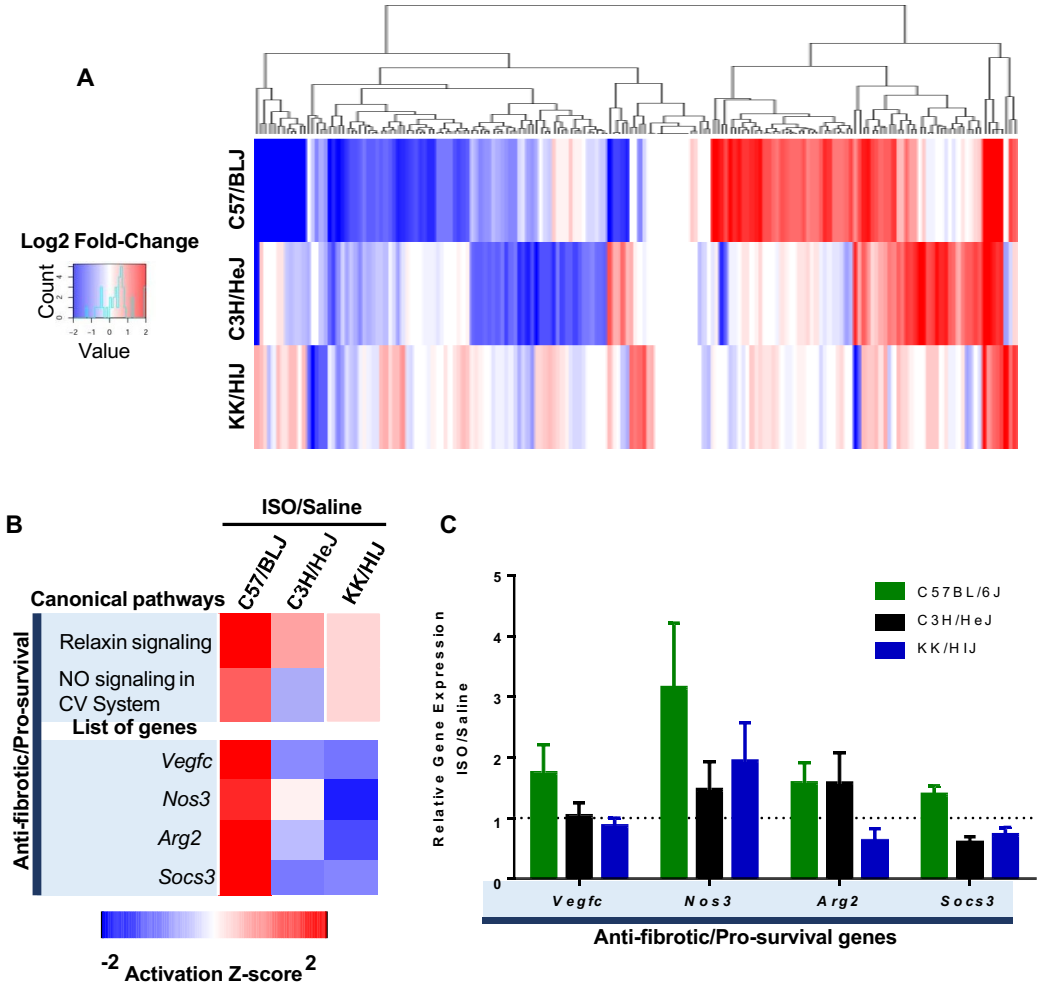

Supplementary Figure IV. Comparison of CFbs gene expression from all three strains reveal potential role of anti-fibrotic/pro-survival pathways. (A) Heat map showing log2 fold change of differentially expressed genes in CFbs of all strains after ISO treatment. **(B)** Ingenuity Pathway Analysis (IPA) was used to generate a list of canonical pathways with significant expression levels in CFbs treated with ISO compared to saline. Shown pathways were selected based on the trends that correlated with the extent of fibrosis seen *in vivo*. **(C)** Reverse transcription-PCR (RT-qPCR) validation of selected canonical pathway genes from the RNA-sequencing data. Relative gene expression was found by normalizing each strain's ISO-treated group with their respective saline-treated groups. NO: Nitric Oxide, CV: Cardiovascular. Data presented as mean ± SEM.

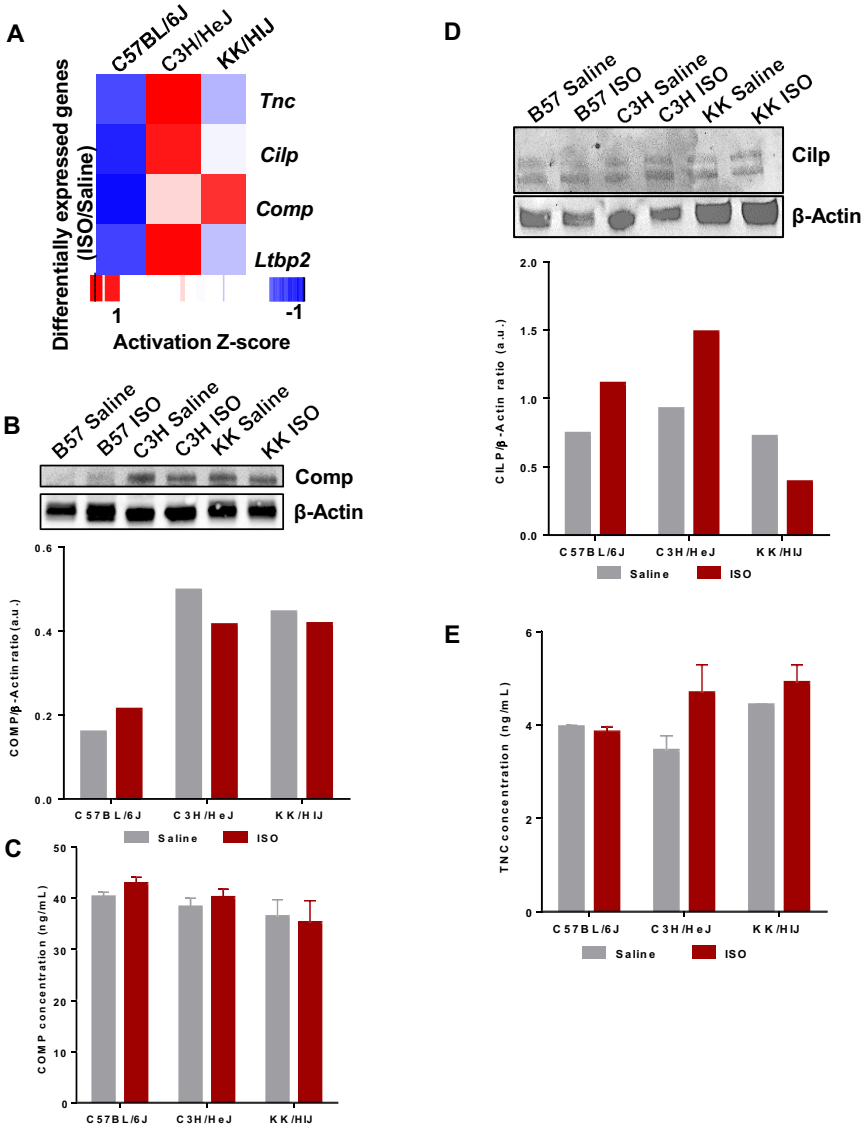

Supplementary Figure V. Most commonly upregulated genes do not exhibit trends in mouse plasma levels. (A) Expression level of commonly upregulated genes among all strains in response to ISO treatment. The protein level of COMP in plasma of all three strains after saline/ISO treatment was measured by Western blot **(B)** and ELISA **(C).** The thickness of the bands was quantified by ImageJ in **(B)** (n=3-4 plasma/strain/condition). **(D)** CILP expression levels in plasma after saline or ISO treatment. The thickness of the bands were quantified by ImageJ (n=3-4 plasma/strain/condition). **(E)** ELISA for TNC in all three strains after saline or ISO treatment. Data presented as mean ± SEM.

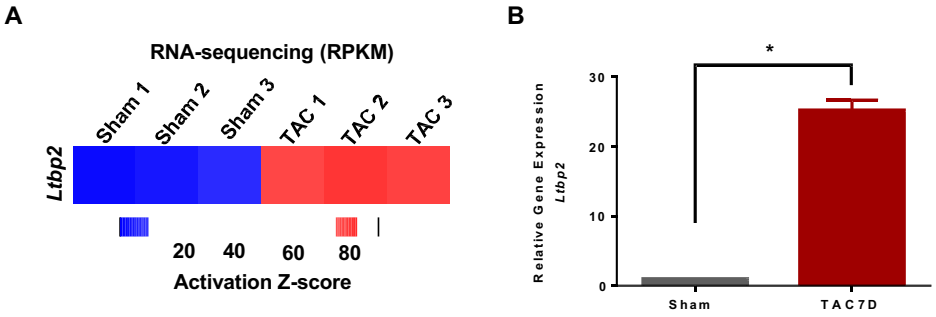

Supplementary Figure VI. *Ltbp2* gene expression is upregulated in CFbs after TAC injury. RNA-sequencing **(A)** and RT-qPCR analysis **(B)** of *Ltbp2* gene expression in CFbs isolated from C57BL/6J, 7 days post-sham or TAC operation. (n=3/mice/condition). Data presented as mean ± SEM. T-test, *P < 0.05.

Supplementary Figure I. **Severity of cardiac hypertrophy and cardiac dysfunction varies among select strains in response to ISO treatment. (A)** Representative images of adult, female mice (8-12 weeks) from all three strains: C57BL/6J, C3H/HeJ, and KK/HIJ. **(B)** Whole heart images of the different strains after 21 days of saline/ISO treatment (n=6 mice/condition). **(C)** Heart weight/tibia length (HW/TL) ratio after treatment with saline or ISO (n=20 hearts/strain). **(D)** Representative M-mode echocardiographic images of hearts from animals following 21 days of saline or ISO treatment (n=20 mice/strain). **(E)** Fractional shortening was measured by echocardiography in both saline and ISO groups across the different strains (n=20 mice/strain). Data presented as mean ± SEM. Two-way ANOVA, *P < 0.05. Scale bar: 2mm.

Supplementary Figure II. Strain-specific CFbs exhibit similar characteristics in culture. **(A)** Thy1+HE- cells from the hearts of the three strains were isolated by FACS and expanded in culture. **(B-C)** Cultured $Thy1^{+}HE^{-}$ cells expressed fibroblast associated markers Collagen1 (Col1) (red) and PDGFRα (green). **(D-E)** Rare, activated CFbs were observed in the absence of any stimuli. Activated CFbs were marked by co-expression of αSMA (green) and Col1 (red). The bar graph demonstrates the percentage of $Col1^{+}\alpha SMA^{+}$ cells relative to all $Col1^{+}$ cells (n=5 wells/strain/condition). **(F-G)** Proliferating CFbs were identified by nuclear staining for phospho-Histone H3 (pHH3) (red). The percentage of $pHH3^{+}$ nuclei was measured relative to total nuclei (green) (n=5 wells/strain/condition). DAPI was used to stain nuclei. Data presented as mean ± SEM. T-test. Scale bar: 200μm.

Supplementary Figure III. Levels of CFb activation after ISO treatment correlate with extent of collagen deposition, while CFb proliferation does not. (A) Heart sections after ISO treatment were stained for Col1 (red) to visualize extracellular matrix deposition. **(B)** IHC of ISO-treated heart sections stained for periostin (green) and αSMA (red), which both mark activated fibroblasts. **(C)** Fold change of proliferation rates in response to ISO were compared across the different strains. Each ISO-treated group was normalized to their respective control

groups within each strain (n=12/strain/condition). DAPI was used to stain nuclei. Data presented as mean ± SEM. Two-way ANOVA, *P < 0.05. Scale bar: 50μm.

Supplementary Figure IV. Comparison of CFbs gene expression from all three strains reveal potential role of anti-fibrotic/pro-survival pathways. (A) Heat map showing log2 fold change of differentially expressed genes in CFbs of all strains after ISO treatment. **(B)** Ingenuity Pathway Analysis (IPA) was used to generate a list of canonical pathways with significant expression levels in CFbs treated with ISO compared to saline. Shown pathways were selected based on the trends that correlated with the extent of fibrosis seen *in vivo*. **(C)** Reverse transcription-PCR (RT-qPCR) validation of selected canonical pathway genes from the RNA-sequencing data. Relative gene expression was found by normalizing each strain's ISO-treated group with their respective saline-treated groups. NO: Nitric Oxide, CV: Cardiovascular. Data presented as mean ± SEM.

Supplementary Figure V. Most commonly upregulated genes do not exhibit trends in mouse plasma levels. (A) Expression level of commonly upregulated genes among all strains in response to ISO treatment. The protein level of COMP in plasma of all three strains after saline/ISO treatment was measured by Western blot **(B)** and ELISA **(C).** The thickness of the bands was quantified by ImageJ in **(B)** (n=3-4 plasma/strain/condition). **(D)** CILP expression levels in plasma after saline or ISO treatment. The thickness of the bands were quantified by ImageJ (n=3-4 plasma/strain/condition). **(E)** ELISA for TNC in all three strains after saline or ISO treatment. Data presented as mean ± SEM.

Supplementary Figure VI. *Ltbp2* gene expression is upregulated in CFbs after TAC injury. RNA-sequencing **(A)** and RT-qPCR analysis **(B)** of *Ltbp2* gene expression in CFbs isolated from C57BL/6J, 7 days post-sham or TAC operation. (n=3/mice/condition). Data presented as mean ± SEM. T-test, *P < 0.05.

CHAPTER 5

Conclusion and Future Direction

5.1 Developmental Heterogeneity of Cardiac Fibroblasts Does Not Predict Pathological Proliferation and Activation

The developmental origin of cardiac fibroblasts remains a controversial subject. This issue is one worth investigating, as evidence suggests a causal role for these cells in the pathological response to ischemic and pressure overload injuries in animal models [1, 2]. These injury models are analogous to the prevalent cardiovascular diseases in humans that are among the most costly and debilitating conditions globally [3]. Cardiac fibroblasts mediate hypertrophy and scar formation through specific signaling pathways and secreted proteins, hence the identification of a subset of fibroblasts that specifically enact this pathological program is critical. This need stems from the perspective of therapy and drug development, as the ideal drug would only modulate the disease-causing cellular subset without affecting other cell types. However, to achieve this goal, we have to first delineate the different subsets that comprise the fibroblast population in the heart. Although several studies have provided strong evidence for the contribution of certain lineages to the cardiac fibroblast population, the most pressing problem in this field is the lack of markers that are specific for the entire fibroblast population [4]. To this end, we first sought to develop a panel of surface markers that would most specifically allow us to account for the majority of cardiac fibroblasts without contamination from other cell types. Next, we attempted to clarify the precise lineage origins of cardiac fibroblasts and explored the implications of this developmental heterogeneity in normal physiology and after pathological insults to the heart.

Herein, we characterized the Thy1+CD45-CD31-CD11b-Ter119- cells in great detail and presented rigorous evidence for their fibroblast identity. Next, with the aid of our well-characterized surface markers and numerous transgenic mouse strains, we comprehensively examined various lineages as potential progenitors for cardiac fibroblasts including; Tbx18Cre [5] and Wt1CreERT2 [6-9] for epicardium; Tie2Cre for endothelium [10]; Pax3Cre for neural crest [11]. This enabled us to identify the epicardium as the primary source of cardiac fibroblasts (~75%) in healthy adult mice, while endothelium contributed to a smaller population of fibroblasts (~12%). Additionally, there was a minor contribution from neural crests to fibroblast pool (~3-5%). Next, we induced pressure overload injury by transaortic constriction (TAC) and showed that the developmental programs that generate fibroblasts in utero do not seem to mediate the levels of proliferation after injury.

The results from our study have also been confirmed by the Evans group [12]. Despite the fact that our group and others have shown that epicardial cells generate cardiac fibroblasts during development through epithelial to mesenchymal transition (EMT), our work revealed that pressure overload injury does not generate fibroblasts through this mechanism. However, it is technically possible that inefficient recombination in the inducible Cre system or the short time course before analysis may have led to underestimation of fibroblasts being generated from EMT in the Wt1CreERT2/+ model. Therefore, using a more specific inducible transgenic mouse model such as MsInCreER/+, which has been previously shown to mark all epicardial cells [13, 14], would be a potential future direction of our study. Our data also corroborated some of the

findings of Zeisberg et al. [15] in identifying endothelial-derived fibroblasts as a subset of cardiac fibroblasts; however, in contrast to their work we observed an absence of evidence for active endothelial to mesenchymal transition (EndMT) upon pressure overload injury. Finally, we performed bone marrow transplantation and parabiosis experiments to explore the potential contribution of bone marrow (either hematopoietic stem cells or stromal cells) or circulating cells to scar forming fibroblasts after injury. The bone marrow transplantation model obviated questions about ectopic transgene expression or transgene silencing that complicated interpretation of Cre-based lineage-tracing models from previously reported studies [15, 16]. Our findings showed that there was no contribution from the bone marrow to cardiac fibroblasts in both physiological and pathological settings. Our data suggested that perhaps a shared mechanism stimulates proliferation of distinct fibroblast subsets in response to injury.

Overall, we believe that prospective isolation of cardiac fibroblasts using our panel of surface markers, along with gene expression profiling, could lead to an accurate understanding of the signaling pathways that regulate each developmental subset and the entire fibroblast population in response to injury.

5.2 The Cardiac Microenvironment Supersedes Developmental Origin for Fibroblast-to-Cardiomyocyte Reprogramming

While cell-based regenerative therapies hold promise, direct reprogramming of endogenous cardiac fibroblasts to cardiomyocytes is an attractive alternative strategy that can potentially regenerate the myocardium from endogenous fibroblasts and reduce scar

formation [17, 18]. Emerging studies have reported the remarkable predisposition of resident cardiac fibroblasts to be reprogrammed more efficiently to iCMs in vivo, especially in the injury milieu, when compared to in vitro reprogramming [19-22]. However, a fundamental and unresolved issue in the field of direct reprogramming is to identify key components that drive the conversion of a mature cell type to another. It is unclear whether the developmental origin or/and the microenvironment of the fibroblasts is the critical factor for efficient reprogramming. Indeed, a recent study by the Rosenthal group suggested that a subpopulation of CFbs may be more amenable to cardiac reprogramming due to their expression of core cardiogenic genes which are mainly associated with cardiomyocyte ontogenesis [23]. CFbs are known to have multiple discrete developmental origins [24]; however, the hierarchical ontogeny and ancestral relationship of CFbs to other cardiac cell types, particularly cardiomyocytes, has not been fully investigated. To address this issue, we used a combination of transgenic mouse models, transplantation studies and gene expression profiling to show that the majority of CFbs originate from a mesodermal precursor that also generates cardiomyocytes and other major cell types in the heart. We also demonstrated that a minority of the CFb population originates from neural crest-derived precursors. We further explored whether the mesoderm-derived CFbs that share the same ancestral relationship with cardiomyocytes exhibit a higher efficiency of reprogramming to generate iCMs. We provided compelling evidence that, despite distinct developmental origins, all CFbs were able to be successfully converted to beating iCMs through in vitro direct reprogramming. However, when compared to fibroblasts of other organs with similar developmental origin, CFbs generated iCMs with higher efficiency, emphasizing the critical role of the

physiological environment on cell fate conversion. To further confirm our results, it would be interesting to study the in vivo cardiac reprogramming of fibroblasts in tissues other than the heart. For example, by injecting the cardiogenic factors into the lung or dermal and cardiac tissues we can evaluate the effect of endogenous milieu on efficiency and maturity of induced cardiomyocytes after injury.

The in vivo environment of the heart appears to improve the maturity of the generated iCMs through in situ reprogramming, with even higher efficiency being achieved with prior damage [19-21]. However, it is not clear how the injury can overcome the epigenetic hurdles that prevent cardiac reprogramming in vitro and potentially render the cells to be more amenable to fate switch. Furthermore, CFbs expand substantially, especially in the infarct zone after an ischemic injury [24]. Stimulation of cell proliferation is shown to facilitate cell type conversions as the de-condensed chromatin state during mitosis is more accessible to reprogramming factors [25]. Therefore, we aimed to explore whether injury results in differential response within the various CFb subtypes such that it could preferentially stimulate a specific CFb population for reprogramming. Our data from pressure overload injury, revealed a parallel expansion of developmentally-distinct fibroblast populations. Moreover, both subsets generated activated fibroblasts after injury, which are considered to be responsible for the pathological secretion of fibrosis-associated ECM. Despite this indistinguishable response to pressure overload injury, we observed a unique re-expression of early developmental genes in CFbs that corresponded to their developmental origin. One week after induction of pressure overload injury, mesoderm-derived CFbs were enriched in genes associated with early

cardiac development while early neuronal genes were mainly upregulated in neural crest-derived CFbs. These findings further raise the intriguing possibility that Mesp1-derived CFbs may be more susceptible to be reprogrammed to iCMs in vivo due to the re-expression of early mesoderm and cardiac development genes after injury.

Additionally, the changes observed in the re-expression of early developmental genes were no longer present 4 weeks after injury. These intriguing findings suggested that there may exist a discrete temporal period after injury when the unique milieu may allow for endogenous cells to overcome epigenetic barriers that hinder the early stages of reprogramming. Deeper understanding of the molecular mechanisms involved in reverting fibroblasts back to their neonatal stage may be essential for enhancing the reprogramming efficiency of fibroblasts to cardiomyocytes. By understanding how environmental factors overcome epigenetic barriers in vivo, we can combine them with reprogramming factors to activate and reprogram fibroblasts within the scarred myocardium heart failure patients. In future studies, it would be of great interest to verify the effects of fibroblasts heterogeneity on in vivo cardiac reprogramming. Moreover, it would be interesting to isolate Mesp1- and Pax3 derived cardiac fibroblasts from both sham and TAC injured hearts and compare their efficiency of cardiomyocyte generation by in vitro reprogramming. The data from this experiment may further reveal how endogenous microenvironment (injured/non-injured) can affect the fibroblasts lineage conversion. Moreover, we used pressure overload injury model; whereas most previous in vivo reprogramming studies have been performed in acute ischemic heart models. Therefore, it would be interesting to explore whether acute injury would affect the re-

expression of early developmental genes in cardiac fibroblasts and whether the effect is also lineage dependent.

Overall, we believe the knowledge from our studies will not only prove to be critical for future developmental studies of cardiac fibroblasts, but it will also be essential for elucidating molecular mechanisms that efficiently drive in vivo CFb reprogramming to cardiomyocytes, particularly in the setting of cardiac injury for potential clinical translation.

5.3 Genetic Regulation of Fibroblast Activation and Proliferation in Isoproterenol-induced Cardiac Fibrosis

It is known that, in both mice and humans, genetic variability contributes to the development and progression of disease. This variability is an obstacle for evaluation and treatment of complex diseases such as heart failure [26], which is characterized by a large number of pathological changes, such as contractile dysfunction, cardiomyocyte hypertrophy, edema, and myocardial fibrosis [27, 28]. The onset and severity of these pathological manifestations are highly heterogeneous among heart failure patients, likely due to complex interactions between genetic variants. Thus, dissecting the genetic contributions to specific pathological changes in the failing heart would provide important insights for the future development of personalized diagnoses and targeted therapies.

Herein, we have conducted a comprehensive phenotypic characterization of CFbs from different inbred strains of mice from the Hybrid Mouse Diversity Panel (HMDP) following chronic treatment with a β-adrenergic agonist, isoproterenol (ISO). Through our analysis,

we identified three mouse strains; C57BL/6J, C3H/HeJ, and KK/HlJ which, after ISO treatment, exhibited minimal, moderate, and extensive levels of fibrosis, respectively. This finding indicated that the genetic background of mice significantly influences the observed phenotype of cardiac fibrosis after injury. Both our in vitro and in vivo experiments demonstrated that, in response to ISO, levels of fibroblast activation appeared to correlate with the extent of fibrosis seen in each strain. However, we observed similar levels of fibroblast proliferation in all three mice strains, regardless of the degree of fibrosis. Our findings indicate that activation of cardiac fibroblasts seems to be a prominent factor contributing to the generation of cardiac fibrosis. For future studies, it would be of great interest to investigate whether there is a direct correlation between fibroblast proliferation and the degree of activation. For example, observing whether blocking or downregulating proliferation in cardiac fibroblasts, both in vitro and in vivo, would affect the degree of fibroblasts activation or cardiac fibrosis. Furthermore, gene expression profiling of cardiac fibroblasts from all three strains unveiled distinct characteristics in the transcriptomes of these cells. We identified LTBP2, a TGFβ-associated protein as commonly upregulated in all three mouse strains after ISO. LTBP2 level was found to be elevated in the plasma after injury and was strictly localized in fibrotic myocardial tissue in both mice and human subjects with heart failure. The discovery of LTBP2 as a unique marker for fibrosis is exciting because future research in how LTBP2 may regulate fibrosis could unravel pathways that can be targeted for therapeutic intervention. In future studies, we are interested to explore how overexpression or downregulation of LTBP2 in cardiac fibroblasts of different strains may affect the levels of CFb proliferation and activation.

Overall, these findings have significant clinical relevance to the understanding of human cardiac fibrosis and disease progression. In our study, we present for the first-time a thorough and detailed characterization of cardiac fibroblasts using an innovative approach of comparing multiple mouse strains treated with the β-adrenergic agonist ISO. From the various comparisons made, we were able to identify several unique, strain-specific mechanisms in which cardiac fibroblasts may modulate ISO-mediated fibrosis. These mechanisms provide new insight into cardiac fibroblast physiology and the cellular processes contributing to the development of cardiac fibrosis.

1. Thum, T., et al., MicroRNA-21 contributes to myocardial disease by stimulating MAP kinase signalling in fibroblasts. Nature, 2008. 456: p. 980-4.

2. Takeda, N., et al., Cardiac fibroblasts are essential for the adaptive response of the murine heart to pressure overload. J. Clin. Invest., 2010. 120: p. 254-265.

3. Organization, W.H. The Global Burden Of Disease: 2004 Update. 2004.

4. Krenning, G., E.M. Zeisberg, and R. Kalluri, The origin of fibroblasts and mechanisms of cardiac fibrosis. J. Cell. Physio., 2010.

5. Cai, C.-L., et al., A myocardial lineage derives from Tbx18 epicardial cells. Nature, 2008. 454(7200): p. 104-108.

6. Quinn, T.A., et al., Electrotonic coupling of excitable and nonexcitable cells in the heart revealed by optogenetics. Proceedings of the National Academy of Sciences of the United States of America, 2016. 113(51): p. 14852-14857.

7. von Gise, A., et al., WT1 regulates epicardial epithelial to mesenchymal transition through β-catenin and retinoic acid signaling pathways. Developmental biology, 2011. 356(2): p. 421-431.

8. Zhou, B. and W.T. Pu, Genetic Cre-loxP assessment of epicardial cell fate using Wt1-driven Cre Alleles. Circulation research, 2012. 111(11): p. e276-e280.

9. Rudat, C. and A. Kispert, Wt1 and epicardial fate mapping. Circ Res, 2012. 111(2): p. 165-9.

10. Zeisberg, E.M., et al., Endothelial-to-mesenchymal transition contributes to cardiac fibrosis. Nat. Med., 2007. 13: p. 952-61.

11. Lang, D., et al., Pax3 functions at a nodal point in melanocyte stem cell differentiation. Nature, 2005. 433: p. 884-7.

12. Moore-Morris, T., et al., Resident fibroblast lineages mediate pressure overload–induced cardiac fibrosis. The Journal of Clinical Investigation, 2014. 124(7): p. 2921-2934.

13. Koyama, Y., et al., Mesothelin/mucin 16 signaling in activated portal fibroblasts regulates cholestatic liver fibrosis. The Journal of Clinical Investigation, 2017. 127(4): p. 1254-1270.

14. Rinkevich, Y., et al., Identification and prospective isolation of a mesothelial precursor lineage giving rise to smooth muscle cells and fibroblasts for mammalian internal organs, and their vasculature. Nat Cell Biol, 2012. 14(12): p. 1251-1260.

15. Zeisberg, E.M., et al., Endothelial-to-mesenchymal transition contributes to cardiac fibrosis. Nat Med, 2007. 13(8): p. 952-61.

16. Ruiz-Villalba, A., et al., Interacting resident epicardium-derived fibroblasts and recruited bone marrow cells form myocardial infarction scar. J Am Coll Cardiol, 2015. 65(19): p. 2057-66.

17. Sanganalmath, S.K. and R. Bolli, Cell therapy for heart failure: a comprehensive overview of experimental and clinical studies, current challenges, and future directions. Circ Res, 2013. 113(6): p. 810-34.

18. Qian, L. and D. Srivastava, Direct cardiac reprogramming: from developmental biology to cardiac regeneration. Circ Res, 2013. 113(7): p. 915-21.

19. Qian, L., et al., In vivo reprogramming of murine cardiac fibroblasts into induced cardiomyocytes. Nature, 2012. 485(7400): p. 593-8.

20. Song, K., et al., Heart repair by reprogramming non-myocytes with cardiac transcription factors. Nature, 2012. 485(7400): p. 599-604.

21. Jayawardena, T.M., et al., MicroRNA induced cardiac reprogramming in vivo: evidence for mature cardiac myocytes and improved cardiac function. Circ Res, 2015. 116(3): p. 418-24.

22. Mohamed, T.M.A., et al., Chemical Enhancement of In Vitro and In Vivo Direct Cardiac Reprogramming. Circulation, 2016.

23. Furtado, M.B., et al., View from the heart: cardiac fibroblasts in development, scarring and regeneration. Development, 2016. 143(3): p. 387-97.

24. Ali, S.R., et al., Developmental Heterogeneity of Cardiac Fibroblasts Does Not Predict Pathological Proliferation and Activation. Circulation Research, 2014. 115(7): p. 625-635.

25. Gaspar-Maia, A., et al., Open chromatin in pluripotency and reprogramming. Nature reviews. Molecular cell biology, 2011. 12(1): p. 36-47.

26. Altshuler, D., M.J. Daly, and E.S. Lander, Genetic Mapping in Human Disease. Science (New York, N.Y.), 2008. 322(5903): p. 881-888.

27. Beltrami, C.A., et al., Structural basis of end-stage failure in ischemic cardiomyopathy in humans. Circulation, 1994. 89(1): p. 151-63.

28. Kong, P., P. Christia, and N.G. Frangogiannis, The pathogenesis of cardiac fibrosis. Cell Mol Life Sci, 2014. 71(4): p. 549-74.